Ivane Javakhishvili Tbilisi State University

Faculty of Exact and Natural Sciences

Doctoral Program: Physics

Revaz Beradze

Some Cosmological and Astrophysical Implications of Mirror World Model

The thesis work is performed to obtain a PhD academic degree in Physics

Scientific Supervisors:

Merab Gogberashvili
Assoc. Prof.

Zurab Berezhiani
Prof.

Tbilisi, 2022

Abstract

Direct detection of gravitational waves using Laser Interferometer Gravitational-Wave Observatory (LIGO) opened a new window in the field of physics and began a new era in multi-messenger astronomy. Conducting three observing runs, 90 confirmed gravitational-wave signals produced by mergers of binary compact objects, were summarized in Gravitational-Wave Transient Catalog-3. While general properties of detected radiation are consistent with theory of general relativity, the models of massive stars' evolution challenge to explain some of the features: absence of counterpart electromagnetic radiation in majority of events, rate of mergers higher then predicted, masses of compact objects falling within the expected gaps.

In this thesis, we want to address these troublesome aspects to the particular dark matter model - mirror world theory. Mirror matter model states that all elementary particles have their twin mirror partners that are governed through the same microphysical laws. Mirror and ordinary particles are invisible for each other, but they can interact via gravity. Mirror matter is thought to be colder and dominated by helium. This leads to formation of massive stars with short lifespans. So, in mirror world, great amount of massive compact objects are expected to be formed in early times.

We suggest that, if observed gravitational waves originated from mirror compact binaries, then dearth of electromagnetic radiation is natural, as mirror photons stay unnoticed by our detectors. Besides that, mirror matter abundance, as it is a candidate for dark matter, can exceed ordinary matter abundance five times. Altogether, large number of massive compact objects will increase binary merger rates, making it compatible with observations. In addition, odd mass-gap event could potentially be overcame by mirror world scenario.

Acknowledgments

Contents

Chapter 1

Introduction

More than a century ago, in his famous paper "On the Electrodynamics of Moving Bodies", published in 1905, Albert Einstein proposed his Special theory of Relativity (SR) and began a whole new chapter in the history of physics. Einstein came up with two postulates: 1. The laws of physics are invariant in all inertial reference frames; 2. The speed of light in vacuum is same for all observers, regardless the motion of observer or the source of light. The theory assumed that interaction speed between objects is finite and properly described motions of objects with the velocities comparable with the speed of light (relativistic velocities). The postulates lead to an ambitious statement that time is not absolute! Clocks in different reference frames may tick at different rates! Newtonian physics was not any more as inviolable as it used to be. Space and time were not as distinct and they were unified in a notion of space-time that entered entangled in Lorentz transformations, replacing Galilean transformation rules. Three-dimensional Euclidean space was replaced by four-dimensional Minkowskian spacetime, that became a main field where SR is operated.

In fact, for that time, Newtonian mechanics already showed incompatibility with Maxwell's equations of electromagnetism. By the time, null result of Michelson-Morley experiment finally ruled out an idea of luminiferous aether. Based on earlier works by Hendrik Lorentz and Henri Poincare, Einstein's SR dealt with all these problems. It stated, that there are no privileged frames of reference, though the eather must not exist; and it incorporated Newtonian mechanics with the theory of electromagnetism, in which the interaction speed is finite. By the way, in the limit when the velocity of objects is small compared to the speed of light, or if one assumes that interaction between objects is immediate, SR nicely recovers the Newtonian physics.

But that was not a whole story. SR does not directly address acceleration and about gravity - two important quantities in Newtonian physics. Einstein moved on and in 1915 published general theory of relativity (GR), where he generalized SR and refined Newton's law of universal gravitation, providing unified description of gravity as a geometric property of four-dimensional spacetime. Einstein proposed that, what we observe as gravitational force, is a curvature of spacetime, and the curvature is caused by the energy-momentum that matter has. GR uses Riemannian geometry and it's main formula is given by Einstein's equations

$$R_{\mu\nu} - \frac{1}{2}Rg_{\mu\nu} = 8\pi G T_{\mu\nu} \ , \tag{1.1}$$

where $g_{\mu\nu}$ is a metric tensor, R and $R_{\mu\nu}$ are, correspondingly, Ricci scalar and Ricci tensor and they both are the functions of metric tensor, so the left hand side of the equation (1.1) is poorly geometric. $T_{\mu\nu}$ on the right hand side is energy-momentum tensor and G is Newton's

gravitational constant. So, Einstein's equations (1.1) govern the response of spacetime curvature to the presence of matter and energy.

Einstein used another cornerstone in this theory - the equivalence principle. A somewhat similar concept was introduced by Galileo when he realized, that objects of different mass fall on the Earth at the same time, i.e., in later formulation, the proportionality parameter in the Newton's law of gravitation

$$F = -m_g \nabla \phi \ , \quad (F \ - \ \text{gravitational force}, \ \phi \ - \ \text{gravitational potential}) \tag{1.2}$$

- the gravitational mass of a body m_g, and proportionality parameter between force F and acceleration a in Newton's second law

$$F = m_i a \ , \tag{1.3}$$

- the inertial mass of a body m_i, are the same characteristics of the given object

$$m_g = m_i \tag{1.4}$$

and, so

$$a = -\nabla \phi \ . \tag{1.5}$$

This leads to Einstein's famous thought experiment: observer in a enclosed elevator of sufficiently small size, has no way to distinguish whether the elevator is hanging in the field of gravitating body, or is accelerating in an empty space.

Now we arrive to the description of the motion of test particles, i.e. response of matter to the curvature of spacetime. Free particles move along the path of shortest possible distance, called geodesics. In other words, particles tend to move on straight lines, but in curved spacetime there might not be straight lines in a sense we know it from Euclidean geometry. Here comes the definition of parameterized path $x^\mu(\lambda)$, obeying geodesic equation

$$\frac{d^2 x^\mu}{d\lambda^2} + \Gamma^\mu_{\sigma\rho} \frac{dx^\sigma}{d\lambda} \frac{dx^\rho}{d\lambda} = 0 \quad (\Gamma^\mu_{\sigma\rho} \text{ is Christoffel symbol}) \ , \tag{1.6}$$

that serves as the shortest possible distance particle takes through spacetime. In Newtonian mechanics, acceleration of a particle is governed by external force (1.3), in particular case by gravitational force (1.5). In GR, gravity is not actually a "force"; curvature of spacetime is what particle feels like a gravitational force and the path of the particle is described by the geodesic equation (1.6). So, in the framework of GR, a ball being in a free fall is more truly "unaccelerated", then a ball lying on a table; the ball on the table is deflected away from the geodesic it would like to be on - that is why, it feels the curvature of spacetime as a gravitational force.

GR predicted the anomalous perihelion shift of Mercury, that gave a good point that it was a correct theory of gravity. However, more powerful proof in favor of GR came in 1919, when Eddington measured the deflection of starlight by Sun during a total solar eclipse of May 29. The experiment confirmed that Sun really does warp the spacetime and light from stars follow geodesics in that curved spacetime. Later on, GR was verified many times by observations like measuring gravitational redshift of light, light travel time delay by Shapiro, frame-dragging tests, gravitational lensing, cosmological expansion of the Universe and many more.

Soon after GR was published, Karl Schwarzschild found the first non-trivial exact solution to Einstein's equations. Spherically symmetric metric, known as Schwarzschild metric that solved

Einstein's equations predicted the existence of elusive object - black hole (BH) - singular point in a fabric of spacetime. Massive stars, in the final stage of their evolution collapse under their gravity and create objects so compact that even light is unable to escape it. BHs immediately became very attractive objects for physicists and they remains such for today.

Another consequence of GR was existence of gravitational waves (GW). As said before, presence of mass curves spacetime; moving mass generates changes in curvature and, in certain cases, this curvature can propagate in wave-like manner. This propagating phenomenon is known as gravitational wave, but it cannot be generated by constant or spherically symmetric motions. In order to produce GWs, changes in quadrupole moment of massive body is required. The most profound mechanism for generation of GWs is a binary star system - two massive objects orbiting each other. A supernova can also radiate GWs, suppose the explosion is not a perfectly symmetric process. Also, cosmic inflation at the early stage of the Universe may have created a gravitational wave background.

Gravitational waves carry energy and lose of energy of its source, served as the first indirect evidence for the existence of GWs. Hulse-Taylor binary - a pair of stars, one of which is a pulsar, was used to calculate how much energy should be radiated through GWs, describing binary trajectories in the framework of GR. Measuring the decrease in orbital period of this binary due to lose of energy, the existence of GWs was proved by indirect way.

However, more important discovery came in 2015, when Laser Interferometer Gravitational-Wave Observatory (LIGO), located in Hanford and Livingston (both in USA), directly detected GWs for the first time, emitted by a merger of binary black hole system (BBH). Unlike to Hulse-Taylor binary case, which used the binary properties to get the information about GWs, LIGO discovery used GWs to study the properties of its source. This opened completely new window for physicists and humanity acquired absolutely novel tool for observing and exploring the Universe. Several detection of GWs from BBH mergers by LIGO, was followed by the discovery of GWs from binary neutron star (BNS) merger by LIGO together with Virgo detector (located in Cascina, Italy). Such a huge discovery started a new era in multimesenger astronomy.

Many theories are capable of producing the BBH and BNS systems, that radiate GWs detectable by LIGO/Virgo. The most profound models are isolated binaries formed through common-envelope or, via chemically homogeneous evolution; also dynamical processes in dense stellar clusters. However, high number of binaries' merger rates obtained by LIGO observations, require some specific assumptions in all existing models. Moreover, several detection contained compact objects in the mass range that are disfavored in currently accepted theories of massive stars' evolution. So, the origin of many compact objects that are detected by LIGO remain speculative. Therefore, we may need to invent some new models, in order to explain LIGO signals.

All modern physics relies on Special Relativity. But there is a gap between General Relativity, that portrays gravitational force and incorporates SR, and quantum description of other three fundamental forces - electromagnetic, weak and strong nuclear interactions - unified in the Standard Model (SM) of particle physics that is a relativistic theory as well. SM is based on quantum field theory and all fundamental particles are presented as the oscillations in corresponding quantum fields. Particles with half-integer spin - fermions - are matter particles; gauge bosons with integer spin, are force carriers and the only scalar particle is Higgs boson. Quantum chromodynamics (QCD) with $SU(3)$ symmetry group, defines the strong interaction between quarks and gluons. While Electroweak theory unifies quantum electrodynamics (QED) and weak force with $SU(2) \times U(1)$ symmetry. And Higgs mechanism generates mass to all fundamental particles.

However, there is no well-defined quantum description of gravity. All quantum fields corresponding to the fundamental particles of SM, are constructed in spacetime. But, according to GR, gravity is not a real "force" but is a curvature of spacetime itself, it's hard to properly define corresponding quantum field. Hypothetical massless spin-2 boson called graviton is thought to be the quantum of gravity. However, due to an outstanding mathematical problem with renormalization in GR, still there is no complete quantum field theory of gravitons.

Besides the incompatibility of GR with quantum field theory, there are also cosmological observations that cannot be explained within the SM of particle physics. A widely accepted standard cosmological model called Lambda cold dark matter, shortly ΛCDM, is based on GR, and says, that the Universe started from a singular point as a result of the Big Bang and is continuously expanding after that. According to ΛCDM and cosmological observations, at about 68% of the total energy density of the Universe is constituted by dark energy (DE) associated with cosmological constant Λ. At about 27% comes on dark matter (DM) and our ordinary baryonic matter contributes only 5%. True nature of DE and DM is unclear. DE is identified with vacuum energy and is thought to be responsible for the expansion of the Universe. But there is a huge difference between the measured value of the vacuum energy and its theoretical prediction. DM is believed to be constituted by weakly interacting massive particles, but none of the observations is able to confirm any DM model yet. Therefore, SM of particle physics is truly incomplete, as it describes only ordinary matter and does not account for the rest 95% of the Universe.

That is why, there are many expansions to SM, including Supersymmetry, Grand unified theory, string theory and more. One possible expansion is a class of Left-Right symmetry models. SM is Lorentz invariant theory and the current terms are allowed to be assembled in a way to remain unchanged under Lorentz transformations. Terms satisfying such invariance must be type of either scalar, pseudoscalar, vector, axial vector or tensor. Weak interaction violates parity and SM is experimentally verified to be a chiral theory, where currents have 'vector minus axial vector' (V-A) type. This means, that only left-handed particles and right-handed antiparticles participate in weak interactions. It implies, that parity in not a symmetry of our Universe. However, one can introduce a mirror sector of particles, that have right-handed interactions and restore a parity conservation globally. But, mirror sector should somehow be invisible or have a very weak interaction with ordinary matter, as we do not see them in particle experiments.

Mirror matter or mirror world model states, that each SM particle has its mirror partner with opposite chirality. All particle physics in mirror sector is similar to that of SM, except, chiralities are opposite; right-handed particles are participating in mirror weak interaction and currents have (V+A) type. Mirror particles are invisible for ordinary observers and visa-versa. One can consider a theory with two identical gauge groups $G \times G'$ and with identical particle concept. So if G is symmetry group of ordinary world physics, e.g., $SU(3) \times SU(2) \times U(1)$ in Standard Model, the symmetry group $G' = SU(3)' \times SU(2)' \times U(1)'$ corresponds to the mirror world. Mirror particles are singlets of ordinary matter and vice versa, i.e., ordinary particles are mirror particle singlets.

But as gravity stays outside the theory of particle physics, it can be equivalently sensible for ordinary and mirror particles. So, the only possibility for the interaction between these two worlds can be gravity and maybe some other unknown weak forces. Alternatively, one can imagine the mirror world scenario as a five-dimensional theory, with parallel 3D-branes located in two fixed points; ordinary matter being localized on the left-brane and mirror matter localized on the right-brane, while gravity can freely pass between these two branes.

If mirror sector exists, it was also created by the Big Bang, along with the ordinary matter. However, mirror world should have a lower temperature, as Big Bang Nucleosynthesis puts the constraints on the cosmological abundance of ordinary and mirror particle. Therefore, cosmological evolution of these two worlds cannot be identical. The lower temperature of mirror world can imply that baryon asymmetry there is higher than in ordinary world. Certain baryo-leptogenesis mechanism can give a ~ 5 times higher baryon number density in mirror world compared to ordinary world. Recalling the difference between the energy density of DM and ordinary matter, mirror matter can stand as dark matter and completely explain it.

The lower initial temperature will affect cosmological evolution of mirror world. In fact, mirror sector is expected to be dominated by helium. Due to lower temperature, all cosmological processes happen earlier. Matter-radiation decoupling occurs at early times and star formation begins earlier as well. Besides, star are born with high initial masses and, therefore, evolve faster. As a result, in mirror world there should be higher abundance of neutron stars and black holes - the final products of the evolution of massive stars.

In the present thesis, we discuss the possibilities that the gravitational waves detected by LIGO/Virgo detectors, may have emerged from mirror world. As mentioned above, the binary compact objects' merger rate calculated relying on LIGO observations, is higher than it was predicted in majority of models. Mirror world with large abundance of compact objects, can be a good candidate to explain high merger rates. But what is more important, only 1 out of 90 GWs detected so far were accompanied by electromagnetic counterpart - gamma-ray bursts. That is strange, as such cataclysmic events is expected to generate other type of radiation as well. However, if merger of compact objects occur in mirror world, any type of radiation except gravitational will be invisible for us. Mirror photons and neutrinos will pass our detectors, while gravitational waves can be observable. Besides that, models of massive stars' evolution predict existence of mass gaps; supernova explosions cannot produce black holes with mass in certain intervals. However, LIGO data contains many objects within these forbidden regions, that is challenging to be explained by standard models. Mirror world model can assist in this matter as well.

In the upcoming chapters, we discuss in more details the theory of relativity (2), theoretical prospects of gravitational waves (3), their detection and existing data (4); then the standard model of particle physics and its expansion in mirror world model (5). Finally, we present our analyses on how LIGO events can be related to mirror world scenario (6), with summary and conclusion given in the chapter (7).

The thesis is based on the papers that have been published during the PhD studies: [1–5], regarding implication of gravitational-wave data in the context of mirror world. Although, two other studies that have been released as well during the PhD, but that are not directly connected with GW-physics, are mentioned. One of them concerns CKM matrix unitarity problem [6] and it can be related to mirror world physics. Another one [7] considers one of the hottest topics of modern cosmology - the Hubble tension problem, that is discussed in the context of recently suggested quasi-molecular mechanism of recombination that could affect the cosmic microwave background physics.

Chapter 2

Theory of Relativity

2.1 Special Theory of Relativity

In this chapter we briefly review the basic concepts of Einstein's special theory of relativity. Most of our discussion follows the book *Spacetime and Geometry: An Introduction to General Relativity* [8] by Sean Carroll. Unless otherwise indicated, we use the Natural Units $\hbar = c = 1$.

2.1.1 Galilean and Lorentz Transformations

In Newtonian mechanics we have one dimension for time and three dimensions for space, defined in Euclidean geometry. Time passes only in forward direction, while objects can move back and forth in spatial coordinates. All inertial frames share a universal time; i.e. when two events happen simultaneously in one reference frame, they happen simultaneously in any other reference frame. The relationship between the coordinates (t, x, y, z) and (t', x', y', z') of a single arbitrary event, as measured in two coordinate systems S and S', in uniform relative motion with velocity V in their common x and x' directions, with their spatial origins coinciding at time $t = t' = 0$, are given by Galilean transformation rules:

$$
\begin{aligned}
t' &= t \\
x' &= x - Vt \\
y' &= y \\
z' &= z
\end{aligned}
\tag{2.1}
$$

Distance between two objects in space is an invariant quantity

$$
\Delta l^2 = \Delta x^2 + \Delta y^2 + \Delta z^2 \ .
\tag{2.2}
$$

That means, if one measures the distance between the same points in the coordinate system, that is rotated or translated relative to original reference frame, will get the same result

$$
\Delta l^2 = \Delta x'^2 + \Delta y'^2 + \Delta z'^2 \ .
\tag{2.3}
$$

Rotations, for example in $x - y$ plane, are presented by a matrix

$$
\begin{pmatrix}
\sin(\theta) & \cos(\theta) & 0 \\
-\sin(\theta) & \cos(\theta) & 0 \\
0 & 0 & 1
\end{pmatrix} ,
\tag{2.4}
$$

while for translations we have expressions similar to (2.1), if instead of Vt one takes some constant.

In special relativity (SR) there is maximum speed that object can have relative to any inertial reference frame - the speed of light c. As a consequence, time is not absolute, but is relative, i.e. two simultaneous events in one coordinate system may not be simultaneous in other reference frame. So spatial distance between two points (2.2) is not invariant any more. Instead of Euclidean geometry, SR uses four-dimensional spacetime called Minkowski space, that has a signature $(-1, 1, 1, 1)$ and a new invariant, called spacetime interval between two events, is defined:

$$(\Delta s)^2 = -(c\Delta t)^2 + (\Delta x)^2 + (\Delta y)^2 + (\Delta z)^2 , \tag{2.5}$$

that is unchanged in any other reference frame

$$(\Delta s)^2 = -(c\Delta t')^2 + (\Delta x')^2 + (\Delta y')^2 + (\Delta z')^2 . \tag{2.6}$$

Spacetime interval (2.5) can be positive, negative, or zero even for two non-identical points. As there exists the maximum speed c, which in Natural units equal to 1, it is enlightening to consider paths $x = \pm t$. A set of points that are all connected to a single event by straight lines moving at the speed of light is the light cone. Light cones are naturally divided into future and past; the set of all points inside the future and past light cones of a given point are called timelike, those outside the light cones are spacelike and those on the cones are lightlike or null. Interval is negative for timelike, positive for spacelike, and zero for lighlike events (2.5). The motion of a particle is a curve through spacetime, called worldline. The path of massless particles, photons, follow the lightlike curves, while the wordline of massive particles is always timelike. Spacelike worldline requires travel with the speed $v > c$ and so is impossible.

Galilean transformation rules (2.1) are not valid in SR. Instead, Lorentz transformation rules are used, which are given by:

$$\begin{aligned}
t' &= \gamma(t - vx/c^2) \\
x' &= \gamma(x - vt) \\
y' &= y \\
z' &= z ,
\end{aligned} \tag{2.7}$$

where

$$\gamma = \frac{1}{\sqrt{1 - \frac{v^2}{c^2}}} . \tag{2.8}$$

Besides the rotations in spatial planes (2.4), SR describes rotations between space and time directions, i.e. in $x - t$, $y - t$, $z - t$ planes, called Lorentz boosts. For example, the boost in x-direction is given by:

$$\begin{pmatrix} \sinh(\phi) & \cosh(\phi) & 0 & 0 \\ -\sinh(\phi) & \cosh(\phi) & 0 & 0 \\ 0 & 0 & 1 & 0 \\ 0 & 0 & 0 & 1 \end{pmatrix} . \tag{2.9}$$

Unlike to the rotational angle θ that is defined with period 2π, the boost parameter ϕ is defined from $-\infty$ to $+\infty$. Three rotations and three boosts represent Lorentz group, which is nonabelian, as Lorentz transformations do not commute. Adding four translations gives a ten-parameter nonabelian group, called Poincare group.

7

At this point, we have to introduce some basic concepts. SR uses 4-vector formalism and spacetime coordinates are denoted by Greek superscripts that runs from 0 to 4, with 0 referring to time and 1-3 to spatial coordinates:

$$x^\mu : \quad \begin{array}{l} x^0 = ct \\ x^1 = x \\ x^2 = y \\ x^3 = z \ . \end{array} \tag{2.10}$$

Sometimes we will need to refer only to spatial coordinates and in that case Latin superscripts, that runs from 1 to 3 are used:

$$x^i : \quad \begin{array}{l} x^1 = x \\ x^2 = y \\ x^3 = z \ . \end{array} \tag{2.11}$$

A 4-dimensional version of Kronecker delta symbol is represented as

$$\delta^{\mu'}_\mu = \begin{cases} 1 & \text{when } \mu' = \mu, \\ 0 & \text{when } \mu' \neq \mu, \end{cases} \tag{2.12}$$

and we introduce 4×4 matrix, called metric, written by two lower indices:

$$\eta_{\mu\nu} = \begin{pmatrix} -1 & 0 & 0 & 0 \\ 0 & 1 & 0 & 0 \\ 0 & 0 & 1 & 0 \\ 0 & 0 & 0 & 1 \end{pmatrix} \tag{2.13}$$

Then spacetime interval (2.5) can be rewritten in more compact way

$$(\Delta s)^2 = \eta_{\mu\nu} \Delta x^\mu \Delta x^\nu \ . \tag{2.14}$$

This formula introduces Einstein's summation convention, in which indices appearing both as superscripts and subscripts are summed over all possible values.

Lorentz transformations can be represented by six-set of matrices $\Lambda^{\mu'}_\mu$, one of which is given by (2.9). Then, coordinate transformations are

$$x^{\mu'} = \Lambda^{\mu'}_\nu x^\nu \ , \tag{2.15}$$

or in shortened matrix notations $x' = \Lambda x$. Coming from the invariance of the interval

$$(\Delta s)^2 = (\Delta x)^T \eta (\Delta x) = (\Delta x')^T \eta (\Delta x') = (\Delta x)^T \Lambda^T \eta \Lambda (\Delta x) \ , \tag{2.16}$$

Lorentz transformations are the kind of transformations, that satisfy

$$\eta = \Lambda^T \eta' \Lambda \ , \tag{2.17}$$

or

$$\eta_{\rho\sigma} = \Lambda^{\mu'}_\rho \Lambda^{\nu'}_\sigma \eta_{\mu'\nu'} \ . \tag{2.18}$$

2.1.2 Vectors and Tensors

To describe spacetime, we need basis $\hat{e}_{(\mu)}$, that can be defined in a way, that basis vector $\hat{e}_{(1)}$ is what we would normally think of pointing along the x-axis. Then comes the definition of contravariant or tangent vector

$$A = A^\mu \hat{e}_{(\mu)} \ . \tag{2.19}$$

The coefficients A^μ are components of the vector A. Upon change of the basis, components contra-vary (here comes the name) to compensate that change and leave entire vector unchanged. In other words, the matrix that transforms the vector components is the inverse of the matrix that transforms the basis vectors.

A parameterized curve or path through spacetime is specified by the coordinates as a function of the parameter $x^\mu(\lambda)$. The tangent vector $V(\lambda)$ of the type (2.19) has components

$$V^\mu = \frac{dx^\mu}{d\lambda} \ . \tag{2.20}$$

The entire vector is

$$V = V^\mu \hat{e}_{(\mu)} = \frac{dx^\mu}{d\lambda} \hat{e}_{(\mu)} \ . \tag{2.21}$$

Taking into account (2.15), we derive transformation rules for components of vector

$$V^\mu \to V^{\mu'} = \Lambda^{\mu'}_{\ \nu} V^\nu \ . \tag{2.22}$$

However, vector V is itself invariant under Lorentz transformations, so we can write

$$V = V^\mu \hat{e}_{(\mu)} = V^{\nu'} \hat{e}_{(\nu')} = \Lambda^{\nu'}_{\ \mu} V^\mu \hat{e}_{(\nu')} \ , \tag{2.23}$$

which implies

$$\hat{e}_{(\mu)} = \Lambda^{\nu'}_{\ \mu} \hat{e}_{(\nu')} \ . \tag{2.24}$$

Using the relation

$$\Lambda^\mu_{\ \rho} \Lambda^\rho_{\ \nu} = \delta^\mu_\nu \tag{2.25}$$

will give us transformations rules for the basis vector

$$\hat{e}_{(\nu')} = \Lambda^\mu_{\ \nu'} \hat{e}_{(\mu)} \ . \tag{2.26}$$

As a result, the set of basis vectors, that are labeled with lower indices, transform via the inverse Lorentz transformation of the coordinates or vector components, that were labeled with upper indices. Combination of two objects, one with upper and one with lower indices, gives Lorentz invariant quantity, called contravariant vector, or sometimes referred as just vector.

However, there are also different class of vectors with lower indices, called covariant, cotangent or dual vectors, that, in combination with contravariant vectors give a scalar. Basis vectors of covariant vectors should satisfy:

$$\hat{\theta}^{(\nu)} \left(\hat{e}_{(\mu)} \right) = \delta^\nu_\mu \ . \tag{2.27}$$

Every covariant vector can be written in terms of components, which are labeled with lower indices:

$$\omega = \omega_\mu \hat{\theta}^{(\mu)} \ . \tag{2.28}$$

Action of covariant vector on contravariant vector gives:

$$\omega(V) = \omega_\mu \hat{\theta}^{(\mu)} \left(V^\nu \hat{e}_{(\nu)} \right) = \omega_\mu V^\nu \hat{\theta}^{(\mu)} \left(\hat{e}_{(\nu)} \right) = \omega_\mu V^\nu \delta^\mu_\nu = \omega_\mu V^\mu \in \mathbf{R} \ . \tag{2.29}$$

The transformation properties for the components and for the basis of contravariant vector are derived in the same manner, and have a form:

$$\omega_{\mu'} = \Lambda^{\nu}{}_{\mu'}\omega_{\nu} \tag{2.30}$$

$$\theta^{(\rho')} = \Lambda^{\rho'}{}_{\sigma}\theta^{(\sigma)} . \tag{2.31}$$

$$\tag{2.32}$$

The components of a dual vector transform under the inverse transformation of those of a vector. Example of dual vector is a gradient of a scalar function, the set of partial derivatives with respect to the spacetime coordinates, denoted by a lowercase d:

$$d\phi = \frac{\partial\phi}{\partial x^{\mu}}\theta^{(\mu)} \tag{2.33}$$

Using a chain rule and equation (2.15), transformation rules for the components of this dual vectors are:

$$\frac{\partial\phi}{\partial x^{\mu'}} = \frac{\partial x^{\mu}}{\partial x^{\mu'}}\frac{\partial\phi}{\partial x^{\mu}} = \Lambda^{\mu}{}_{\mu'}\frac{\partial\phi}{\partial x^{\mu}} . \tag{2.34}$$

The fact that the gradient is a dual vector leads to the useful shorthand notations for partial derivatives:

$$\frac{\partial\phi}{\partial x^{\mu}} = \partial_{\mu}\phi . \tag{2.35}$$

A straightforward generalization of vectors and dual vectors is the notion of a tensor. Just as action of dual vector on vectors gives scalar, a tensor T of rank (k, l) is a map from a collection of dual vectors and vectors to **R**:

$$T : \ T^*_P \underbrace{\times \cdots \times}_{\text{(k times)}} T^*_P \times T_P \underbrace{\times \cdots \times}_{\text{(l times)}} T_P \to \mathbf{R} . \tag{2.36}$$

Here, " $*$ " denotes dual and " $\times$ " denotes Cartesian product, so for example, $T_P \times T_P$ is a space of ordered pairs of vectors. A normal vector is a type $(1, 0)$ tensor, a dual vector is a type $(0, 1)$ tensor and a scalar is a type $(0, 0)$ tensor. Basis for (k, l) tensor can be constructed by taking tensor product $\otimes$ of basis vectors and dual vectors:

$$\hat{e}_{(\mu_1)} \otimes \cdots \otimes \hat{e}_{(\mu_k)} \otimes \hat{\theta}^{(\nu_1)} \otimes \cdots \otimes \hat{\theta}^{(\nu_l)} . \tag{2.37}$$

In 4-dimensional spacetime we will have 4^{k+l} basis tensors. In a component notation arbitrary tensor will be written as:

$$T = T^{\mu_1\cdots\mu_k}{}_{\nu_1\cdots\nu_l}\hat{e}_{(\mu_1)} \otimes \cdots \otimes \hat{e}_{(\mu_k)} \otimes \hat{\theta}^{(\nu_1)} \otimes \cdots \otimes \hat{\theta}^{(\nu_l)} . \tag{2.38}$$

So, a (k, l) tensor has k upper and l lower indices and the order of indices is important. The transformation of tensor components under Lorentz transformations can be derived by applying the transformation rules of basis vectors and dual vectors and has a form:

$$T^{\mu'_1\cdots\mu'_k}{}_{\nu'_1\cdots\nu'_l} = \Lambda^{\mu'_1}{}_{\mu_1}\cdots\Lambda^{\mu'_k}{}_{\mu_k}\Lambda^{\nu'_1}{}_{\nu_1}\cdots\Lambda^{\nu'_l}{}_{\nu_l}T^{\mu_1\cdots\mu_k}{}_{\nu_1\cdots\nu_l} . \tag{2.39}$$

Thus, each upper index gets transformed like a vector, and each lower index gets transformed like a dual vector.

Example of $(1,1)$ tensor is the Kronecker delta symbol (2.12). The metric tensor (2.13) is $(0,2)$ tensor. Using these two objects, one can define $(2,0)$ tensor with two upper indices $\eta^{\mu\nu}$, called the inverse metric:

$$\eta^{\mu\nu}\eta_{\nu\rho} = \eta_{\rho\nu}\eta^{\nu\mu} = \delta^\mu_\rho \ . \tag{2.40}$$

The action of the metric on two vectors is called the inner product (also scalar or dot product):

$$\eta(V,W) = \eta_{\mu\nu}V^\mu W^\nu = V \cdot W \ . \tag{2.41}$$

The norm of a vector is defined to be the inner product of a vector with itself, and this number is not positive definite, as it was in Euclidean space. In fact, spacetime interval (2.14) is such object, and as we already said, it can be spacelike $(\Delta s)^2 < 0$, timelike $(\Delta s)^2 > 0$, or lightlike $(\Delta s)^2 = 0$.

Now we have to discuss some properties of tensors. The metric and inverse metric can be used to raise and lower indices on tensors:

$$T^{\alpha\beta\mu}{}_\delta \ = \ \eta^{\mu\gamma}T^{\alpha\beta}{}_{\gamma\delta} \tag{2.42}$$

$$T_\mu{}^\beta{}_{\gamma\delta} \ = \ \eta_{\mu\alpha}T^{\alpha\beta}{}_{\gamma\delta} \ . \tag{2.43}$$

Summing over one upper and one lower index is called contraction, and it turns (k,l) tensor into $(k-1, l-1)$ tensor:

$$S^{\alpha\beta}{}_\gamma = T^{\alpha\beta\nu}{}_{\gamma\nu} \ . \tag{2.44}$$

Trace is a scalar and for $(1,1)$ tensor it is a sum of a diagonal elements of the matrix and often denoted without index: $X = X^\mu{}_\mu$. For $(0,2)$ tensor, one should at first rise one index and then sum. For example, for metric tensor we have:

$$\eta^{\mu\nu}\eta_{\mu\nu} = \delta^\mu_\mu = 4 \ . \tag{2.45}$$

In flat spacetime with inertial coordinates, the partial derivative of (k,l) tensor is a $(k, l+1)$ tensor:

$$T_\alpha{}^\mu{}_\nu = \partial_\alpha R^\mu{}_\nu \tag{2.46}$$

and transforms properly under Lorentz transformations. The important thing is that, partial derivatives commute:

$$\partial_\mu\partial_\nu(\cdots) = \partial_\nu\partial_\mu(\cdots) \ . \tag{2.47}$$

Tensor is said to be symmetric in any of its indices if it is unchanged under exchange of those indices:

$$S_{\mu\nu\sigma} = S_{\nu\mu\sigma} \ . \tag{2.48}$$

Tensor is antisymmetric in any of its indices if it changes sign under exchange of those indices:

$$A_{\mu\nu\sigma} = -A_{\nu\mu\sigma} \ . \tag{2.49}$$

2.1.3 Energy and Momentum

For infinitesimal coordinate displacement dx^μ, we introduce infinitesimal interval, or line element:

$$ds^2 = \eta_{\mu\nu}dx^\mu dx^\nu \ . \tag{2.50}$$

Considering a path through spacetime as a parameterized curve, $x^\mu(\lambda)$, for timelike paths we define proper time:

$$d\tau = \int \sqrt{-\eta_{\mu\nu} \frac{dx^\mu}{d\lambda} \frac{dx^\nu}{d\lambda}} d\lambda , \tag{2.51}$$

which will be positive. Tangent vector along the path is known as four-velocity, U^μ:

$$U^\mu = \frac{dx^\mu}{d\tau} , \tag{2.52}$$

and since $d\tau^2 = -\eta_{\mu\nu} dx^\mu dx^\nu$, the four-velocity is automatically normalized:

$$\eta_{\mu\nu} U^\mu U^\nu = -1 . \tag{2.53}$$

In the rest frame of a particle $U^\mu = (1,0,0,0)$. Momentum four-vector is defined as

$$p^\mu = mU^\mu , \tag{2.54}$$

where m is a mass of a particle, often referred as the rest mass. Energy is a 0th component of four-momentum, $E = p^0$, and is not invariant under Lorentz transformations. In the rest frame $p^0 = m$ and recalling that we had set $c = 1$, we recover famous $E = mc^2$. For a particle moving with three-velocity $v = dx/dt$ along the x axis, we can perform Lorentz transformations and get:

$$p^\mu = (\gamma m, v\gamma m, 0, 0) , \tag{2.55}$$

where $\gamma = 1/\sqrt{1 - v^2}$. For small v, $p^0 = m + \frac{1}{2}mv^2$ and $p^1 = mv$. In general,

$$p_\mu p^\mu = -m^2, \tag{2.56}$$

is invariant scalar quantity and energy

$$E = \sqrt{m^2 + \mathbf{p}^2} , \tag{2.57}$$

where $\mathbf{p}^2 = \delta_{ij} p^i p^j$ is usual 3-momentum.

When speaking about systems comprised of huge numbers of particles, we describe system as a fluid - a continuum characterized by macroscopic quantities such as density, pressure, entropy, viscosity, and so on. Four-momentum is insufficient to describe the energy and momentum of a fluid, so one defines the $(2,0)$ tensor, called energy-momentum tensor, $T^{\mu\nu}$. Thinking of a rest-frame fluid, it's T^{00} component is simply energy density ρ. Similarly, in this frame, $T^{0i} = T^{i0}$ is the momentum density. The spatial components T^{ij} are the momentum flux; they represent the forces between neighboring infinitesimal elements of the fluid. Off-diagonal terms in T^{ij} represent shearing terms, such as those due to viscosity. And the diagonal terms give the pressure components $p_i = T^{ii}$ in x, y and z directions (no summation is carried here).

Dust is defined as a collection of particles at rest with respect to each other. If n is a number density of particles in their rest frame, one can construct the number-flux four-vector

$$N^\mu = nU^\mu . \tag{2.58}$$

N^0 will be the number density of particles as measured in any other frame, and N^i will be the flux of particles in the x^i direction. If one considers that each of the particles has the same mass m, then in the rest frame, the energy density of the dust is given by

$$\rho = mn . \tag{2.59}$$

12

Then, energy-momentum tensor for the dust is defined as

$$T_{\text{dust}}^{\mu\nu} = p^\mu N^\nu = mnU^\mu U\nu = \rho U^\mu U^\nu \ . \tag{2.60}$$

A slight generalization of the dust is a perfect fluid. It is described by two parameters: rest-frame energy density ρ and an isotropic rest-frame pressure p. General form of energy-momentum tensor for a perfect fluid is given by

$$T^{\mu\nu} = (\rho + p)U^\mu U^\nu + p\eta^{\mu\nu} \ , \tag{2.61}$$

which, in a rest frame equals to

$$T^{\mu\nu} = \begin{pmatrix} \rho & 0 & 0 & 0 \\ 0 & p & 0 & 0 \\ 0 & 0 & p & 0 \\ 0 & 0 & 0 & p \end{pmatrix} \ . \tag{2.62}$$

The concept of perfect fluid is quite general and to describe an evolution of such fluid one needs to specify the equation of state, i.e. relation between pressure and energy density $p = p(\rho)$. There are three special cases that are discussed in cosmology. As we already said, for dust $p = 0$. Isotropic gas of photons is given by $p = \frac{1}{3}\rho$. And for vacuum energy, $p_{\text{vac}} = -\rho_{\text{vac}}$, and energy-momentum tensor is proportional to the metric $T_{\text{vac}}^{\mu\nu} = -\rho_{\text{vac}}\eta^{\mu\nu}$.

The very important property of energy-momentum tensor is that, it is being conserved. In this context, conservation is expressed as the vanishing of the "divergence":

$$\partial_\mu T^{\mu\nu} = 0 \ . \tag{2.63}$$

However, in general relativity, when one considers the spacetime that may not be flat, the equations given above get slightly modified.

2.2 General Theory of Relativity

Keeping in mind the basic concepts of special relativity described in the previous chapter, now we make a brief review of Einstein's general theory of relativity (GR). Again, our discussion follows Sean Carroll's book *Spacetime and Geometry: An Introduction to General Relativity* [8] and the reviews of the Particle Data Group [9].

2.2.1 Metric, Covariant Derivative and Parallel Transport

The metric tensor $\eta_{\mu\nu}$ introduced in the previous chapter describes the Minkowski metric, i.e. flat spacetime. For curved spacetime metric tensor is denoted by $g_{\mu\nu}$ and it is not constant. It is a symmetric $(0,2)$ tensor, with so called pseudo-Riemannian signature $(-1, 1, 1, 1)$, and is usually considered to be nondegenerate, meaning that its determinant $g = |g_{\mu\nu}| \neq 0$. Then inverse metric $g^{\mu\nu}$ is defined as:

$$g^{\mu\nu}g_{\nu\alpha} = g_{\lambda\sigma}g^{\lambda\mu} = \delta^\mu_\sigma \ . \tag{2.64}$$

And the interval for curved spacetime is given by:

$$ds^2 = g_{\mu\nu}dx^\mu dx^\nu \ . \tag{2.65}$$

A generalization of a partial derivative in a curved spacetime is a covariant derivative. It is denoted by ∇ and its action on a contravariant vector is given as:

$$\nabla_\mu V^\nu = \partial_\mu V^\nu + \Gamma^\nu_{\mu\lambda} V^\lambda \ . \tag{2.66}$$

$\Gamma^\nu_{\mu\lambda}$ is a connection coefficient, called a Christoffel symbol and it accounts for the curvature effects. Introducing a condition of metric-compatibility, $\nabla_\sigma g^{\mu\nu} = 0$, and assuming that the connection is symmetric in its lower indices, $\Gamma^\sigma_{\mu\nu} = \Gamma^\sigma_{\nu\mu}$, i.e. it is torsion-free, the Christoffel symbol can be written using the metric tensor:

$$\Gamma^\sigma_{\mu\nu} = \frac{1}{2} g^{\sigma\lambda} \left(\partial_\mu g_{\nu\lambda} + \partial_\nu g_{\lambda\mu} - \partial_\lambda g_{\mu\nu} \right) \ . \tag{2.67}$$

Covariant derivative of a dual vector has the form:

$$\nabla_\mu \omega_\nu = \partial_\mu \omega_\nu - \Gamma^\nu_{\mu\lambda} \omega_\lambda \ . \tag{2.68}$$

The concept of moving a vector along a path, keeping constant all the while, is known as parallel transport. In flat spacetime, given a curve $x^\mu(\lambda)$, it means that the components of the vector stay constant along this path:

$$\frac{d}{d\lambda} V^\mu = \frac{dx^\nu}{d\lambda} \frac{\partial}{\partial x^\nu} V^\mu = 0 \ . \tag{2.69}$$

In curved spacetime, one can generalize this approach by replacing the partial derivative with covariant derivative, defining a directional covariant derivative as:

$$\frac{D}{d\lambda} = \frac{dx^\mu}{d\lambda} \nabla_\mu \ . \tag{2.70}$$

So, equation for the parallel transport of a vector in curved spacetime will have a form:

$$\frac{d}{d\lambda} V^\mu + \Gamma^\mu_{\nu\sigma} \frac{dx^\nu}{d\lambda} V^\sigma = 0 \ . \tag{2.71}$$

In Euclidean space, a straight line is a path that parallel transports its own tangent vector. The curved-space generalization of the straight line is a geodesic. The tangent vector to a path $x^m(\lambda)$ is $dx^\mu/d\lambda$ and the condition that it is parallel transported is given as

$$\frac{D}{d\lambda} \frac{dx^\mu}{d\lambda} = 0 \ , \tag{2.72}$$

or alternatively

$$\frac{dx^\mu}{d\lambda^2} + \Gamma^\mu_{\nu\sigma} \frac{dx^\nu}{d\lambda} \frac{dx^\sigma}{d\lambda} = 0 \ . \tag{2.73}$$

The equation (2.73) is called the geodesic equation.

2.2.2 Curvature Tensors

The Riemann tensor is a measure of a curvature of spacetime. It is a function of the metric tensor and is defined as:

$$R^\mu{}_{\alpha\nu\beta} = \partial_\nu \Gamma^\mu_{\alpha\beta} - \partial_\beta \Gamma^\mu_{\alpha\nu} + \Gamma^\sigma_{\alpha\beta} \Gamma^\mu_{\sigma\nu} - \Gamma^\sigma_{\alpha\nu} \Gamma^\mu_{\sigma\beta} \ . \tag{2.74}$$

If there exist a coordinate system, in which the components of the metric tensor are constant, the Riemann tensor vanishes and this means, that spacetime is flat. The Riemann tensor has some important properties. It is antisymmetric in its first two indices

$$R_{\mu\nu\alpha\beta} = -R_{\nu\mu\alpha\beta} \; , \tag{2.75}$$

in its last two indices

$$R_{\mu\nu\alpha\beta} = -R_{\mu\nu\beta\alpha} \; , \tag{2.76}$$

and symmetric under exchange of pair of indices

$$R_{\mu\nu\alpha\beta} = R_{\alpha\beta\mu\nu} \; . \tag{2.77}$$

Besides, sum of cyclic permutations of the last three indices vanishes:

$$R_{\mu\nu\alpha\beta} + R_{\mu\alpha\beta\nu} + R_{\mu\beta\nu\alpha} = 0 \; . \tag{2.78}$$

Also, taking the covariant derivative of the Riemann tensor and writing a sum of cyclic permutations of the first three indices equals to zero:

$$\nabla_\sigma R_{\mu\nu\alpha\beta} + \nabla_\mu R_{\nu\sigma\alpha\beta} + \nabla_\nu R_{\sigma\mu\alpha\beta} = 0 \; . \tag{2.79}$$

It is known as Bianchi identity. The contraction of the Riemann tensor is called the Ricci tensor:

$$R_{\mu\nu} = R^\sigma{}_{\mu\sigma\nu} \; , \tag{2.80}$$

and it is symmetric $R_{\mu\nu} = R_{\nu\mu}$. The contraction (or the trace) of the Ricci tensor is called the Ricci scalar:

$$R = R^\mu{}_\mu = g^{\mu\nu} R_{\mu\nu} \; . \tag{2.81}$$

Contracting twice on the Bianchi identity (2.79), one gets:

$$\nabla_\sigma R = 2\nabla^\mu R_{\mu\alpha} \; . \tag{2.82}$$

Defining the Einstein tensor as

$$G_{\mu\nu} = R_{\mu\nu} - \frac{1}{2} R g_{\mu\nu} \; , \tag{2.83}$$

the twice-contracted Bianchi identity is equivalent to

$$\nabla^\mu G_{\mu\nu} = 0 \; . \tag{2.84}$$

2.2.3 Einstein's Equations

Einstein figured out that matter and energy warp spacetime and the curvature of spacetime is what we observe as gravitational force. He found a formulation for the equations that correctly describes the relation between matter and curvature and recovers the Newtonian gravity in the static weak field limit. He explicitly wrote the equality between the curvature $G_{\mu\nu}$ and the energy-momentum tensor $T_{\mu\nu}$, with appropriate coefficient

$$G_{\mu\nu} = 8\pi G T_{\mu\nu} \; , \tag{2.85}$$

where G is Newtons constant of gravity. But in more formal way, Einstein equations are derived through the principle of least action. The total action for gravitation is defined as:

$$S = S_H + S_{\text{Matter}}, \tag{2.86}$$

where first term is Hilbert or Einstein-Hilbert action

$$S_H = \frac{1}{16\pi G} \int d^4x \ \sqrt{-g} \ R \ , \tag{2.87}$$

and the second term S_{Matter} is the action for matter field. In (2.87) R is the Ricci scalar (2.81) and $d^4x\sqrt{-g}$ is a volume element, where g is a determinant of metric tensor and $\sqrt{-g}$ was introduced to take care for correct transformation properties. Varying (2.87) with respect to metric, we get:

$$\delta S_H = \frac{1}{16\pi G} \int d^4x \ \delta(\sqrt{-g} \ R) \ . \tag{2.88}$$

Remembering (2.81), the following three terms have to be examined:

$$\delta S_H = \frac{1}{16\pi G} \int d^4x \left(R\delta\sqrt{-g} + \sqrt{-g}R_{\mu\nu}\delta g^{\mu\nu} + \sqrt{-g}g^{\mu\nu}\delta R_{\mu\nu} \right) \ . \tag{2.89}$$

We skip the detailed calculation which are given in the appendix, and give the final results. It turns up, that the first term in (2.89) is simplified as

$$R \ \delta\sqrt{-g} = \frac{1}{2}R\sqrt{-g} \ g^{\mu\nu}\delta g_{\mu\nu} \ , \tag{2.90}$$

and the last term is just a boundary term and so goes to zero if variation vanishes at infinity. So we are left with:

$$\delta S_H = -\frac{1}{16\pi G} \int d^4x\sqrt{-g} \left(R^{\mu\nu} - \frac{1}{2}R \ g^{\mu\nu} \right) \delta g_{\mu\nu} \ . \tag{2.91}$$

Equating to zero the variation of Hilbert action with respect to metric

$$\frac{1}{\sqrt{-g}}\frac{\delta S_H}{\delta g_{\mu\nu}} = -\frac{1}{16\pi G} \left(R^{\mu\nu} - \frac{1}{2}R \ g^{\mu\nu} \right) = 0 \tag{2.92}$$

yields Einstein's equations in vacuum

$$R^{\mu\nu} - \frac{1}{2}R \ g^{\mu\nu} = 0 \ . \tag{2.93}$$

Now, boldly defining the energy-momentum tensor as

$$T_{\mu\nu} \equiv -2\frac{1}{\sqrt{-g}}\frac{\delta S_{\text{Matter}}}{\delta g_{\mu\nu}} \ , \tag{2.94}$$

and equating to zero the variation of the total action (2.86) gives the Einstein equations in its canonical form

$$R_{\mu\nu} - \frac{1}{2}R \ g_{\mu\nu} = 8\pi G \ T_{\mu\nu} \ . \tag{2.95}$$

To account for the expansion of the universe, we can also add a cosmological constant term Λ in the total action:

$$S = \frac{1}{16\pi G} \int d^4x \ \sqrt{-g} \ (R - 2\Lambda) + S_{\text{Matter}} \ . \tag{2.96}$$

This will yield Einstein equations in complete form:

$$R_{\mu\nu} - \frac{1}{2}R \ g_{\mu\nu} + \Lambda g_{\mu\nu} = 8\pi G \ T_{\mu\nu} \ . \tag{2.97}$$

2.2.4 Schwarzschild Solution and Kerr's Black Hole

The most profound solution to Einstein equations, after the flat Minkowski spacetime, is a spherically symmetric static vacuum solution - the Schwarzschild metric. In spherical coordinates (t, r, θ, ϕ) the metric is given by

$$ds^2 = -\left(1 - \frac{r_s}{r}\right) dt^2 + \left(1 - \frac{r_s}{r}\right)^{-1} dr^2 + r^2 d\Omega^2 \ , \tag{2.98}$$

where $d\Omega^2$ is the metric on a unit two-sphere

$$d\Omega^2 = d\theta^2 + \sin^2 \theta d\phi^2 \ , \tag{2.99}$$

and r_s is called Schwarzschild radius. The Schwarzschild metric (2.98) is a solution to the Einstein equations in vacuum

$$R_{\mu\nu} = 0, \tag{2.100}$$

describing the spacetime outside a static spherically symmetric gravitating body of mass M. The Schwarzschild radius is proportional to the mass of a gravitating body $r_s = 2GM$. As $M \to 0$ we recover the flat Minkowski spacetime. Also, as $r \to \infty$, the spacetime progressively becomes flat, that is known as asymptotic flatness.

The metric (2.98) has two singularities, at $r = 0$ and $r = 2GM$. The $r = 0$ point is a real singularity, where curvature goes to infinity. But it turns up, that the Schwarzschild radius $r = r_s$ is just a coordinate singularity and with an appropriate change of coordinates the metric at this point can become regular. However, r_s is still an interesting point.

The metric (2.98) describes the spacetime outside a spherical massive object, like star or planet and each of them has its own Schwarzschild radius, which is less then the radius of the object. But the metric also predicts the existence of compact objects called black holes (BH), that have Schwarzschild radius outside; or in other words r_s is its boundary. In their final stage of evolution, massive stars can collapse under their own curvature (i.e. due to their own gravitational force) and create a singularity, elusive object named BH. The center of this object is a true gravitational singularity and its Schwarzschild radius is called an event horizon. The event horizon is a point of no return; once passing this line no particle or even light can escape it. The existence of such objects had no doubt for physicists for decades, however, the recent image of central BH of M87 galaxy finally confirmed their reality.

But the Schwarzschild BH is an idolized case and such objects do not exist in nature. Real BH is parametrized by three quantities: mass, electric charge and angular momentum. Charged Reissner-Nordström BHs quickly get neutralized so in reality BHs have only a tiny charge. But, considering a complex mechanism of BH creation from a rotating star, all BHs do rotate, so they have an angular momentum. Rotating BH is described by a Kerr metric:

$$
\begin{aligned}
ds^2 = \ & - \left(1 - \frac{2GMr}{\bar{r}^2}\right) dt^2 - \frac{2GMAr \sin^2 \theta}{\bar{r}^2} (dt \ d\phi + d\phi \ dt) \\
& + \frac{\bar{r}^2}{\Delta} dr^2 + \bar{r}^2 d\theta^2 + \frac{\sin^2 \theta}{\bar{r}^2} \left[(r^2 + A^2)^2 - A^2 \Delta \sin^2 \theta\right] d\phi^2,
\end{aligned}
\tag{2.101}
$$

where A is an angular momentum per unit mass,

$$\Delta(r) = r^2 - 2GMr + A^2 \tag{2.102}$$

17

and

$$\bar{r}^2(r, \theta) = r^2 + a^2 \cos^2 \theta. \tag{2.103}$$

So, the Kerr metric describes the geometry of empty spacetime around a rotating uncharged axially-symmetric black hole with a quasispherical event horizon.

2.2.5 Friedmann-Robertson-Walker Universe

On the large enough scales, the Universe in isotropic and homogeneous. Isotropy states that the space looks the same no matter in what direction you look and homogeneity means that the metric is the same in every part of the space. These assumptions together are known as the Cosmological Principle, implying that a space is maximally symmetric and stating that all spatial positions in the Universe are essentially equivalent. Accounting also that the Universe is evolving in time, it is described using the Robertson-Walker metric:

$$ds^2 = dt^2 - a^2(t) \left[\frac{dr^2}{1 - kr^2} + r^2 \left(d\theta^2 + \sin^2 \theta d\phi^2 \right) \right], \tag{2.104}$$

where a(t) is a dimensionless scale factor $(a(t) = R(t)/R(t_0)$, where $R(t)$ is a scale factor at a moment t and $R(t_0)$ is a present epoch scale factor), and k is a curvature constant that takes discrete values $+1$, -1, 0, corresponding to closed, open, or spatially flat geometries. Considering the matter content of the Universe as a perfect fluid, similar to (ref(.61)), energy-momentum tensor has a form

$$T_{\mu\nu} = -pg_{\mu\nu} + (p + \rho)U_\mu U_\nu, \tag{2.105}$$

where now $g_{\mu\nu}$ is spacetime described by Robertson-Walker metric (2.104). With the perfect fluid source, Einstein's equations lead to the Friedmann equations

$$H^2 \equiv \left(\frac{\dot{a}}{a} \right) = \frac{8\pi G \rho}{3} - \frac{k}{a^2} + \frac{\Lambda}{3} \tag{2.106}$$

and

$$\frac{\ddot{a}}{a} = \frac{\Lambda}{3} - \frac{4\pi G}{3} \left(\rho + 3p \right), \tag{2.107}$$

where H is a Hubble parameter. These two equations give a third useful equation:

$$\dot{\rho} = -3H(\rho + p). \tag{2.108}$$

The Friedmann equation (2.106) can be used to define a critical density such that $k = 0$ when $\Lambda = 0$,

$$\rho_{\rm c} \equiv \frac{3H^2}{8\pi G}. \tag{2.109}$$

Then the cosmological density parameter $\Omega_{\rm tot}$ is defined as the energy density relative to the critical density

$$\Omega_{\rm tot} = \frac{\rho}{\rho_{\rm c}} \tag{2.110}$$

and the Friedmann equation (2.106) can be rewritten as

$$\Omega_{\rm tot} - 1 = \frac{k}{H^2 a^2}. \tag{2.111}$$

One can see that when $\Omega_{\text{tot}} > 1$, $k = +1$ and the Universe is closed, when $\Omega_{\text{tot}} < 1$, $k = -1$ and the Universe is open, and when $\Omega_{\text{tot}} = 1$, $k = 0$, and the Universe is spatially flat.

It is often necessary to distinguish different contributions to the density parameter. Therefore, it is convenient to define present-day density parameters for pressureless matter Ω_{m} that consists of baryonic matter Ω_{b} and dark matter Ω_{DM}, relativistic particles Ω_{r} – photons and neutrinos, and the contribution from vacuum energy $\Omega_{\Lambda} = \Lambda/3H^2$. The Friedmann equation (2.111) then becomes

$$\Omega_{\text{m}} + \Omega_{\text{r}} + \Omega_{\Lambda} - 1 = \frac{k}{H_0^2 a_0^2}, \tag{2.112}$$

where the subscript 0 indicates present-day values. Thus, it is the sum of the densities in matter, relativistic particles, and vacuum that determines the overall sign of the curvature.

2.2.6   ΛCDM Model

The ΛCDM (Lambda cold dark matter) model is a parameterization of the Big Bang cosmological model in which the universe contains three major components: a cosmological constant Λ associated with dark energy, cold dark matter and ordinary matter. It is frequently referred to as the standard model of Big Bang cosmology as it provides a reasonably good account of the main properties of the Universe: the existence and structure of the cosmic microwave background (CMB); the large-scale structure (LSS) in the distribution of galaxies; the observed abundances of hydrogen, helium, and lithium; the accelerating expansion of the universe observed in the light from distant galaxies and supernovae.

The expansion rate of the Universe is given by the Friedmann equation (2.106) and accounting that the densities of various species scale as different powers of a, it can be conveniently rewritten in terms of the various density parameters as

$$H(a) = H_0\sqrt{(\Omega_{\text{b}} + \Omega_{\text{CDM}})a^{-3} + \Omega_{\text{r}}a^{-4} + \Omega_{\text{k}}a^{-2} + \Omega_{\Lambda}a^{-3(1+\omega)}}, \tag{2.113}$$

where $\omega = p/\rho$ is equation of state of dark energy and $H_0 = 100h$ km s^{-1}Mpc^{-1} is a present-day value of the Hubble constant, with h being the reduced Hubble constant.

The measurements of the CMB anisotropy lead us to believe that Ω_{tot} is very close to unity and so the Universe is flat $k = 0$. The radiation density is very small today and it is negligible. For the rest of the values, the current CMB data gives [10]:

$$\Omega_{\text{b}} = 0.05, \quad \Omega_{\text{CDM}} = 0.27, \quad \Omega_{\Lambda} = 0.68 \ . \tag{2.114}$$

So visible baryonic matter constitutes only 5% is the total energy budget of the Universe. 27% is elusive dark matter and 68% is dark energy, that governs accelerated expansion of the Universe.

2.2.7   The Hubble Tension

Determination of the Hubble constant (2.113) using a distance ladder in the local Universe gives [9]

$$H_0 = 73.2 \pm 1.3 \ \ \text{km sec}^{-1} \ \text{Mpc}^{-1} \ . \tag{2.115}$$

But the Hubble parameter is also measured in earlier cosmological epochs through CMB and assuming ΛCDM model it estimates current expansion rate, that is equal to [10]

$$H_0 = 67.4 \pm 0.5 \ \ \text{km sec}^{-1} \ \text{Mpc}^{-1} \ , \tag{2.116}$$

being in 5% conflict with (2.115), creating the so-called Hubble tension. In our paper [7], we discussed the possibility recently suggested quasi-molecular mechanism of recombination [11] can be that missing ingredient, that increases the CMB-based Hubble constant determination (2.116) and makes it compatible with (2.115).

2.2.8 Dark Matter

As already mentioned, matter content of the Universe, consists of visible matter – that is baryonic matter and non-luminous dark matter,

$$\Omega_{\mathrm{m}} = \Omega_{\mathrm{b}} + \Omega_{\mathrm{DM}}. \tag{2.117}$$

Dark matter is thought to account for approximately 85% of the matter in the universe. It is called "dark" because it does not appear to interact with the electromagnetic field, which means it does not absorb, reflect, or emit electromagnetic radiation. However, its gravitational effects seems to be confirmed with many different observations.

Galaxy rotation curves does not agree with Kepler's Second Law, according to which, the rotation velocities must decrease with distance from the center, similar to the Solar System. Instead, the galaxy rotation curve remains flat as distance from the center increases. This could be explained, if besides luminous matter, there is also some dark matter, distributed in different manner.

Structure formation in the Universe would have been different if there were no dark matter. If there were only ordinary matter in the Universe, there would not have been enough time for density perturbations to grow into the galaxies and clusters currently seen.

In the early universe, when ordinary matter recombined and cosmic microwave background was formed, dark matter affected it by its gravitational potential (mainly on large scales) and by its effects on the density and velocity of ordinary matter. Ordinary and dark matter perturbations, therefore, evolve differently with time and leave different imprints on the CMB. The observed CMB angular power spectrum provides powerful evidence in support of dark matter, as its precise structure is well fitted by the ΛCDM model, but difficult to reproduce with any competing model.

With many more evidence coming from velocity dispersions, gravitational lensing, baryon acoustic oscillations, bullet clusters and etc., existence of DM is inevitable. However, there is no definite vision about its composition. There are many possible candidates of DM, for the review of their properties and possibility of detection see [9, 12, 13].

Weakly interacting massive particles (WIMPs) are hypothetical elementary particles that constitute DM. There is no formal definition of a WIMP, but broadly, a WIMP is a new elementary particle which interacts via gravity and some other unknown weak force, that is not a part of the standard model of particle physics. For the review of WIMPs see [14,15]. Axions are other popular candidates of DM that are widely discussed in literature [16,17]. Most probable, dark matter is thought to be cold (CDM), that refers to the fact that is should move slowly compared to the speed of light. Among other candidates of DM like sterile neutrinos [18], supersymmetric particles [19], gravitinos [20] and so on, there is a mirror matter model. It assumes that DM is made of mirror partners of well known elementary particles of standard model. Mirror particles do not interact with ordinary particles except of gravitational force. We will review mirror matter model in chapter (5).

Chapter 3

Theory of Gravitational Waves

The general theory of relativity also suggests the existence of gravitational radiation. The Einstein equations, assuming the field is weak and static (i.e. all time derivatives are zero) and particles are moving slowly, restores Newtonian physics. However, considering the weak field that can vary in time, GR predicts a phenomena that is absent in Newtonian physics: gravitational waves. This chapter is denoted to the theoretical foundations of gravitational-wave physics.

3.1 Equation for Gravitational Wave

To get the equations for the gravitational waves, one has to impose the weakness of the field, write Einstein's equations in this limit and solve it with the appropriate choice of gauge. The weakness of gravitational field means that the metric can be decomposed as flat Minkowski metric plus a small perturbation,

$$g_{\mu\nu} = \eta_{\mu\nu} + h_{\mu\nu}, \qquad |h_{\mu\nu}| \ll 1 \ . \tag{3.1}$$

Ignoring high order terms of $h_{\mu\nu}$, one immediately obtains

$$g^{\mu\nu} = \eta^{\mu\nu} - h^{\mu\nu} \ , \tag{3.2}$$

where $h^{\mu\nu} = \eta^{\mu\rho}\eta^{\nu\sigma}h_{\rho\sigma}$. The theory is Lorentz invariant, because we know that $\eta_{\mu\nu}$ is invariant and $h_{\mu\nu}$ transforms as

$$h_{\mu'\nu'} = \Lambda^{\mu'}_{\ \mu}\Lambda^{\nu'}_{\ \nu}h_{\mu\nu} \ . \tag{3.3}$$

In order to find the equation of motion for $h_{\mu\nu}$, we have to examine Einstein's equation to first order. For that, at first we need the Christoffel symbol

$$\Gamma^{\sigma}_{\mu\nu} = \frac{1}{2}g^{\sigma\lambda}\left(\partial_\mu g_{\nu\lambda} + \partial_\nu g_{\lambda\mu} - \partial_\lambda g_{\mu\nu}\right) = \frac{1}{2}\eta^{\sigma\lambda}\left(\partial_\mu h_{\nu\lambda} + \partial_\nu h_{\lambda\mu} - \partial_\lambda h_{\mu\nu}\right) \ . \tag{3.4}$$

In Riemann tensor Γ^2 terms can be neglected, so we are left with

$$R_{\mu\nu\rho\sigma} = \eta_{\mu\lambda}\partial_\rho\Gamma^\lambda_{\nu\sigma} - \eta_{\mu\lambda}\partial_\sigma\Gamma^\lambda_{\nu\rho} = \frac{1}{2}\left(\partial_\rho\partial_\nu h_{\mu\sigma} + \partial_\sigma\partial_\mu h_{\nu\rho} - \partial_\sigma\partial_\nu h_{\mu\rho} - \partial_\rho\partial_\mu h_{\nu\sigma}\right) \ . \tag{3.5}$$

Contracting over μ and ρ, we get the Ricci tensor

$$R_{\mu\nu} = \frac{1}{2}\left(\partial_\sigma\partial_\nu h^\sigma_{\ \mu} + \partial_\sigma\partial_\mu h^\sigma_{\ \nu} - \partial_\mu\partial_\nu h - \Box h_{\mu\nu}\right) \ , \tag{3.6}$$

where h is a trace of the perturbation $h = \eta^{\mu\nu}h_{\mu\nu} = h^\mu{}_\mu$, and $\Box$ is a simple d'Alambertian. Contracting once again yields the Ricci scalar

$$R = \partial_\mu\partial_\nu h^{\mu\nu} - \Box h \ . \tag{3.7}$$

Putting it all together we obtain the linearized Einstein tensor

$$G_{\mu\nu} = R_{\mu\nu} - \frac{1}{2}\eta_{\mu\nu}R = \frac{1}{2}\left(\partial_\sigma\partial_\nu h^\sigma{}_\mu + \partial_\sigma\partial_\mu h^\sigma{}_\nu - \partial_\mu\partial_\nu h - \Box h_{\mu\nu} - \eta_{\mu\nu}\partial_\lambda\partial_\sigma h^{\lambda\sigma} + \eta_{\mu\nu}\Box h\right) \ . \tag{3.8}$$

The linearized field equation will be

$$G_{\mu\nu} = 8\pi G T_{\mu\nu} \ , \tag{3.9}$$

where $G_{\mu\nu}$ is given by (3.8) and $T_{\mu\nu}$ is calculated to zeroth order in $h_{\mu\nu}$.

3.2   Fixing a Gauge

However, the decomposition of the metric into a flat background plus a perturbation is not unique. One can find a different coordinate system in which metric can still be written as the Minkowski metric plus a perturbation, but the perturbation may be different. Here comes the idea of gauge invariance. It turns up, that for sufficiently small ϵ,

$$h_{\mu\nu}^{(\epsilon)} = h_{\mu\nu} + 2\epsilon\partial_{(\mu}\xi_{\nu)} \ , \tag{3.10}$$

where ξ is some vector field. The equation (3.10) tells us what kind of metric perturbations denote physically equivalent spacetimes - those related to each other by $2\epsilon\partial_{(\mu}\xi_{\nu)}$ for some vector ξ^μ. Examining the Riemann tensor under such transformations, we see that it stays unchanged:

$$\begin{aligned}
\delta R_{\mu\nu\rho\sigma} &= \frac{1}{2}(\partial_\rho\partial_\nu\partial_\mu\xi_\sigma + \partial_\rho\partial_\nu\partial_\sigma\xi_\mu + \partial_\sigma\partial_\mu\partial_\nu\xi_\rho + \partial_\sigma\partial_\mu\partial_\rho\xi_\nu \\
&\quad - \partial_\sigma\partial_\nu\partial_\mu\xi_\rho - \partial_\sigma\partial_\nu\partial_\rho\xi_\mu - \partial_\rho\partial_\mu\partial_\sigma\xi_\nu - \partial_\rho\partial_\mu\partial_\sigma\xi_\nu) = 0 \ .
\end{aligned} \tag{3.11}$$

So, in order to solve the linearized Einstein's equations (3.9), at first one needs to choose the gauge. But before that, its useful to decompose the components of the metric perturbation. $h_{\mu\nu}$ is a symmetric $(0,2)$ tensor and under spatial rotations its 00 component transforms as scalar, the 0i components as 3-vector and ij components as 2-index tensor. So one can represent the components of the metric perturbation as:

$$\begin{aligned}
h_{00} &= -2\Phi \\
h_{0i} &= \omega_i \\
h_{ij} &= 2s_{ij} - 2\psi\delta_{ij} \ ,
\end{aligned} \tag{3.12}$$

where the tensor part was further split into the trace Ψ and the traceless (also referred as the strain tensor) s_{ij} parts:

$$\begin{aligned}
\Psi &= -\frac{1}{6}\delta^{ij}h_{ij} \\
s_{ij} &= \frac{1}{2}\left(h_{ij} - \frac{1}{3}\delta^{kl}h_{kl}\delta_{ij}\right) \ .
\end{aligned} \tag{3.13}$$

The entire metric can be written as:

$$ds^2 = -(1 - 2\Phi)^2 dt^2 + \omega_i (dt dx^i + dx^i dt) + [(1 - 2\Phi)\delta_{ij} + 2s_{ij}] dx^i dx^j . \tag{3.14}$$

Taking metric in this decomposition (3.12) the gauge transformations (3.10) now take the form:

$$\begin{aligned}
\Phi &\rightarrow \Phi + \partial_0 \xi^0 \\
\omega_i &\rightarrow \omega_i + \partial_0 \xi^i - \partial_i \xi^0 \\
\Psi &\rightarrow \Psi - \frac{1}{3} \partial_i \xi^i \\
s_{ij} &\rightarrow s_{ij} + \partial_{(i} \xi_{j)} - \frac{1}{3} \partial_k \xi^k \delta_{ij}
\end{aligned} \tag{3.15}$$

(we dropped ϵ and assumed that ξ^μ is small itself). Now we take the so-called transverse gauge:

$$\begin{aligned}
\partial_i s^{ij} &= 0 \\
\partial_i \omega^i &= 0 ,
\end{aligned} \tag{3.16}$$

by choosing ξ^μ in the way to satisfy

$$\begin{aligned}
\nabla^2 \xi^j + \frac{1}{3} \partial_j \partial_i \xi^i &= -2 \partial_i s^{ij} \\
\nabla^2 \xi^0 - \partial_0 \partial_i \xi^i &= \partial_i \omega^i .
\end{aligned} \tag{3.17}$$

Writing the linearized Einstein equations (3.9) using the metric perturbations decomposed as (3.12) in the transverse gauge (3.16), one gets:

$$G_{00} = 2\nabla^2 \Psi = 8\pi G T_{00} \tag{3.18}$$

$$G_{0j} = -\frac{1}{2} \nabla^2 \omega_j + 2 \partial_0 \partial_j \Psi = 8\pi G T_{0j} \tag{3.19}$$

$$G_{ij} = (\delta_{ij} \nabla^2 - \partial_i \partial_j)(\Phi - \Psi) - \partial_0 \partial_{(i} \omega_{j)} + 2\delta_{ij} \partial_0^2 \Phi - \Box s_{ij} = 8\pi G T_{ij} . \tag{3.20}$$

Our goal is to write the equations for gravitational waves, that are the free propagating degrees of freedom and require no local source (but of course they can be generated by such source). That is why we set to zero the entire energy-momentum tensor $T_{\mu\nu} = 0$. Then 00 equation is just

$$\nabla^2 \Psi = 0 , \tag{3.21}$$

which with well-behaved boundary condition implies $\Psi = 0$. Using that, $0j$ equation is

$$\nabla^2 \omega_j = 0 , \tag{3.22}$$

which from its side implies $\omega_j = 0$. Plugging this results the trace part of ij equations gives

$$\nabla^2 \Phi = 0 , \tag{3.23}$$

implying $\Psi = 0$. So the only thing is left is the trace-free part of ij equation, which becomes a wave equation for the traicless strain tensor:

$$\Box s_{ij} = 0 . \tag{3.24}$$

23

So from the entire metric perturbation $h_{\mu\nu}(\Phi, \omega_i, \Psi, s_{ij})$ all degrees of freedom except s_{ij} were set to zero and only the trace part survived. $h_{\mu\nu}$ is purely spatial, traceless and transverse:

$$
\begin{aligned}
h_{0\nu} &= 0 \\
\eta^{\mu\nu} h_{\mu\nu} &= 0 \\
\partial_\mu h^{\mu\nu} &= 0 \; .
\end{aligned}
\tag{3.25}
$$

This is known as transverse-traceless gauge

$$
h_{\mu\nu}^{\mathrm{TT}} = \begin{pmatrix} 0 & 0 & 0 & 0 \\ 0 & & & \\ 0 & & 2s_{ij} & \\ 0 & & & \end{pmatrix}
\tag{3.26}
$$

and the equation of motion is given by

$$
\Box h_{\mu\nu}^{\mathrm{TT}} = 0 \; .
\tag{3.27}
$$

3.3 Plane Wave Solution

Plane waves are particularly useful solutions for these wave equations

$$
h_{\mu\nu}^{\mathrm{TT}} = C_{\mu\nu} e^{ik_\sigma x^\sigma} \; ,
\tag{3.28}
$$

where $C_{\mu\nu}$ is a constant, symmetric $(0,2)$ tensor, which is purely spatial $\eta^{\mu\nu} C_{\mu\nu} = 0$ and traceless $C_{0\nu} = 0$. k_σ is a wave vector that, by inserting (3.28) in (3.27) must satisfy

$$
k_\sigma k^\sigma = 0 \; .
\tag{3.29}
$$

This means that plane wave is a solution if the wave vector is null, implying that gravitational waves propagate at the speed of light. The timelike component of the wave vector is the frequency of the wave ω, and the vector can be written as $k^\sigma = (\omega, k^1, k^2, k^3)$ and the condition that it is null vector, becomes

$$
\omega^2 = \delta_{ij} k^i k^j \; .
\tag{3.30}
$$

Recalling that the perturbation should be transverse, implies

$$
k_\mu C^{\mu\nu} = 0 \; ,
\tag{3.31}
$$

that is the wave vector must be orthogonal to $C^{\mu\nu}$.

3.4 Effect of Gravitational Wave Propagation

The solution becomes more explicit if one chooses spatial coordinates in a way that the wave is propagating in x^3 direction, that is:

$$
k^\mu = (\omega, 0, 0, k^3) = (\omega, 0, 0, \omega) \; .
\tag{3.32}
$$

In this case, $C_{0\nu} = 0$ and (3.31) together imply that $C_{3\nu} = 0$ and only nonzero components of $C_{\mu\nu}$ are C_{11}, C_{12}, C_{21} and C_{22}. But as $C_{\mu\nu}$ is traceless and symmetric, one can write:

$$C_{\mu n} = \begin{pmatrix} 0 & 0 & 0 & 0 \\ 0 & C_{11} & C_{12} & 0 \\ 0 & C_{12} & -C_{11} & 0 \\ 0 & 0 & 0 & 0 \end{pmatrix} . \tag{3.33}$$

So, for a plane wave in this gauge traveling in the x^3 direction, the two components C_{11} and C_{12} and the frequency ω completely characterize the wave.

To illustrate the effect of passing gravitational wave, it is useful to consider relative motion of nearby particles that are positioned at a ring-shape at initial moment. The motion would be described by geodesic deviation equation:

$$\frac{D^2}{d\tau^2} S^\mu = R^\mu{}_{\nu\rho\sigma} U^\nu U^\rho S^\sigma , \tag{3.34}$$

where S^μ is a separation vector and $U^\mu(x)$ are the four-velocities of particles. Admitting that our test particles are moving slowly and keeping the terms at the first order in $h^{\mathrm{TT}}_{\mu\nu}$, the equation (3.34) becomes:

$$\frac{\partial^2}{\partial t^2} S^\mu = \frac{1}{2} S^\sigma \frac{\partial^2}{\partial t^2} h^{\mathrm{TT}\mu}{}_\sigma . \tag{3.35}$$

For the wave traveling in x^3 direction only S^1 and S^2 will be affected. Considering effects of C_{11} and C_{12} separately, for C_{11} we have the equations

$$\frac{\partial^2}{\partial t^2} S^1 = \frac{1}{2} S^1 \frac{\partial^2}{\partial t^2} C_{11} e^{ik_\sigma x^\sigma} \tag{3.36}$$

and

$$\frac{\partial^2}{\partial t^2} S^2 = -\frac{1}{2} S^2 \frac{\partial^2}{\partial t^2} C_{11} e^{ik_\sigma x^\sigma} . \tag{3.37}$$

Solving to the lowest order, one has:

$$S^1 = \left(1 + \frac{1}{2} C_{11} e^{ik_\sigma x^\sigma}\right) S^1(0) \tag{3.38}$$

and

$$S^2 = \left(1 - \frac{1}{2} C_{11} e^{ik_\sigma x^\sigma}\right) S^2(0) \tag{3.39}$$

These solutions tell, that particles initially separated in the x^1 direction will oscillate in the x^1 direction and particles initially separated in the x^2 direction will oscillate in the x^2 direction. So, starting with a ring-shape, particles will bounce back and forth in the shape of a "+", as the wave passes. The equations for C_{22} will have slightly different solutions, telling that particles will move in "×" shape. Hence, C_{11} and C_{22} are often denoted correspondingly by h_+ and $h_\times$, and these patterns are shown in the figure (3.1).
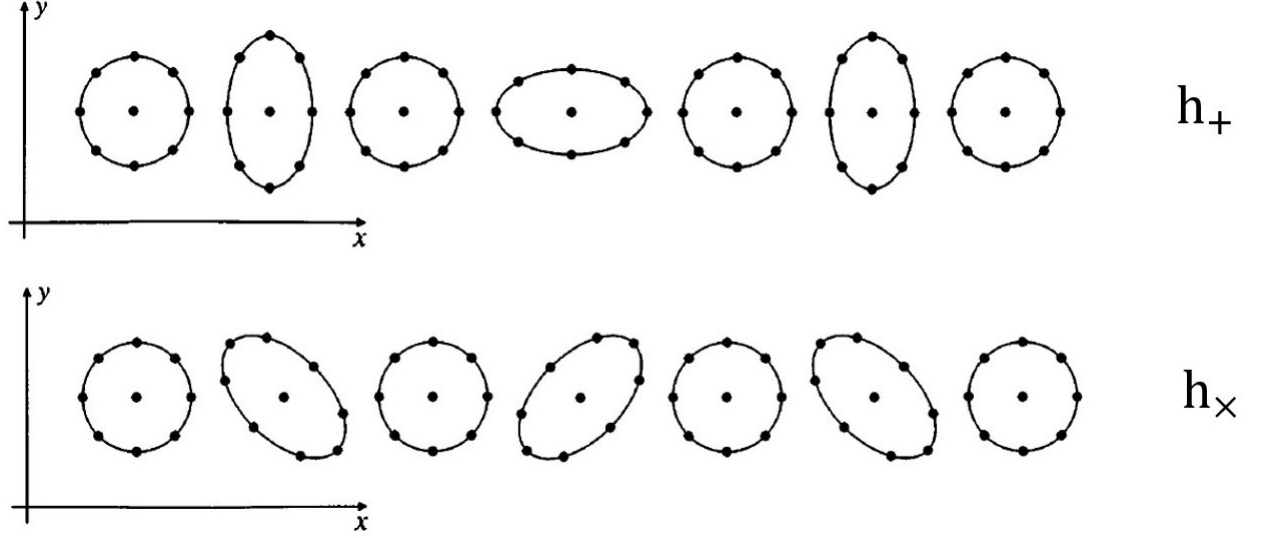
Figure 3.1: Effect of gravitational wave passing in z direction, with plus (top) and cross (bottom) polarization on a ring of particles.

3.5 Production of Gravitational Waves

To discuss the generation of GWs by source, one should consider Einstein's equations coupled to matter $G_{\mu\nu} = 8\pi G T_{\mu\nu}$. Now, metric perturbation will include not only strain tensor, but also non-zero scalar and vector components. It is convenient to define trace-reversed perturbation

$$\bar{h}_{\mu\nu} = h_{\mu\nu} - \frac{1}{2}h\eta_{\mu\nu} \ , \tag{3.40}$$

that is not transverse in general, but in a vacuum far away from the source $\bar{h}^{\text{TT}}_{\mu\nu} = h^{\text{TT}}_{\mu\nu}$. Choosing gauge parameter ξ_μ satisfying $\Box\xi_\mu = -\partial_\lambda \bar{h}^\lambda{}_\mu$ and imposing the Lorentz gauge $\partial_\mu \bar{h}^{\mu\nu} = 0$, gives Einstein tensor in a form:

$$G_{\mu\nu} = -\frac{1}{2}\Box\bar{h}_{\mu\nu} \tag{3.41}$$

and linearized Einstein equation is this gauge is

$$\Box\bar{h}_{\mu\nu} = -16\pi G T_{\mu\nu} \ . \tag{3.42}$$

Writing the solution using Green's function

$$\bar{h}_{\mu\nu}(x^\sigma) = -16\pi G \int G(x^\sigma - y^\sigma)T_{\mu\nu}(y^\sigma)d^4y \ , \tag{3.43}$$

where

$$G(x^\sigma - y^\sigma) = -\frac{1}{4\pi|\boldsymbol{x} - \boldsymbol{y}|}\delta[|\boldsymbol{x} - \boldsymbol{y}| - (x^0 - y^0)]\theta(x^0 - y^0) \ , \tag{3.44}$$

where boldface denotes spatial 3-vectors and θ is Heaviside function that equals to 1 if $x^0 > y^0$ and performing the integral over y^0, gives

$$\bar{h}_{\mu\nu}(t, \boldsymbol{x}) = 4G \int \frac{1}{|\boldsymbol{x} - \boldsymbol{y}|}T_{\mu\nu}(t - |\boldsymbol{x} - \boldsymbol{y}|, \boldsymbol{y})d^3y \ , \tag{3.45}$$
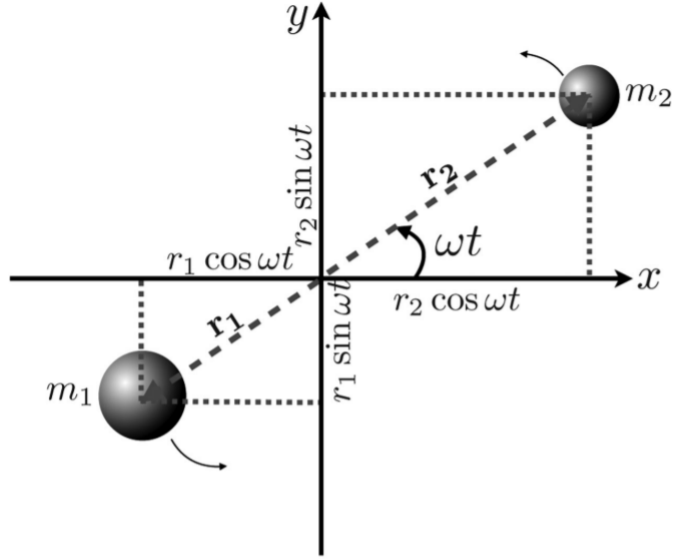
Figure A1 A two-body system, m_1 and m_2 orbiting in the xy-plane around their C.O.M.

Figure 3.2: Figure adopted from [21]

where $t = x^0$ and $t - |\boldsymbol{x} - \boldsymbol{y}| = t_r$ is called a retarded time. Assuming that the source is isolated, far away and slowly moving, one can approximate $|\boldsymbol{x} - \boldsymbol{y}| = r$, where r is distance between the source and observer. Now, taking a Fourier transform of the metric perturbation, one obtains

$$\tilde{h}_{\mu\nu}(\omega, \boldsymbol{x}) = \frac{1}{2\pi} \int dt e^{i\omega t} \, \bar{h}_{\mu\nu}(t, \boldsymbol{x}) = \frac{4G}{2\pi} \int dt d^3 y e^{i\omega t_r} \frac{e^{i\omega r}}{r} T_{\mu\nu}(t_r, \boldsymbol{y}) = 4G \frac{e^{i\omega r}}{r} \int d^3 y \, \tilde{T}_{\mu\nu}(\omega, \boldsymbol{y}).$$
(3.46)

Considering spatial parts $\tilde{h}_{ij}(\omega, \boldsymbol{x})$, using integration by parts and Fourier-space version of $\partial_\mu T^{\mu\nu} = 0$, mainly $-\partial_k \tilde{T}^{k\mu} = i\omega \tilde{T}^{0\mu}$, one has

$$\int d^3 y \, \tilde{T}_{\mu\nu}(\omega, \boldsymbol{y}) = -\frac{\omega^2}{2} \int y^i y^j \, \tilde{T}^{00} d^3 y \,.$$
(3.47)

Defining the quadrupole moment tensor of the energy density of the source,

$$I_{ij}(t) = \int y^i y^j \, T^{00} d^3 y \,,$$
(3.48)

and taking the inverse Fourier transform, we obtain the quadrupole formula

$$\bar{h}_{ij}(t, \boldsymbol{x}) = \frac{2G}{r} \frac{d^2 I_{ij}}{dt^2}(t_r) \,.$$
(3.49)

Sometimes it is more convenient to use the reduced quadrupole moment

$$Q_{ij} = I_{ij} - \frac{1}{3} \delta_{ij} \delta^{kl} I_{kl}$$
(3.50)

and of course the transverse-traceless part of strain tensor (3.49) is not affected with this change.

27

The most interesting case is to discuss gravitational radiation emitted by the binary star system. The following discussion follows [21]. Consider two stars of mass m_1 and m_2 orbiting each other in $X - Y$ plane (as shown in the figure (3.2)). The distances from the stars to their common center of mass are r_1 and r_2 correspondingly and $r = r_1 + r_2$ is the distance between the stars. We treat the motion of the stars in Newtonian approximation and assume that their orbits are circular. Suppose the radii of the stars are small compared to their separation distance, the binary system's mass density distribution function can be written using Dirac's delta function:

$$\rho(x, y, z) = m_1 \delta(x - x_1)\delta(y - y_1)\delta(z) + m_2 \delta(x - x_2)\delta(y - y_2)\delta(z) . \qquad (3.51)$$

Then, reduced quadrupole moment of the system will have a form:

$$Q_{ij} = \int d^3 x \rho(\boldsymbol{x}) \left(x^i x^j - \frac{1}{3} r^2 \delta_{ij} \right) . \qquad (3.52)$$

Writing stars' coordinates explicitly using angular frequency ω of the system

$$
\begin{aligned}
x_1 &= -r_1 \cos \omega t \\
y_1 &= -r_1 \sin \omega t \\
x_2 &= r_2 \cos \omega t \\
y_2 &= r_2 \sin \omega t
\end{aligned}
\qquad (3.53)
$$

and using a center-of-mass reference frame

$$m_1 r_1 = m_2 r_2 , \qquad (3.54)$$

appearance of Delta function allows to integrate (3.52) to get:

$$Q_{ij} = \frac{1}{2}\mu r^2 \begin{pmatrix} \frac{1}{3} + \cos 2\omega t & \sin 2\omega t & 0 \\ \sin 2\omega t & \frac{1}{3} - \cos 2\omega t & 0 \\ 0 & 0 & -\frac{2}{3} \end{pmatrix}, \qquad (3.55)$$

where $\mu = \frac{m_1 m_2}{m_1 + m_2}$ is reduced mass of the system. The gravitational wave strain tensor at a luminosity distance d_L is given by

$$h_{ij} = \frac{2G}{c^4 d_L}\frac{d^2 Q_{ij}}{dt^2} = \frac{4G\mu}{c^4 d_L}r^2\omega^2 \begin{pmatrix} -\cos 2\omega t & -\sin 2\omega t & 0 \\ -\sin 2\omega t & \cos 2\omega t & 0 \\ 0 & 0 & 0 \end{pmatrix} \qquad (3.56)$$

(hereafter we recover the presence of c). The rate at which energy is carried away by the gravitational waves is found to be

$$\frac{dE_{GW}}{dt} = \frac{c^3}{16\pi G}\int\int \sum_{i,j=1}^{3} \frac{dh_{ij}}{dt}\frac{dh_{ij}}{dt}dS = \frac{1}{5}\frac{G}{c^5}\sum_{i,j=1}^{3}\frac{d^3 Q_{ij}}{dt^3}\frac{d^3 Q_{ij}}{dt^3} = \frac{32}{5}\frac{G}{c^5}\mu^2 r^4 \omega^6. \qquad (3.57)$$

Orbital energy is given as

$$E_{\text{orb}} = -\frac{GM\mu}{2r} , \qquad (3.58)$$

where $M = m_1 + m_2$ is a total mass of the system. The loss of energy through gravitational radiation drains the orbital energy

$$\frac{dE_{\mathrm{orb}}}{dt} = \frac{GM\mu}{2r^2}\frac{dr}{dt} = -\frac{dE_{GW}}{dt} \ . \tag{3.59}$$

Assuming that the energy radiated away over each orbit is small compared to E_{orb}, one can describe each orbit as approximately Keplerian. Using Kepler's third law and its derivative

$$r^3 = \frac{GM}{\omega^2} \ , \qquad \dot{r} = -\frac{2}{3}\frac{\dot{\omega}}{\omega}r \ , \tag{3.60}$$

and inserting (3.57) in (3.59), one gets

$$\dot{\omega} = \frac{96}{5}\frac{G^{5/3}}{c^5}\mu M^{2/3}\omega^{11/3} = \frac{96}{5}(G\mathcal{M}_c)^{5/3}\omega^{11/3} \ , \tag{3.61}$$

where $\mathcal{M}_c = (\mu^3 M^2)^{1/5}$ notation was introduced and it is called a chirp mass.

A phenomenological form of the gravitational waveform is given by

$$h(t) = h_0 \cos\phi(t) \ , \tag{3.62}$$

where h_0 is called a scaling amplitude and equals to the coefficient of non-zero components of the strain (3.56)

$$h_0 = \frac{4G\mu}{c^4 d_L}r^2\omega^2 = \frac{4(G\mathcal{M})^{5/3}}{c^4 d_L}\omega^{2/3} \tag{3.63}$$

(here we used the Kepler's 3rd law). $\phi(t)$ is the gravitational wave phase and it evolves in time as:

$$\phi(t) = 2\omega t + \dot{\omega}t^2 + \phi_0 \ , \tag{3.64}$$

where ϕ_0 is the initial phase of binary. Inserting a solution $\omega(t)$ of (3.61) in (3.63) and (3.64) one gets a gravitational waveform of merging binary (3.62).

Chapter 4

Detection of Gravitational Waves

4.1 Gravitational Wave Detectors

Gravitational waves (GW) were directly detected for the first time in 2015. Since then about 100 events have been recorded by LIGO, Virgo and KAGRA observatories, that have been operating with necessary sensitivity.

The Laser Interferometer Gravitational-Wave Observatory (LIGO) is a system of two detectors in USA designed to detect GWs. One detector is located in Hanford, Washington and the second in Livingston, Louisiana. It began observations in 2002, but only after the upgrade to Advanced LIGO in 2015, it reached enough sensitivity to detect GWs. Virgo interferometer is a GW observatory located in Cascina, Italy. After the upgrade to Advanced Virgo it joined Advanced LIGO to make its first detection in 2017. The Kamioka Gravitational Wave Detector (KAGRA) was built underground in the Kamioka Observatory in Gifu Prefecture, Japan. It become operational in February 2020, but was shut down in two months due to pandemic.

All these three observatories are interferometers and they are based on similar working principle. Each of the detectors consist of two perpendicular arms of few kilometers. A single laser beam is split at the intersection of the two arms, the light is reflected from the end points of the arms and returns to the intersections where they interfere. If the lengths of both arms have remained unchanged, then the two combining light waves should destructively interfere and there will be no light observed at the output of the detector. However, if a GW passed through the detector, according to Einstein's general relativity, spacetime inside arm will be warped; one arm will be stretched, other compressed and the two light beams would no longer completely subtract each other, yielding light patterns at the detector output. This light pattern encodes the information about relative change of arms' lengths and though gives ability to reconstruct gravitational waveform.

However, detecting GW is technically extremely difficult. Passage of GW is expected to change the arm length by about 1/1000 the diameter of a proton. Equivalently, this is a relative change in distance of approximately one part in 10^{21}. Many things on Earth can cause such small changes, so one should be able to subtract all noise that distorts GW signal. Detectors optical components are sustained under ultra-high vacuum to ensure that the light travels in straight lines and it is not bent due to slight temperature differences across the arm. The positions of the mirrors are adjusted to account for terrestrial noise, local vibrations, seismic activities and even the change of the tidal force of the Sun and the Moon. Improving the noise subtraction and signal analyses technologies through the years, finally the detectors reached the sufficient sensitivities to detect GW for the first time.

4.2 Gravitational Wave Data

4.2.1 LIGO-Virgo-KAGRA Events

Since the upgrade to the Advanced LIGO, it conducted three observing runs. The first observing run (O1) took place between 12 September 2015 - 19 January 2016 with runtime of 4.26 months and it observed two confirmed signals form merging Binary Black Holes (BBH) GW150914 [22], GW151226 [23].

During the second observing run (O2) (30 November 2016 - 25 August 2017), with advanced Virgo joining on 1 August, it has detected three more events GW170104 [24], GW170814 [25], GW170608 [26] from BBH system and one signal from merging neutron stars GW170817 [27]. Later on, novel methods for reanalyzing first two runs, revealed five more GW signals from BBHs (GW170729, GW170809, GW170818, GW170823 and GW151012 [28]). In total, during O1&O2 LIGO observed 10 GWs from BBH mergers and one signal from binary neutron stars and the results were summarized in Gravitational-Wave Transient Catalog-1 [28]. It is important that the neutron star event and two BBH signals (GW170814 and GW170818) were triple-coincidence events, observed by two LIGO observatories together with Virgo detector.

The third observing run (O3) began on 1 April 2019 and it was divided into O3a, from 1 April to 30 September 2019, and O3b, from 1 November 2019 to 27 March 2020. Suspension of observation during October 2019 was for instrument upgrades and fixes, and cessation in March 2020 was due to the COVID-19 pandemic.

O3a already revealed several unexpected discoveries. The theory of evolution of stars predicts the absence of compact objects with masses in between the most massive neutron stars and least massive black holes, approximately $3-5M_\odot$; this is called a lower mass gap and it was somehow supported by electromagnetic observations. Also, many models suggest existence of so-called upper mass gap, black holes with masses in the range of about $\sim 50-120M_\odot$ should not exist due to pair-instability supernovae. We will explain the reasons for the mass gaps in more details below.

The first odd event in O3a was GW190425, a compact binary coalescence with total mass $\sim 3.4M_\odot$ [29]. The masses of binary components and of the final object are at the edge of the lower mass gap. The event GW190521, a binary black hole merger with a total mass of $150M_\odot$ presumably falls in the upper mass gap [30]. There were also events with very asymmetric component masses [31,32]. The results of O3a were outlined in Gravitational-Wave Transient Catalog-2 [33], that included 39 events. Later, the GWTC-2 was extended to GWTC-2.1 [34] with 8 additional events. The second half of the third observing run also revealed two interesting events of neutron star - black hole mergers [35]. The results of O3b, with 35 new events were presented in GWTC-3 [36]. To sum up, the analysis of three observing runs that have been conducted so far, in overall revealed 90 events with probability $P_{astro} > 0.5$ being of an astrophysical origin [36]. Among these 90 events, the majority are BH-BH mergers, with few of them containing BHs from the upper mass gap. Two events are from the merger of BH with an object of lower mass gap. Two more events are from NS-BH coalescence, and other two from NS-NS merger. It is important to notice, that the event GW170817 of binary NS coalescence still remains the only GW detection accompanied by a gamma-ray counterpart [37, 38]. No other electromagnetic radiation associated with GW has been found yet [39, 40].

The fourth run, O4, is planned to begin in March 2023.

4.2.2 Merger Rates

As a result of the analyses of the three observing runs, merger rates for different systems were estimated [43]. The merger rate for BBH systems, accounting that coalescence rate evolves with redshift, was calculated to be

$$\mathcal{R}_{\mathrm{BBH}} = 17.9 - 44 \ \mathrm{Gpc}^{-3}\mathrm{yr}^{-1} \tag{4.1}$$

at a fiducial redshift $z = 0.2$. For BH-NS and BH-mass gap systems, the merger rates were inferred to be

$$\mathcal{R}_{\mathrm{BH-NS}} = 7.8 - 140 \ \mathrm{Gpc}^{-3}\mathrm{yr}^{-1} \tag{4.2}$$

and

$$\mathcal{R}_{\mathrm{BH-mass \ gap}} = 9.4 \times 10^{-5} - 25 \ \mathrm{Gpc}^{-3}\mathrm{yr}^{-1} \tag{4.3}$$

correspondingly. BNS are estimated to coalescence at a rate

$$\mathcal{R}_{\mathrm{BNS}} = 10 - 1700 \ \mathrm{Gpc}^{-3}\mathrm{yr}^{-1} \tag{4.4}$$

and NS-mass gap objects are expected to merge at a rate

$$\mathcal{R}_{\mathrm{NS-massgap}} = 0.02 - 39 \ \mathrm{Gpc}^{-3}\mathrm{yr}^{-1} \ . \tag{4.5}$$

Still having relatively high uncertainties in the measured merger rates, many models of compact binary formation and evolution can fit with the observations.

4.3 Binary Black Holes

The population properties of LIGO-Virgo-Kagra (LVK) compact objects and their astrophysical interpretations have been discussed in the papers accompanying the GW transient catalogs: [41–43]. We start with reviewing the possible scenarios for binary black hole formation and merger.

The most common way for creating a BH is gravitational collapse of a heavy star. The final step of evolution of the stars is still speculative [44], but according to the most common description, by the time the star runs out of fuel, if its core mass remains heavy enough, it explodes, creating a supernova and leaving a BH as a stellar remnant. However, the mass of the remnant BH is not in one-to-one match with the mass of the progenitor star. Stellar wind is the main reason by which star loses its mass and its strength is found to be dependent on the metallicity of the star. Low metallicity reduces opacity, radiation transport becomes easier and decreases wind strength. So only the stars with a certain amount of metal content (below $\simeq 1/2 \ Z_\odot$) are thought to be capable of creating BHs with mass $\gtrsim 25 M_\odot$.

Binary black hole systems could be created through different mechanisms. Despite increasing number of BBH mergers, their origin is not clearly understood, but several formation channels are under close investigation. Isolated massive binaries in the galactic field could form BBH through common-envelope [45, 46], through stable Roche-lobe overflow [47, 48] or via chemically homogeneous evolution [49, 50]. BBH might also be created in dense stellar cluster by some dynamical processes [51]. Alternatively, triple or quadrupole systems can also produce BBH mergers [52, 53]. Finally, BBHs can have a primordial origin [54–58].

4.3.1 Primordial Black Holes

Some authors suggested explanations for the sources of GW signals by so-called Primordial Black Holes (PBH) [54–58]. PBHs are BHs that could have been formed in the early universe, when no astrophysical objects existed yet. The most popular mechanism for PBH formation is the direct gravitational collapse of primordial density inhomogeneities. As in the very early times, the universe was radiation dominated and ordinary matter was not yet formed, we can think of PBH as the direct collapse of Dark Matter (DM) density fluctuations, and it is common to define a fraction of PBHs in DM

$$f_{\mathrm{PBH}} = \frac{\Omega_{\mathrm{PBH}}}{\Omega_{\mathrm{DM}}} \ , \tag{4.6}$$

where Ω_{PBH} and Ω_{DM} are PBH and DM density parameters, respectively.

Existing constraints on f_{PBH} in different mass ranges from various experiments are reviewed in [56]. The mass interval relevant for LVK events is

$$1 \ M_\odot < M < 100 \ M_\odot \ . \tag{4.7}$$

However, microlensing surveys say that PBHs in the mass range

$$10^{-7} \ M_\odot < M < 30 \ M_\odot \tag{4.8}$$

cannot fill dominant parts of Ω_{DM} [59, 60]; higher mass PBHs ($43 M_\odot \lesssim$) are excluded by wide binaries [61] and the mass range $1 - 100 \ M_\odot$ is constrained by the non-detection of cosmic microwave background (CMB) spectral distortion [62]. This suggests that upper bound on f_{PBH} is order of 10^{-4}–10^{-3} in the mass range (4.7). Several models can be responsible for the explanation of LVK signals using the PBHs. These models differ with the value of f_{PBH} and use distinct mechanism for binary system formation:

- When two PBHs accidentally pass each other with sufficiently small impact parameter, they can form BBHs due to energy loss by gravitational radiation [63]. In this scenario, in order to explain the event rate estimated by LVK, the fraction of PBHs in DM (4.6) is required to be the order of unity. This is in contradiction with the CMB anisotropies, but in [63], it is assumed that constraints from CMB require modeling of several complex physical processes and, therefore, could have a significant uncertainty.

- A different mechanism for estimating a PBH merging rate was suggested in [54]. Cosmic expansion pulls PBHs away from each other, while gravitation tries to keep them together. If gravitational energy between two PBHs exceeds expansion energy, they start to free-fall on one another. However, neighboring PBH can exert torque on their system, avoiding their head-on collision and forming an eccentric binary in this way. In [54] it was assumed that PBHs are massive stellar halo objects (MACHO) with monochromatic mass function equal to $0.5 \ M_\odot$, PBHs are initially randomly distributed in space and $f_{\mathrm{PBH}} \approx 1$. After the LIGO discovery, this theory was rewritten for PBHs with mass $30 \ M_\odot$ [55] and (4.6) was treated as a free parameter. It was derived that, in order to get a merging rate compatible with LVK's estimates, f_{PBH} is required to be of order 10^{-4}. Intriguingly, it appears close to the PBH abundance estimated from the lack of CMB spectral distortion. More GWs data is needed to test this model.

- In different model the mean mass of PBH is expected to be $\sim 10 M_\odot$ [57] that is in accordance with data [36]. Taking an initial log-normal mass spectrum, existing LVK data can be described by PBHs [58].

Withal, more data is required to encourage the PBH scenario for LVK events.

4.3.2 Astrophysical Black Holes

Currently, most models are mainly concerned with astrophysical origin of LVK binary BHs. These models estimate BBH merging rate as a function of the efficiency of BBH merging ϵ, the distribution of times elapsed between creating and merging of a binary system P and BH's number density N_{BH} [64],

$$\mathcal{R} = \frac{1}{2} \ \epsilon P(\tau) N_{\mathrm{BH}} \ . \tag{4.9}$$

Dimensionless coefficient

$$\epsilon \equiv f_{\mathrm{bin}} \times f_{\mathrm{m_1/m_2}} \times f_{\mathrm{surv}} \times f_{\mathrm{t}} < 1 \tag{4.10}$$

defines the efficiency of BBH merging [64]. Current models predict that half of the stars are in binaries $f_{\mathrm{bin}} \sim 0.5$ [65], $f_{\mathrm{m_1/m_2}} \sim 0.1$ is the fraction of binary systems of stars, which have the mass ratio near unity $m_1/m_2 \sim 1$ [65], which corresponds to the LVK data, and $f_{\mathrm{surv}} \sim 0.1$ is fraction of massive stars that survive as BH pairs after stellar evolution. Finally, $f_{\mathrm{t}} < 1$ is a fraction of BBHs with orbital configuration that makes them available to merge before the present day. As we see, ϵ depends on many factors and can vary significantly in the interval

$$\epsilon \simeq 0.01 - 0.001 \ . \tag{4.11}$$

Delay time $P(\tau)$ is also very speculative as it depends on the masses, metallicities, orbital configurations of the binary system of progenitor stars and it can even exceed the Hubble time. BH number density can be written as [64]

$$N_{\mathrm{BH}} = \mathrm{SFR}(z) \int \phi(m) \ N(m) \int f(Z, m) \int \xi(M) \ dM \ dZ \ dm \ . \tag{4.12}$$

Here $\xi(M)$ is a stellar initial mass function (which usually is integrated in the interval $5 \ M_\odot < M < 150 \ M_\odot$ to match the LVK data), $f(Z, m)$ is a metallicity distribution function of the galaxy of the mass m (usually the metallicity range $0.0002 < Z < 0.02$ is considered), $N(m)$ is total number of stars in the galaxy of mass m, which is normalized as

$$N(m) = \frac{m}{\int M \ \xi(M) \ dM} \ , \tag{4.13}$$

$\phi(m)$ is a galactic stellar mass function and $\mathrm{SFR}(z)$ is a star formation rate, which is typically adopted from the best-fit-function of experimental data [66],

$$\mathrm{SFR}(z) = 0.015 \frac{(1+z)^{2.7}}{1 + [(1+z)/2.9]^{5.6}} \ \mathrm{M}_\odot \ \mathrm{Mpc}^{-3} \ \mathrm{yr}^{-1} \ . \tag{4.14}$$

This function peaks at $z \sim 2$ corresponding to the luminosity distance $\sim$15 Mpc and lookback time $\sim$10 Gyr.

In the scenario for isolated binaries formed throughout common envelope evolution [46], simulations were carried out for different values of metallicities. Derived local BBH merging

rate spans from $\sim 10^{-1}$ to 7×10^{3} Gpc^{-3} yr^{-1}. Such a high uncertainty comes from tight dependence on metallicity distribution function of progenitor stars. In order to fall in merging rate estimated by LVK, lower values of metallicities are favored.

Simulations for chemically homogeneous stellar binaries [49] suggest $\mathcal{R} \approx 10$ Gpc^{-3} yr^{-1}. They find that typical time delay between formation and merger $P(\tau)$ ranges from 4 to 11 Gyr and mergers beyond $z \gtrsim 1.6$ did not take place as the Universe was too young. They conclude that over cosmic time, merger rate rises as mergers with longer delay times start to contribute, but in the present age Universe it start to fall, as low-metallicity SFR decreases, leading to a peak of ~ 20 Gpc^{-3} yr^{-1} at $z \lesssim 0.5$.

In [51] thousands of dense star cluster models with different initial conditions were simulated and coalescing BBHs that escaped or merged inside the clusters were studied. The local merger rate density of BBHs originated from globular clusters is obtained to be 5.4 Gpc^{-3} yr^{-1}.

All these models [46, 49, 51] estimate a theoretical BBH merger rate

$$\mathcal{R}_{\mathrm{BBH}}^{\mathrm{theor}} \sim 5 - 10 \text{ Gpc}^{-3} \text{ yr}^{-1} \ , \tag{4.15}$$

which is near the LVK's lower bound (4.1).

4.3.3 The Sources from the Upper Mass Gap

Several events of LVK data contain unusually heavy BHs that fall in the so-called upper mass gap, produced by pair-instability supernova processes. Current models for evolution of heavy stars predict that temperature in a He core reaches the point when production of electron-positron pairs is allowed. So, part of the energy of photons that was providing pressure against gravity, is consumed by pair production and the star becomes unstable. Stars with He core mass $\sim 32 - 64 M_{\odot}$ are subject to pulsational pair instability, decreasing mass by ejection of some amount of matter, and leaving remnants with mass less than $\sim 65 M_{\odot}$. Stars with He mass $\sim 65 - 135 M_{\odot}$ are affected by pair instability, disrupting the entire star and leaving no remnant compact object. Stars with He core $\gtrsim 135 M_{\odot}$ are considered to directly collapse to intermediate mass BHs [67, 68]. So, the collapse of a heavy star is unable to produce BHs in the mass range $\sim 65 - 150 M_{\odot}$.

Despite this fact, LVK were able to detect GWs coming from the systems in which one or both components are BH with masses in the range $50 - 107 M_{\odot}$. The most massive binary GW190426_190642 contained components with masses $107 M_{\odot}$ and $77 M_{\odot}$, producing a BH with mass $175 M_{\odot}$ after merger and radiating $11 M_{\odot}$ energy through gravitational waves [36]. The second most massive system GW190521 consisted of BHs with masses $95 M_{\odot}$ and $69 M_{\odot}$, radiating $8 M_{\odot}$ energy and producing a final BH with mass $156 M_{\odot}$ [30].

BHs with such high masses are currently discussed to be formed by a hierarchical mergers of smaller BHs [69–71]. In order to coalesce again, initial first generation BHs should be formed in triple or higher multipole systems, or such systems must be assembled in the dense stellar clusters. However, merger product receives a recoil kick from the anisotropic GW emission [72, 73], and it may eject them from clusters and leave unavailable to form new generations of binary BHs [74]. Also, even if effective spin parameter of binary BH system was almost zero, BH formed after their merger is characterized by high spin; so spin value may be a good indication for genealogy of BHs [75, 76]. In [69], the analyses of the ten BHs coalescence events from the first two observing runs of LIGO-Virgo detectors was made and no definite evidence of hierarchical mergers was found.

Merger rate of the events in which mass of one of the components lies in $50-100 M_\odot$ was estimated to be

$$\mathcal{R}_{50-100M_\odot} = 0.099 - 0.4 \text{ Gpc}^{-3}\text{yr}^{-1} \tag{4.16}$$

(Table IV in [43]). Simulations done for nuclear stellar clusters (where the hierarchical mergers are orders of magnitude more common than in globular and young star clusters) with low spin and broad distribution of escape velocities, yield $10^{-2} - 0.2 \text{ Gpc}^{-3}\text{yr}^{-1}$ [70]. In order to obtain such high merger rates, some optimistic assumptions are required. More specifically, in [71], merger rate of GW190521-like events was estimated as,

$$\mathcal{R}_{\text{GW190521}} = \mathcal{R}_{\text{1G}} \times f_{\text{triple}} \times f_{\text{survival}} \times f_{\text{merger}} , \tag{4.17}$$

where $\mathcal{R}_{\text{1G}} \sim 10 - 100 \text{ Gpc}^{-3}\text{yr}^{-1}$ is merger rate of first generation BHs and the value obtained from the first two observing runs [28]. Assuming a high survival, $f_{\text{survival}} \simeq 60\%$, and the large merger fraction, $f_{\text{merger}} \simeq 20\%$, together with the admission that formation fraction of stellar triple systems is $f_{\text{triple}} \simeq 50\%$, the coalescence rate of GW190521-like events was calculated to be [71]

$$\mathcal{R}_{\text{GW190521}} = 0.6 - 6 \text{ Gpc}^{-3}\text{yr}^{-1} . \tag{4.18}$$

We update this merger rate using the value from GWTC-3, $\mathcal{R}_{\text{1G}} \sim 2.5 - 6.3 \text{ Gpc}^{-3}\text{yr}^{-1}$ (Table IV in [43]), obtained for the systems in which the mass of the first component is $20-50 M_\odot$ and $5-50 M_\odot$ for the second component, i.e. systems that can potentially give 'heavy' systems through hierarchical mergers. Inserting this new value of $\mathcal{R}_{\text{1G}}$ in (4.17), one gets

$$\mathcal{R}_{\text{GW190521}} = 0.15 - 0.38 \text{Gpc}^{-3}\text{yr}^{-1} , \tag{4.19}$$

being in agreement with LVK estimations (4.16), but in the price of some extreme postulations.

Possibility of primordial origin of BHs of the event GW190521 was also considered [77]. But, as already mentioned there are tight constraints on mass distribution of primordial BHs [56] and some theories of primordial BH formation predict small component spins [78], that is inconsistent with GW190521. PBH mass can evolve during its cosmological evolution due to accretion [79]. Suppose that PBHs accrete efficiently before the reionization epoch, even the most massive event GW190521 can fit into the PBH scenario [80]. Opportunity of strong gravitational lensing by galaxies or galaxy clusters for the signal GW190521 was also discussed. However, low expected lensing rate and optical depth, and the absence of a multi-image counterpart, disfavor strong lensing hypothesis [77].

4.4 Binary Neutron Star and Neutron Star - Black Hole Systems

In this section we discuss BNS and BH-NS that will form and merge within a Hubble time. Stars within mass range from $\simeq 8 M_\odot$ to $\simeq 50 M_\odot$ will evolve up to a core collapse supernova explosion. The resulting remnant will be a NS if the mass of progenitor star is bellow $20 M_\odot$ otherwise a BH will be formed. Such heavy stars should arrive to the stage of supergiants of size about $30 R_\odot$, at the end of their life. If the initial separation of the components in BNS exceeds the size of the progenitor supergiants, the pure GWs inspiral time will be several order of magnitude the age of the Universe. In order to merge within the age of the Universe (Hubble time), initial separation of canonical BNS system must be less than five solar radius, $\lesssim 5 R_\odot$, in case the

inspiral is dominated by radiation of gravitational waves [81–83]. This implies that BNS system is formed through a common-envelope stage, where either both massive stars are not distinct or the primary forms a compact object before being enveloped by the secondary during its supergiant phase. Thus, the inspiral proceeds much faster and leads to tighter initial separation of the two compact objects. Also, NSs and BHs inside globular cluster could gravitate towards its center due to dynamical friction, leading to both a higher likelihood of dynamical capture and an accelerated inspiral aided by three-body interactions with other objects [84]. The two compact objects of BNS and BH-NS systems will lose energy to GWs, causing the objects to inspiral towards one another. The inspiral time scale ranges from $\simeq 85$ Myr to Hubble time. Thus, after long time of inspiraling the compact objects merge releasing GWs signal of great luminosity ($\simeq 10^{53}$ erg/s [85]). GWs emitted by a binary system are omnidirectional, however not isotropic [86]. In particular, it is strongest along the total angular momentum axis of the system (for inclination angles $l = 0°, 180°$) and weakest along the orbital plane ($l = 90°$).

4.4.1 Electromagnetic Counterpart Radiation

In some seconds after merging the NSs (NS in case of BH-NS merger) get disrupted releasing matter which is supposed to accrete the remnant object powering collimated ultra-relativistic polar jets [83, 87] and mildly relativistic quasi-isotropic outflows [88–90] that produce known electromagnetic and even neutrino counterparts. The jet results in a short gamma ray burst (SGRB) which is a luminous flare of highly variable up to MeV energy gamma radiation lasting less than 2 seconds. The emission from collimated ultra-relativistic jet can only be detected by an observer within jet opening angle, θ_i, due to Doppler beaming limiting the visibility region to inverse Lorentz factor Γ^{-1} (typically $\Gamma \sim 100$). Being launched, the jet must propagate trough to successfully break-out and move outwards at nearly c. The jet reaches the photometric radius where light can escape for the first time and may release the prompt SGRB emission due to collisions of internal shocks.

After the prompt emission the jet is still speeding away interacting with the surrounding circumburst material [91]. The bulk Lorentz factor of the interacting jet slows down, the observable angle grows, the jet starts to emit synchrotron radiation across nearly entire electromagnetic spectrum, which can be detected from radio to GeV energies [91] as SGRB afterglow.

The unbound matter from a merger behaves differently than the bound material that powers the ultra-relativistic jet causing a SGRB. In this case, the neutron rich ejecta containing from $10^{-3} M_\odot$ to $0.1 M_\odot$ moves outwards at a ~ 0.1-0.3 c. The ejecta expands and rapidly cools down losing the energy through thermal neutrino emission. Eventually, in ~ 10-100 ms, it enters relatively slow homologous expansion and the period of synthesis of heavy elements in the so-called r-process. Nuclei freshly synthesized by the r-process are radioactive and decay back to stability. The energy released via β decays and fission can power a thermal transient lasting days to weeks, commonly known as a kilonova [88–90]. Kilonovae are promising electromagnetic counterparts of BNS and BH-NS mergers because their emission is approximately isotropic (in contrast to beamed SGRBs) and can peak at optical, ultra violet and infrared wavelengths. Brightness, duration, and colors of kilonovae are diagnostics of physical processes taking place in mergers [83, 88–90]. When ejection energy ends the kilonova cools down and fades. The quasi isotropic ejecta will continue to move outwards to go, in next few months and years, into the nebula phase. At deceleration radius where the ejecta swept up a comparable amount of material from the surrounding environment, it will transform to a blast wave that releases synchrotron radiation in the radio bands [92–94], analogously described as a kilonova afterglow.

The earliest observable signal from BNS and BH-NS mergers are GWs. They are used in both the detection and characterization of these events as well as in providing localization information for search with other instruments. The merger rate of BNS and BH-NS systems, inferred form LVK data was presented above by the equations (4.4) and (4.2) correspondingly. As we described above the NSs mergers should be accompanied by electromagnetic signals of various wavelengths generated in the evolution of central remnants. First, we focus on the joint searches for GWs and prompt SGRB emission. The total rate of SGRBs depends on the half-jet opening angle distribution, which, in its turn, can be estimated with the measured jet break in the afterglow light curve [95]. Since, the jet breaks are rarely detected the total rate of SGRBs is quite uncertain and reads 1109^{+1432}_{-657} Gpc^{-3}yr^{-1} [96]. Moreover, neglecting one SGRB with particularly narrow half-jet opening angle one arrives to 162^{+140}_{-83} Gpc^{-3}yr^{-1} [96]. Both estimates lie within the range (4.4) inferred by LVK. Because of the solid angle effect only a fraction of successful SGRBs jets can be oriented towards the Earth. Since the emission of gravitation waves is omnidirectional one expects that this fraction of SGRBs would be associated with gravitationally detected BNS or BH-BNS mergers. Recall, that the gravitation emission is stronger when a binary system is more face on. Therefore, the ultra-relativistic jet, which is believed to be aligned with the polar axis of the remnant, should correlate with the strength of the GW signal. The observed inclination angle probability density for gravitationally detected NS mergers is maximized at $l \simeq 30°$ [86]. It was found in [83] that a comparison of the observed inclination angle distribution for NS mergers detected through GWs [86] and prompt SGRBs distribution [91] tells us that roughly 1 in 8 BNS (BH-NS) mergers with detected gravitational signal can spot the Earth within the jet angle. If we restrict ourselves only with the more likely face on systems similar to those like GW170817, where $l < 55°$ [27], the joint observation rate of GW and SGRB signals can become somewhat higher, namely 1 in about 5. Finally, assuming an improvement in signal to noise ratio in gravitational measurements of the NS systems, which would probably give $l < 27°$ for GW170817 [97], one may expect a sort of 1 to 1 correspondence for systems less than 30° off from being face on.

Beyond SGRB detection, the joint observations of GWs and electromagnetic counterparts can be performed through finding of SGRB afterglows, kilonovae, and other expected electromagnetic transients from NS mergers. In general, follow-up searches should not expect to recover those events that occur near the Sun [83]. For the space based searches the constraint spreads out over about 45° of the Sun, for many narrow-field space-based telescopes like Swift, Hubble, Chandra etc. It is clear that the ground-based limitations are stricter, namely a few hours of RA from the Sun, for a compatible size exclusion zone obtained from the GW triggering facilities. An exception could be events detectable long enough that the Sun moves across the sky, which typically requires months of detectibility. Usually, the events are getting identified within a week or so. Either case rules out about 15% of the sky. Also, one should not rely on recovery of SGRB afterglow and kilonovae in case they occur within several degrees of the galactic plane, because of extinction and high rate of transients at lower energies. Following the claim of [83], one can accept that follow-up observations are capable to recover up to 80% of GW triggers.

We assume that every BNS (BH-NS) system triggered in GWs should produce observable signatures in electromagnetic messengers across wide ranges of energies and time. The particular attention we pay the canonical types of counterparts such as SGRBs, SGRB afterglows and kilonovae. Relying on the discussion above, we accept that it is very likely that at least one type of the counterpart should be recovered in prompt and follow up observations. Since all analyzed canonical signals from NS mergers are brighter when observed from polar position

than from equatorial one, especially likely recovery is expected for those BNS (BH-NS) mergers detected not too much off (that means within $\sim 30°$) from its face on position with respect to GWs observations.

As already pointed out, no electromagnetic counterpart has been reported in O3 data and GW170817 remains as the only multimessenger event. Of course, not each of the pottential multimessenger events are well localized because the lack of triggers in one of three detectors. Also, because of the lack of the information about the estimation on inclination angles one cannot be confident that each ultra-relativistic jet putatively producing a SGRB is somehow aligned with the polar axis of the remnant and hence well orientated for recovery of the SGRB or its afterglow. Kilonovae counterparts could also escape the detection as being subluminous in the BNS range of $\simeq 200$ Mpc accessible for current advanced LVK sensitivity or being localized around Sun or the galactic plane. Although, the joint GW-kilonovae detection rate could achieve 21 per year within the BNS horizon of the advance LVK network, as estimated in [83].

4.4.2 The Sources Near the Lower Mass Gap

The latest version of GW catalog [36] includes some notable events near the lower mass gap:

- GW190425 is probably the merger of BNS system with masses $2.0^{+0.6}_{-0.3}M_\odot$ and $1.4^{+0.3}_{-0.3}M_\odot$ [29];

- GW200105 with component masses $8.9^{+1.2}_{-1.5}M_\odot$ and $1.9^{+0.3}_{-0.2}M_\odot$ and GW200115 with component masses $5.9^{+2.0}_{-2.5}M_\odot$ and $1.44^{+0.85}_{-0.29}M_\odot$ are the very first detection of merger of BH-NS systems [35];

- GW190814 is a merger of a $23.2^{+1.1}_{-1.0}M_\odot$ BH with a $2.59^{+0.08}_{-0.09}M_\odot$ compact object [32] and GW200210_092254 is coalescence of $24.2^{+7.5}_{-4.7}M_\odot$ BH with a $2.83^{+0.48}_{-0.43}M_\odot$ compact object.

Uncertainties are given at the 90% credible level. It is important to notice, that none of these events had accompanying electromagnetic radiation, while it is expected that such cataclysmic events should emit GRBs.

Moreover, what matters is that the distribution of masses of X-ray binaries reveal apparent so-called lower mass gap $2.5 - 5M_\odot$ between NSs and BHs [102, 103]. The aforementioned components of LVK events lie on the edge of that mass gap. Some theoretical models of supernova explosions predict existence of the observed mass gap [104, 105]. Nonetheless, some models suggest a smooth transition from NS to BH masses [106, 107].

In principle, both components of GW190425 are consistent with being NSs. While the mass of the one component, $1.4^{+0.3}_{-0.3}M_\odot$, falls in a typical range of observed pulsars, the heavier component with the mass $2.0^{+0.6}_{-0.3}M_\odot$ also can be a NS, as far as existence of pulsars with mass of $\sim 2M_\odot$ were confirmed by observations [108, 109]. But there was no optical counterpart to GW190425, unlike the famous NS-NS merging event GW170817. With the source-frame chirp mass $1.44M_\odot$ and the total mass $3.4M_\odot$, the GW190425 system is significantly more massive than any binary NS system observed through electromagnetic radiation.

The most common mechanism for formation of binary NS systems is an isolated binary evolution channel (for a review see [110]). Following this path, GW190425 may suggest a population of binary NSs formed in ultra-tight orbits with sub-hour orbital period [29]. In order to achieve the system like this, it is required to have a phase of mass transfer from post-helium main sequence star onto NS. If the mass ratio between He-star and NS is high

enough, a common-envelope phase is formed that would shrink the binary orbit to sub-hour periods [111]. If binary survives this common envelope phase, the subsequent supernova kick may be suppressed, as the secondary would likely be ultra-stripped [112]. The small supernova kick, together with very tight orbital separation, increases the chance for binary to remain bound after supernova. Hierarchical mergers of NSs or mass accretion in active galactic nuclei disks, may also be responsible for the creation of compact objects in the lower mass gap [113]. Other possible scenarios, like dynamical formation channels in globular clusters or gravitational lensing of the source of GW190425, is also discussed [29]. However, lack of objects discovered with given properties, does not allow to have a definite theory for their formation mechanism for now.

In the case of GW190814 and GW200210_092254, the first components are definitely a BHs. But the second objects certainly lay in the lower mass gap, if such really exists. They are heavier than the most massive known pulsar and lighter than any BH discovered so far. The masses of the secondary components $2.59^{+0.08}_{-0.09}$ and $2.83^{+0.48}_{-0.43}M_\odot$ exceed the possible maximum mass allowed for a stable NS in most of the models [114, 115]. However, due to theoretical uncertainties the NS-BH scenario cannot be ruled out, e.g. the second components can be a NSs in view of some stiffer equation of state of dense nuclear matter [116]. It is also possible that they are a quark stars in which the original NS was transformed due the fallback of the material after the gravitational collapse of a progenitor star [117]. Thus, GW190814 and GW200210_092254 can be viewed as a BH-NS (or quark star) merger which in principle could have an associated GRB and optical counterpart. The probability for the secondary component of GW190814 and GW200210_092254 being exotic compact object, like boson star [118], gravastar [119], strange-quark star [120] or up-down quark star [121] was also considered.

For the completeness, note that the secondaries of the LVK events named GW190814 and GW200210_092254 are presumably BHs, which may have formed by coalescence of NSs, e.g. the remnant of the event GW170817 has the similar mass [27]. But to merge again, hierarchical triple system in the field [52, 122] or in the galactic center [123, 124] must be considered.

4.5   Problems and Our Suggestion

Summarizing the LVK data of GWs, we outline some main disagreements between existing models and observations:

- **Lack of multi-messenger events:** As we have seen in the section (4.4.1), merger of a NS with a NS or with a BH must be accompanied by different types of electromagnetic radiation and in the most of the configurations these signals should be observable on the Earth. However, despite detecting several events involving NSs, the only one event GW170817 had associated SGRB. Even in case of BBH mergers, if they accret matter, they can produce EM radiation as well.

- **Upper mass gap objects:** The theories of stars evolution predict, that if the core of a star becomes heavy enough, pair instability processes ejects some mass or disrupt entire star (section 4.3.3). Therefore, BHs above certain mass were not expected to exist. However, the LVK data contains multiple events involving BHs in this forbidden mass range.

- **Lower mass gap objects:** According to many models, transition between the mass distributions of NSs and BHs cannot be smooth. Thus, there should be a mass gap

between $\sim 2.5 - 5 M_\odot$, that is supported by the observation of X-ray binaries (sec. 4.4.2). Nevertheless, the LVK data includes compact objects that fall in this mass range.

- **Merger rates:** The merger rates for the different kind of systems estimated from the LVK data (sec. 4.2.2) are reproduced in different theories of binary compact objects formation and merger, only in price of some extreme assumptions (sec. 4.3.2).

Intending to deal with these disagreements between the LVK data and the theories, we propose that these GWs have been emerged from a hidden parallel sector - a mirror world. The mirror world is a candidate of dark matter and it assumes, that all elementary particles have their twin mirror partners that are invisible for us. Only way for the interaction between ordinary and mirror worlds is the gravitational force (and maybe also some another weak force). Thus, gravitational waves can pass between the worlds, while electromagnetic radiation will be unnoticeable for our detectors. Besides, mirror sector is colder than ordinary world and it is dominated by helium. This suggests that, mirror stars are born with higher mass and evolve faster, that can potentially explain mass gap objects and high merger rates. In the next chapter we review the mirror world model.

Chapter 5

Mirror World Model

In the previous chapters we have discussed Einstein's theory of General Relativity, that perfectly describes gravitational interactions between massive objects. In principle, hidden sector of the Universe, i.e. dark matter and dark energy could also be a subject to the laws of GR. However, in addition to the gravitational force, there are three other fundamental interaction in nature. The Standard Model (SM) of particle physics describes all known elementary particles and their interactions via electromagnetic and weak and strong nuclear forces. As no DM particle has been detected so far, theory of particle physics has no definite vision about their nature. Phenomenologically, a full Lagrangian of particle physics can be presented as

$$\mathcal{L} = \mathcal{L}_{\mathrm{SM}} + \mathcal{L}_{\mathrm{dark}} + \mathcal{L}_{\mathrm{mix}} \ , \tag{5.1}$$

where $\mathcal{L}_{\mathrm{SM}}$ describes the Standard Model, $\mathcal{L}_{\mathrm{dark}}$ stands for the theory of dark matter particles and $\mathcal{L}_{\mathrm{mix}}$ could be a possible interaction between these two sectors. In the absence of mixing part, no particle physics experiment can tell the existence of hidden sector.

The theory of Mirror World assumes that $\mathcal{L}_{\mathrm{dark}}$ is an exact copy of SM, but with a very weak mixing part. So, all elementary particles have their twin mirror partners that are almost hidden, but as they can also form (mirror) matter, their existence can be sensed via gravitational effects. This chapter is devoted to a review of mirror world theory. But until that, we make a brief introduction to the Standard Model of particle physics.

5.1 Standard Model of Particle Physics

5.1.1 Overview

The current view of elementary particle physics is described by the Standard Model (SM) [125]. It is a fundamental theory based on the assumptions of Lorentz invariance, gauge invariance and renormalizability. According to their intrinsic characteristic - spin, elementary particles are divided into two types: fermions (half integer spin) and interaction carrier bosons (integer spin). Three fundamental forces - strong, electromagnetic and weak are described as a gauge theory of local symmetry group

$$SU(3)_C \times SU(2)_L \times U(1)_Y \ , \tag{5.2}$$

where the subscripts C, L and Y stands for color, left-handed chirality and weak hypercharge respectively. Each type of interactions are mediated by the bosons of their group and are characterized by coupling constants. $SU(3)_C$ is the non abelian local symmetry group of Quantum

Chromodynamics (QCD), which describes strong interaction via the mediation of the eight massless gluons. The direct product $SU(2)_L \times U(1)_Y$ describes electroweak interaction (EW), mediated by the three massive boson $W^\pm$ and Z and the massless photon γ. The fermions are divided into quarks and leptons and are classified in three generations. The three up-type quarks with electric charge $+\frac{2}{3}e$ are the *up* quark (u), *charm* quark (c) and *top* quark (t), and down-type quarks with electric charge $-\frac{1}{3}e$ are the *down* quark (d), *strange* quark (s) and *bottom* quark (b). There are three negatively charged leptons: electron (e), muon (μ) and tau (τ), and corresponding three neutrinos:: electron neutrino (ν_e), muon neutrino (ν_μ) and tau neutrino (ν_τ). These six quarks and six leptons are grouped in three generations, which are given in Table (5.1). The quarks have a baryon number $B = 1/3$ and the leptons have a lepton number $L = 1$.

Electric charge	1st generation	2nd generation	3rd generation
+2/3	u	c	t
−1/3	d	s	b
0	ν_e	ν_μ	ν_τ
−1	e	μ	τ

Table 5.1: Quarks and leptons in the Standard Model

Particle content of SM can be collected in irreducible representation of the EW gauge group. It is important to note that left-handed (L) and right-handed (R) components of the fermion fields belongs to different irreducible representation, therefore, SM is also defined as an *axial* or *chiral* theory. Fermions are represented as Weyl spinors, left-handed quarks and leptons f_L are transforming as doublets and right-handed quarks and leptons f_R as singlets:

$$f_L: \quad q_L = \begin{pmatrix} u_L \\ d_L \end{pmatrix}_i, \quad l_L = \begin{pmatrix} \nu_L \\ e_L \end{pmatrix}_i; \qquad f_R: \quad u_R, \ d_R, \ e_R. \tag{5.3}$$

Index i runs through three generation of particles. Each particle in SM has corresponding antiparticle that has opposite charge. All the analyses stated below employs antiparticles as well, but we will come back to discuss them in more details in other sections.

5.1.2 Strong Interaction

At first we briefly examine the theory of Strong interactions. Quantum Chromodynamics (QCD) is the gauge Quantum Field Theory (QFT) which takes into account interactions between coloured quarks and gluons. All six quarks and six antiquarks are represented in three colours: Green, Blue, Red. Eight generators of adjoint representation of $SU(3)_C$ group - called Gell-Mann matrices - corresponds to eight massless gluons. Gluons carry the color charge and are mediators of quarks interactions via exchanging the color charges. QCD lagrangian is invariant under the $SU(3)_C$ group transformations and has the form:

$$\mathcal{L}_{QCD} = -\frac{1}{4} \sum_{a=1}^{8} G_a^{\mu\nu} G_{\mu\nu}^a + \sum_{j=1}^{n_f} \bar{q}_j \left(i\slashed{D} - m_j \right) q_j \ , \tag{5.4}$$

where q_j are the quark fields of n_f different flavors with mass m_j. The covariant derivative $\slashed{D} = \gamma^\mu D_\mu$ (γ^μ are Dirac matrices) is given by

$$D_\mu = \partial_\mu - ig_s G_\mu \ . \tag{5.5}$$

43

g_s is the strong coupling constant and gauge field is represented as

$$G_\mu = \sum_a \lambda^a G_\mu^a \ , \tag{5.6}$$

where G_μ^a are the gluon fields and λ^a are the generators of $SU(3)_C$.

QCD has the properties of confinement and asymptotic freedom. Confinement says that no isolated colored charge can exist but only color singlet particle. For example the quark-antiquark potential has a Coulomb part at short distances and a linearly rising terms at long distances:

$$V_{q\bar{q}} \propto \left[\frac{\alpha_s(r)}{r} + \cdots + \sigma\, r \right] \tag{5.7}$$

where $\alpha_s = g_s^2/4\pi$. The linearly rising term makes energetically impossible to separate a $q - \bar{q}$ pair. If the pair is created at one space-time point and then the two particles start to moving away from each other in the center of mass frame, it soon become energetically favourable to create additional pairs, which neutralize color and allow the finale state to be reorganized into two jets of colorless hadrons. Property of asymptotic freedom states that if two quarks are close enough they behave like a free, unbound particles.

5.1.3   Electroweak Theory

The SM Lagrangian for Electroweak part consists of three pieces, gauge kinetic term, the Higgs potential, and the Yukawa interaction. It is given as

$$\mathcal{L}_{SM} = \mathcal{L}_{gauge} + \mathcal{L}_{Higgs} + \mathcal{L}_{Yuk}. \tag{5.8}$$

The first part contains the kinetic terms for fermion and gauge fields such as:

$$\mathcal{L}_{gauge} = i \sum_\alpha \bar{f}_{\alpha L} \slashed{D} f_{\alpha L} + i \sum_\alpha \bar{f}_{\alpha R} \slashed{D} f_{\alpha R} - \sum_a \frac{1}{4} F_{\mu\nu}^a F_a^{\mu\nu} \ , \tag{5.9}$$

where f is generic fermionic field, α runs over the fermionic flavours, $F_{\mu\nu}$-s are the gauge-field strengths tensors and index a runs over all electroweak gauge fields. Covariant derivative is defined as $(\slashed{D} = \gamma^\mu D_\mu)$

$$D_\mu = +ig\frac{\tau^a}{2}W_\mu^a + ig'Q_Y B_\mu \ , \tag{5.10}$$

where g and g' are the gauge coupling constants for $SU(2)_L$, and $U(1)_Y$, respectively. τ^a $(a = 1, 2, 3)$ are the Pauli matrices for a $SU(2)$ group

$$\tau_1 = \begin{pmatrix} 0 & 1 \\ 1 & 0 \end{pmatrix} \quad \tau_2 = \begin{pmatrix} 0 & -i \\ i & 0 \end{pmatrix} \quad \tau_3 = \begin{pmatrix} 1 & 0 \\ 0 & -1 \end{pmatrix} \ . \tag{5.11}$$

Masses of the particles are generated via Higgs mechanism and Spontaneous Symmetry Breaking (SSB). SSB occurs when a lagrangian has some exact symmetry but the solution to the equations of motions do not. The Goldstone theorem states that the SSB of a continuous symmetry in QFT implies the existence of massless spin zero particles, the *Goldstone Bosons*. It comes out that if SSB occurs in a gauge theory with massless vector bosons and scalar fields, the Goldstone bosons transfer their degrees of freedom to the longitudinal mode of the vector

fields which therefore becomes massive particles, this is the so called *Higgs Mechanism*. Higgs lagrangian has the form:

$$\mathcal{L}_{Higgs} = (D_\mu \Phi)^\dagger (D^\mu \Phi) - \mu^2 \Phi^\dagger \Phi - \lambda \left(\Phi^\dagger \Phi \right)^2 \tag{5.12}$$

The coefficient λ must be positive to have the Higgs potential bounded from below and μ^2 must be negative in order to have SSB of $SU(2)_L \times U(1)_Y$. The Higgs potential has a set of minimum values in the classical configuration determined by:

$$\Phi^\dagger \Phi = \frac{v^2}{2} = \frac{-\mu^2}{2\lambda} , \tag{5.13}$$

where v is the vacuum expectation value (VEV) of the Higgs field. Since the vacuum state is invariant under gauge transformation of a U(1) group and the vacuum state must be neutral, we can set:

$$\langle \Phi \rangle = \frac{1}{\sqrt{2}} \begin{pmatrix} 0 \\ v \end{pmatrix} . \tag{5.14}$$

As stated before, according to the Goldstone theorem for every SSB the theory must contain a massless particle, in the case of Electroweak theory, the three broken degrees of freedom are absorbed by the three physical weak gauge bosons ($W^\pm$ and Z), which becomes massive particles. In the unitary gauge the Higgs doublet can be written as:

$$\Phi(x) = \frac{1}{\sqrt{2}} \begin{pmatrix} 0 \\ v + H(x) \end{pmatrix} , \tag{5.15}$$

where the field H(x) is the physical Higgs boson, which is an excitation of the neutral field $\Phi(x)$.

Inserting eq. (5.15) in eq. (5.12), H, $W^\pm$ and Z bosons acquire masses, while photon remains massless:

$$\mathcal{L}_{mass} = -M_H^2 H^2 + M_Z^2 Z_\mu^2 + M_W^2 W_\mu^\dagger W^\mu , \tag{5.16}$$

where

$$M_H = \sqrt{2\lambda v^2} \tag{5.17}$$

$$M_W = \frac{g\,v}{2} \tag{5.18}$$

$$M_Z = \frac{g\,v}{2\cos\theta_W} . \tag{5.19}$$

θ_W is weak mixing angle or Weinberg angle

$$\tan\theta_W = \frac{g'}{g} \tag{5.20}$$

and electric charge is

$$e = \frac{gg'}{\sqrt{g^2 + g'^2}} = g\sin\theta_W . \tag{5.21}$$

The mass of the W boson can be related to the Fermi constant via the equation:

$$\frac{G_F}{\sqrt{2}} = \frac{g^2}{8\,M_W^2} \tag{5.22}$$

and measuring the muon lifetime, one can extract interaction constant G_F and using the equations (5.18), (5.22) compute the VEV of the Higgs field:

$$v = \left(\sqrt{2}G_F\right)^{-\frac{1}{2}} \simeq 246 \text{ GeV} .$$
(5.23)

The Lagrangian of the Yukawa term for the quark sector after the SSB acquires the form:

$$\mathcal{L}_{Yuk} = -\left(\frac{v+H}{\sqrt{2}}\right)\left[\bar{q}_L^D Y^D q_R^D + \bar{q}_L^U Y^U q_R^U\right] + h.c.$$
(5.24)

where U and D stand for all up-type and down-type quarks and Y^D and Y^U are Yukawa coupling matrices. Quarks of different generation can decay into one another and so their mass eigenstates need to be linked with physical quark field that participate in weak interaction. Diagonalizing Y^D and Y^U through biunitary transformation, one finds the so-called Cabbibo-Kobayashi-Maskawa (CKM) matrix as a connection that embodies the physical effects of quark mixing:

$$V_{\text{CKM}} = \begin{pmatrix} V_{ud} & V_{us} & V_{ub} \\ V_{cd} & V_{cs} & V_{cb} \\ V_{td} & V_{ts} & V_{tb} \end{pmatrix}$$
(5.25)

After this transformation mass terms obtain the form:

$$\mathcal{L}_{mass} = -\sum_{\alpha=d,s,b} \frac{y_\alpha^D v}{\sqrt{2}} \bar{q}_{L\alpha}^D q_{R\alpha}^D - \sum_{\alpha=u,c,t} \frac{y_\alpha^U v}{\sqrt{2}} \bar{q}_{L\alpha}^U q_{R\alpha}^U$$

where the quark masses are defined as

$$m_\alpha = \frac{y_\alpha^{U,D} v}{\sqrt{2}} ,$$
(5.26)

with y_α being the Yukawa coupling constants.

The mixing matrix (5.25) can be parametrized in terms of three angles and one phase:

$$V_{CKM} = \begin{pmatrix} c_{12}c_{13} & s_{12}c_{13} & s_{13}e^{-i\delta} \\ -s_{12}c_{23} - c_{12}s_{23}s_{13}e^{i\delta} & c_{12}c_{23} - s_{12}s_{23}s_{13}e^{i\delta} & s_{23}c_{13} \\ s_{12}s_{23} - c_{12}c_{23}s_{13}e^{i\delta} & -c_{12}s_{23} - s_{12}c_{23}s_{13}e^{i\delta} & c_{23}c_{13} \end{pmatrix}$$
(5.27)

with: $c_{ij} = \cos\theta_{ij}$ and $s_{ij} = \sin\theta_{ij}$ and it is a very important object that is responsible for a CP-violation, that is discussed in the next section.

5.1.4 C, P and T-symmetries

C-symmetry: Charge conjugation operation is a transformation that switches all particles with their corresponding antiparticles, i.e, changes the sign of their charges (not only electric charge but also baryon number, lepton number, etc). Charge conjugation operation is defined as:

$$C\gamma_\mu C^{-1} = -(\gamma_\mu)^T ,$$
(5.28)

where $(\cdot)^T$ stands for matrix transpose and γ_μ are Dirac gamma matrices that are constructed using Pauli matrices (5.11)

$$\gamma^0 = \sigma^3 \otimes I, \quad \gamma^i = i\sigma^2 \otimes \sigma^i$$
(5.29)

(I is an identity matrix and $\otimes$ stands for Kronecker product). The explicit form that C takes is dependent on the specific representation and, for example, in Dirac basis is equal to $C = \gamma^0 \gamma^2$. Taking the fermionic content of SM:

$$f_L: \quad q_L = \begin{pmatrix} u_L \\ d_L \end{pmatrix}_i, \quad l_L = \begin{pmatrix} \nu_L \\ e_L \end{pmatrix}_i; \qquad f_R: \quad u_R, \ d_R, \ e_R, \tag{5.30}$$

then the field operators $\bar{f}_R = C\gamma_0 f_L^*$ and $\bar{f}_L = C\gamma_0 f_R^*$ describe antifermions that have opposite gauge charges and opposite chiralities:

$$\bar{f}_R: \quad \bar{q}_R = \begin{pmatrix} \bar{u}_R \\ \bar{d}_R \end{pmatrix}_i, \quad \bar{l}_R = \begin{pmatrix} \bar{\nu}_R \\ \bar{e}_R \end{pmatrix}_i; \qquad \bar{f}_L: \quad \bar{u}_L, \ \bar{d}_L, \ \bar{e}_L. \tag{5.31}$$

The fact that left-handed antineutrino, that is a charge conjugated of a left-handed neutrino, does not exist in SM, makes it obvious that C-symmetry is violated in SM.

P-symmetry: Parity transformation is a flip in a sign of spatial coordinates $P : (t, \mathbf{x}) \to (t, -\mathbf{x})$ and for a long time parity was thought to be a symmetry of the nature. That meant, the Universe should look the same if one sees it through the mirror that reverses all spatial axes. Actually, parity was tested to be conserved in electromagnetic and strong interactions, however, Lee and Yang proposed that it may be broken in some β-decays [126].

The particle content of the Standard Model and hence its Lagrangian is not symmetric under the exchange of the L and R particles: $f_L \leftrightarrow f_R$. In particular, the gauge bosons of $SU(2)$ couple to the f_L fields but do not couple to f_R ones.

Soon after Lee&Yang's proposal, Wu observed, that in the decay of radioactive ^{60}Co, less β-particles were emitted in the direction of nuclear spin than in the opposite direction, that served as a experimental confirmation of parity violation [127].

CP-symmetry: It was strongly believed that, besides the violation of C and P symmetries, the combined CP-symmetry should be conserved. That means, that the symmetry between left (right) particles and their right (left) antiparticles $f_L \to \bar{f}_R$ ($f_R \to \bar{f}_L$) must hold, as antiparticles having opposite charge and handedness, are CP-conjugated of corresponding particles. The weak interactions for particles are left-handed ($V - A$); for antiparticles, as the right-handed ones couple to the $SU(2)$ bosons, interactions are right-handed ($V + A$). CP could be an exact symmetry as far as it is respected by gauge interactions, but it is not by Yukawa terms. Diagonalizing the Yukawa matrices in (5.24), irremovable complex phase arises that is present in CKM matrix (5.27). This complex phase is responsible for the CP-violation in SM. In fact, CP-violation is tiny, but it was first observed in the decay of neutral kaons in 1990s and then confirmed by other experiments.

Furthermore, it appears that the CP violation is the mandatory condition for generation of baryon asymmetry in the Universe. Our universe is filled with matter and there are no objects compound of antimatter. This must be a consequence of some processes at the early universe that produced baryons and anti-baryons at different rates. According to Sakharov [128], three conditions are necessary to get such picture: (i) baryon number violation; (ii) C and CP violation; (iii) interactions out of equilibrium.

T-symmetry: Time reversal symmetry is a symmetry of physical laws under the transformation of time reversal $T : t \mapsto -t$. Since the second law of thermodynamics states that entropy increases as time flows toward the future, in general, the macroscopic universe is not symmetric under time reversal. Besides that, weak interaction also demonstrates the violation of time reversal. In certain β-decays, the exchange of initial and final states show the asymmetry between the transition probabilities.

The violation of T is a mandatory condition for a CPT symmetry. According to the CPT theorem, any Lorentz invariant local quantum field theory with a Hermitian Hamiltonian must be invariant when applying charge conjugation, parity transformation and time reversal transformations altogether.

As CP is violated, in order to have CPT invariance, also T must not hold. Besides that, combinations of any two of these transformation does not give a symmetry. But it is believed, that CPT is an exact symmetry of nature at the fundamental level and there is no experimental evidence of its possible violation.

5.2 Mirror World

In this section we turn into investigation of mirror world theory. For the foundation and in-depth description of the model see [129–134].

5.2.1 Restoring Broken Symmetries

As said before, parity symmetry is violated and there is a clear difference between left-handed and right-handed systems. In order to restore this symmetry, existence of other sector of particles was suggested in which parity is violated in an opposite way. Such "mirror" particles would restore the global P-symmetry of nature. At first, antiparticles were considered as these "mirror" particles, as they showed the basic properties demanded for such particles. The absolute values of all their fundamental parameters (mass, charge, lifetimes, the relative probabilities of different decay channels) seemed to be strictly equal to the same parameters of the particles. Indeed, the CP-transformation matches the observed left-handed state of the neutrinos with the right-handed state of antineutrinos

$$CP : \quad \nu_L \to \bar{\nu}_R \tag{5.32}$$

and since the right-handed antineutrino is also born in weak interactions, the symmetry between left and right is restored. Likewise, conversion of P-parity matches the β^+-decay of antinuclei with the β^--decay of polarized nuclei. Theory of P-violating weak interactions predicts the opposite direction of the preferred positron emission compared with the emission of electrons. Consequently, the combination of mirror reflection together with interchange of the particles and antiparticles seemingly supports the equivalence of left-handed and right-handed coordinate systems.

However, the discovery of CP-violation showed the wrong choice of selecting antiparticles as mirror partners, and once again raised the question of finding the true set of mirror particles and their expected properties. It turned out that when the mirror particles are not identified with antiparticles, they can not participate in the same interactions as ordinary particles. The strict symmetry between the ordinary and mirror electrons leads to serious problems in atomic physics, if ordinary and mirror worlds take part in the same electromagnetic interaction. We

should in this case expect doubling of atomic states because of the additional degrees of freedom associated with the mirror electron states [129].

In the paper [129], Kobzarev, Okun and Pomeranchuk postulated the existence of hypothetical mirror particles and mirror world. According to [129], mirror particles cannot participate in ordinary strong and electromagnetic interactions with ordinary particles. The hidden mirror sector must have its own strong and electromagnetic interactions. This means that mirror particles, like ordinary ones, must form mirror atoms, molecules and, under favorable conditions, invisible mirror stars, planets and even mirror life. Being able to create a structure, mirror matter would be capable to interact with ordinary matter via gravitational force. In 1980s and 1990s, mirror world model began to be considered as a dark matter candidate. For the history of development of mirror world theory see [132].

Such a theory can naturally emerge in the context of the heterotic string theory [130], based, for example, on the $E_8 \times E_8'$ gauge group. In such group $E_8 \leftrightarrow E_8'$ symmetry can originate two forms of matter: ordinary and shadow, with the interactions described by the gauge groups E_8 and E_8', respectively. The particular case of the shadow world can be the mirror world.

Also, in the language of extra dimensions and brane-worlds, one can imagine the mirror world as a five-dimensional theory, with parallel 3D-branes located in two fixed points; ordinary matter being localized on the left-brane and mirror matter localized on the right-brane, while gravity can freely pass between these two branes.

In the upcoming sections our discussion mainly follows the review article *"Through the Looking-Glass: Alice's Adventures in Mirror World"* [131] by Z. Berezhiani.

5.2.2   Mirror Standard Model

We have seen that CP violation does not allow us to consider antiparticles as "mirror" particles. However, one can expand the theory and make it symmetric between left and right. Consider that the transformation of coordinates $P : x \rightarrow -x$ is accompanied by the transformation that interchanges ordinary fields f, ϕ into corresponding hypothetical mirror fields f', ϕ', in the following manner [131]:

$$f_L, \bar{f}_L \rightarrow \gamma_0 f_R', \gamma_0 \bar{f}_R', \quad f_R, \bar{f}_R \rightarrow \gamma_0 f_L', \gamma_0 \bar{f}_L', \quad \phi \rightarrow \phi' . \tag{5.33}$$

From now on, all fields and quantities of the mirror (M) sector will be marked by prime $'$ to distinguish from the ones belonging to the observable ordinary (O) world. Such a symmetry can be called matter parity MP. Obviously, it implies that the gauge couplings are exactly the same for two sectors, the Higgs potentials are identical, while for the Yukawa coupling constants we have

$$Y_{u,d,e}' = Y_{u,d,e}^*. \tag{5.34}$$

In this way, introducing M-world does not brings in any new parameter. So, in this case the particle physics of the M-world will be exactly the same in terms of the R-fields $\bar{f}_R', f_R'$ as that of the O-world in terms of L-fields $f_L, \bar{f}_L$. Hence, MP restores the left-right symmetry as a symmetry between two sectors.

Assuming that particle physics is described by SM and gauge symmetry group $SU(3) \times SU(2) \times U(1)$, mirror particle physics would be presented by analogous gauge group $SU(3)' \times SU(2)' \times U(1)'$. As each elementary particle has its mirror partner, fermion content (5.30) has corresponding mirror fermion sector:

$$f_L' : \quad q_L' = \begin{pmatrix} u_L' \\ d_L' \end{pmatrix}_i, \quad l_L' = \begin{pmatrix} \nu_L' \\ e_L' \end{pmatrix}_i ; \quad f_R' : \quad u_R', \ d_R', \ e_R', \tag{5.35}$$

and antifermions (5.31) have corresponding mirror antifermions:

$$\bar{f}'_R: \quad \bar{q}'_R = \begin{pmatrix} \bar{u}'_R \\ \bar{d}'_R \end{pmatrix}_i, \quad \bar{l}'_R = \begin{pmatrix} \bar{\nu}'_R \\ \bar{e}'_R \end{pmatrix}_i; \qquad \bar{f}'_L: \quad \bar{u}'_L, \ \bar{d}'_L, \ \bar{e}'_L. \tag{5.36}$$

We note that we have prescribed mirror baryon number $B' = 1/3$ to quarks q'_L, u'_R, d'_R and mirror lepton number $L' = 1$ to leptons l'_L, e'_R, and so antiquarks $\bar{q}'_R, \bar{u}'_L, \bar{d}'_L$ have $B = -1/3$ and antileptons $\bar{l}'_R, \bar{e}'_L$ have $L' = -1$.

The Lagrangian of QCD (5.4) as well as the electroweak part (5.8) are presented with their mirror analogs. For example, mirror EW Lagrangian has the form:

$$\mathcal{L}'_{SM} = \mathcal{L}'_{gauge} + \mathcal{L}'_{Higgs} + \mathcal{L}'_{Yuk}, \tag{5.37}$$

in which each part consists of primed quantities.

5.2.3 Kinetic Mixing of Ordinary and Mirror Photons

As said before, the full Lagrangian (5.1) can contain the gauge invariant mixing term between the field-strength tensors of the gauge factors $U(1)$ and $U(1)'$. After the electroweak symmetry breaking, this term gives rise to a kinetic mixing term between the the O- and M-photons [131]

$$\mathcal{L}_{\text{mix}} = -\epsilon F^{\mu\nu} F'_{\mu\nu}. \tag{5.38}$$

This term cannot be suppressed by symmetry reasons, and generally the constant ϵ could be of order 1.

Once such a term is introduced, the following situation emerges. One has to diagonalize first the kinetic terms of the ordinary photon field A_μ and the mirror one A'_μ, and identify the physical photon as a their linear combination. Now, once the kinetic terms are brought to canonical form by diagonalization and scaling of the fields, $(A, A') \to (A_1, A_2)$, any orthonormal combination of states A_1 and A_2 becomes good to describe the physical basis. In particular, A_2 can be chosen as a "sterile" state which does not couple to O-particles but only to M-particles. Then, the orthogonal combination A_1 couples not only to O-particles, but also with M-particles with a small charge $\propto 2\epsilon$; in other words, mirror matter becomes "milicharged" with respect to the physical ordinary photon.

In this way, the term (5.38) induces the process $e^+e^- \to e'^+e'^-$ with an amplitude just 2ϵ times the s-channel amplitude for $e^+e^- \to e^+e^-$. This could have striking experimental implications for positronium physics: ordinary positronium mixes to its mirror counterpart which effect could be manifested as an invisible decay mode of the orthopositronium. For the moment, the experimental limits on the orthopositronium decays lead to an upper limit $\epsilon < 3 \times 10^{-7}$ or so.

However, the stronger limit can be obtained from the cosmology. As we will see in the next section, the big bang nucleosynthesis (BBN) constraints require that mirror sector should be colder than the the ordinary one, $T'/T < 0.5$ or so. On the other hand, the reaction $e^+e^- \to e'^+e'^-$, funneling energy from O-sector to M-sector, would heat the latter too much before the BBN epoch, unless $\epsilon < 3 \times 10^{-8}$.

5.3 Mirror World Cosmology

If mirror sector exists, it was also created by the Big Bang, along with the ordinary matter. One could think that due to mirror parity the ordinary and mirror world particles should have same

abundances and their cosmological evolution should be identical. However, this could not be a case. Two main macroscopic parameters, that are the only free parameters of the mirror world model, govern the evolution of mirror sector. These are the fraction of mirror and ordinary photon temperatures:

$$x \equiv \frac{T'_R}{T} \tag{5.39}$$

and the fraction of mirror and ordinary baryon densities:

$$\beta \equiv \frac{\Omega'_b}{\Omega_b}. \tag{5.40}$$

Certain inflationary model [135] can reheat two sectors to different temperatures, that is needed to fit in the BBN bounds on effective number of extra neutrino species [136]. The mechanism of lepto-baryogenesis [137] can produce baryon asymmetry simultaneously in ordinary and mirror worlds. With the possibility of $\Omega'_b \approx 5\Omega_b$, mirror world can be a good candidate for dark matter [138], fitting with cosmic microwave background (CMB) and large scale structures (LSS) power spectrum data [139]. Mirror particles can form stars and galaxies and they can play a role of MACHOS (massive compact halo objects) [140] and can be detected in microlensing experiments.

In the following section we describe these mechanisms in more details.

5.3.1 BBN constraints

BBN puts a constraint on effective number of extra light neutrinos [141]

$$\Delta N_\nu < 1. \tag{5.41}$$

Mirror photons γ', electrons e' and neutrinos $\nu'_e, \nu'_\mu, \nu'_\tau$ would give a contribution in the Hubble expansion rate equivalent to $\Delta N_\nu \simeq 6.14$ [136] and this would violate (5.41). But this problem could be avoided if in the early Universe the M-system had a lower temperature than ordinary world

$$T' < T. \tag{5.42}$$

This could become plausible if following conditions hold:

(i) In post-inflationary epoch the two sectors are reheated to different temperatures, i.e (5.42), that can be naturally achieved in some inflationary models [135];

(ii) The two systems interact very weakly, so they do not come into thermal equilibrium with each other during the Universe expansion. If the systems interact through gravity, this condition is automatically attained;

(iii) Both systems expand adiabatically, without significant entropy production.

If these conditions are fulfilled, two sectors with different initial temperatures, evolving independently during the cosmological expansion, at later stages maintain nearly constant ratio of their temperatures (5.39). In this way, if $x \ll 1$, mirror sector would not affect primordial nucleosynthesis in the ordinary world.

If the two systems were decoupled already after reheating, at later times t they will have different temperatures $T(t)$ and $T'(t)$, and so different energy and entropy densities:

$$\rho(t) = \frac{\pi^2}{30} g_*(T) T^4, \quad \rho'(t) = \frac{\pi^2}{30} g'_*(T') T'^4 , \tag{5.43}$$

$$s(t) = \frac{2\pi^2}{45} g_s(T) T^3, \quad s'(t) = \frac{2\pi^2}{45} g_s'(T') T'^3 . \tag{5.44}$$

The factors g_*, g_s and g_*', g_s' accounting for the effective number of the degrees of freedom in the two systems can in general be different from each other. Let us assume that during the expansion of the Universe the two sectors evolve with separately conserved entropies. Then the ratio $x \equiv (s'/s)^{1/3}$ is time independent while the ratio of the temperatures in the two sectors is simply given by:

$$\frac{T'(t)}{T(t)} = x \cdot \left[\frac{g_s(T)}{g_s'(T')} \right]^{1/3} . \tag{5.45}$$

The Hubble expansion rate is determined by the total energy density $\bar{\rho} = \rho + \rho'$, $H = \sqrt{(8\pi/3) G_N \bar{\rho}}$. Therefore, at a given time t in a radiation dominated epoch we have

$$H(t) = \frac{1}{2t} = 1.66 \sqrt{\bar{g}_*(T)} \frac{T^2}{M_{Pl}} = 1.66 \sqrt{\bar{g}_*'(T')} \frac{T'^2}{M_{Pl}} \tag{5.46}$$

where

$$\bar{g}_*(T) = g_*(T)(1 + x^4), \quad \bar{g}_*'(T') = g_*'(T')(1 + x^{-4}). \tag{5.47}$$

In particular, we have $x = T_0'/T_0$, where T_0, T_0' are the present temperatures of the relic photons in O- and M-sectors. In fact, x is the only free parameter in the model and it is constrained by the BBN bounds.

The observed abundances of light elements are in good agreement with the standard nucleosynthesis predictions. The effective number of degrees of freedom at $T \sim 1$ MeV equals to $g_* = 10.75$ and it is saturated by photons γ, electrons e and three neutrino species ν_e, ν_μ, ν_τ. The contribution of mirror particles would change it to $\bar{g}_* = g_*(1 + x^4)$. Deviations from $g_* = 10.75$ are usually parametrized in terms of the effective number of extra neutrino species, $\Delta g = \bar{g}_* - 10.75 = 1.75 \cdot \Delta N_\nu$. Thus we have:

$$\Delta N_\nu = 6.14 \cdot x^4 \tag{5.48}$$

and the condition (5.41) implies

$$x < 0.64 . \tag{5.49}$$

As far as $x^4 \ll 1$, in a relativistic epoch the Hubble expansion rate (5.46) is dominated by the O-matter density and the presence of the M-sector practically does not affect the standard cosmology of the early ordinary Universe. However, even if the two sectors have the same microphysics, the cosmology of the early mirror world can be very different from the standard one as far as the crucial epochs like baryogenesis, nuclesosynthesis, etc. are concerned. Any of these epochs is related to an instant when the rate of the relevant particle process $\Gamma(T)$, which is generically a function of the temperature, becomes equal to the Hubble expansion rate $H(T)$. Obviously, in the M-sector these events take place earlier than in the O-sector, and as a rule, the relevant processes in the former freeze out at larger temperatures than in the latter.

In the matter domination epoch the situation becomes different. In particular, we know that ordinary baryons provide only a small fraction of the present matter density, whereas the observational data indicate the presence of dark matter with about 5 times larger density. It is interesting to question whether the missing matter density of the Universe could be due to mirror baryons? In the next section we show that this could occur in a pretty natural manner.

It can also be shown that the BBN epoch in the mirror world proceeds differently from the ordinary one, and it predicts different abundances of primordial elements [136, 142]. It is well

known that primordial abundances of the light elements depend on the baryon to photon density ratio $\eta = n_B/n_\gamma$, and the observational data well agree with the WMAP result $\eta \simeq 6 \times 10^{-10}$. As far as $T' \ll T$, the universe expansion rate at the ordinary BBN epoch ($T \sim 1$ MeV) is determined by the O-matter density itself, and thus for the ordinary observer it would be very difficult to detect the contribution of M-sector: the latter is equivalent to $\Delta N_\nu \approx 6.14x^4$ and hence it is negligible for $x \ll 1$. As for nucleosynthesis epoch in M-sector, the contribution of O-world instead is dramatic: it is equivalent to $\Delta N'_\nu \approx 6.14x^{-4} \gg 1$. Therefore, mirror observer which measures the abundances of mirror light elements should immediately observe discrepancy between the universe expansion rate and the M-matter density at his BBN epoch ($T' \sim 1$ MeV) as far as the former is determined by O-matter density which is invisible for him. The result for mirror ^{4}He also depends on the mirror baryon to photon density ratio $\eta' = n'_B/n'_\gamma$. Writing that $\beta = n'_B/n_B$ and $\eta' = (\beta/x^3)\eta$, we see $\eta' \gg \eta$ unless $\beta \ll x^3$. However, if $\beta > 1$, we expect that mirror helium mass fraction Y'_4 would be considerably larger than the observable $Y_4 \simeq 0.24$. Namely, direct calculations show that for x varying from 0.6 to 0.1, Y'_4 would vary in the range $Y'_4 = 0.5 - 0.8$. Therefore, if M-baryons constitute dark matter or at least its reasonable fraction, the M-world is dominantly helium world while the heavier elements can also present with significant abundances.

The 'helium' nature of the mirror universe should have a strong impact on the processes of the star formation and evolution in the mirror sector [140] and it is discussed in upcoming sections.

5.3.2 Lepto-Baryogenesis

When discussing CP violation in the section (5.1.4), we already mentioned that, in order to get a baryon asymmetry (BA) from initially baryon symmetric Universe, Sakharov's three conditions must hold: (i) B violation, (ii) CP violation, (iii) departure from thermal equilibrium [128]. These conditions can be satisfied in the decays of heavy particles of grand unified theories. But, besides that, a certain mechanism of leptogenesis based on $B - L$ violating scattering processes presented in [137], can be responsible to produce BA in ordinary and mirror sectors. In this section we briefly describe this mechanism.

The main idea consists in the following. The mirror sector of particles is not in thermal equilibrium with the ordinary particle world as far as the two systems interact very weakly, via gravity. However, superheavy singlet neutrinos N can mediate very weak effective interactions between the ordinary and mirror leptons. Then, a net $B - L$ could emerge in the Universe as a result of CP-violating effects in the unbalanced production of mirror particles from ordinary particle collisions.

We consider lepton doublets $l_i = (\nu, e)_i$ ($i = 1, 2, 3$ is a family index) and Higgs doublet ϕ from SM and its mirror partners l'_i and ϕ'. Their coupling to the heavy singlet neutrinos are given by:

$$y_{ia}l_i N_a \phi + y'_{ia}l'_i N_a \phi' + \frac{M}{2}g_{ab}N_a N_b + \text{h.c.} , \qquad (5.50)$$

where M is heavy neutrino mass scale and g_{ab} are Yukawa-like constants. M is assumed to be greater than the reheating temperature T_R, and so heavy neutrinos are not thermally produced. After the postinflationary reheating, different temperatures are established in the two sectors: $T'_R < T_R$, i.e. the mirror sector is cooler than the visible one, or ultimately, even completely

"empty". Now, through the $\Delta L = 1$ reactions

$$l_i \phi \rightarrow \bar{l}'_k \bar{\phi}' \tag{5.51}$$

$$\bar{l}_i \bar{\phi} \rightarrow l'_k \phi' \tag{5.52}$$

entropy transfers to the cooler mirror world and it gets slowly occupied by particles. Due to complex Yukawa couplings in (5.50), the processes violate CP and so the cross sections with leptons and anti-leptons in the initial state are different from each other. As a result, leptons leak to the mirror sector with different rate than antileptons and so a non-zero $B - L$ is produced in the Universe.

There are also $\Delta L = 2$ scattering processes like $l\phi \rightarrow \bar{l}\bar{\phi}$. The rates for the $\Delta L = 1$ and $\Delta L = 2$ reactions are:

$$\Gamma_1 = \frac{Q_1 n_{\text{eq}}}{8\pi M^2}; \quad Q_1 = \text{Tr}[(y'^\dagger y')^* g^{-1} (y^\dagger y) g^{-1}],$$
$$\Gamma_2 = \frac{3Q_1 n_{\text{eq}}}{4\pi M^2}; \quad Q_2 = \text{Tr}[(y^\dagger y)^* g^{-1} (y^\dagger y) g^{-1}], \tag{5.53}$$

where $n_{\text{eq}} \simeq (1.2/\pi^2) T^3$ is an equilibrium density per one bosonic degree of freedom. It is essential that these processes stay out of equilibrium, which means that their rates should not exceed much the Hubble parameter $H = 1.66 \, g_*^{1/2} T^2 / M_{Pl}$ for temperatures $T \leq T_R$, where g_* is the effective number of particle degrees of freedom, namely $g_* \simeq 100$ in the SM. In other words, the dimensionless parameters

$$k_1 = \left(\frac{\Gamma_1}{H}\right)_{T=T_R} \simeq 1.5 \times 10^{-3} \frac{Q_1 T_R M_{Pl}}{g_*^{1/2} M^2}$$
$$k_2 = \left(\frac{\Gamma_2}{H}\right)_{T=T_R} \simeq 9 \times 10^{-3} \frac{Q_2 T_R M_{Pl}}{g_*^{1/2} M^2} \tag{5.54}$$

should not be much larger than 1.

In $\Delta L = 1$ processes the CP-odd lepton number asymmetry emerges from the interference between the tree-level and one-loop diagrams of figure (5.1). However, CP-violation takes also place in $\Delta L = 2$ processes (see figure (5.2)). This is a consequence of the very existence of the mirror sector, namely, it comes from the contribution of the mirror particles to the one-loop diagrams of figure (5.2). The direct calculation gives:

$$\sigma(l\phi \rightarrow \bar{l}\bar{\phi}) - \sigma(\bar{l}\bar{\phi} \rightarrow l\phi) = \Delta\sigma \,;$$
$$\sigma(l\phi \rightarrow \bar{l}'\bar{\phi}') - \sigma(\bar{l}\bar{\phi} \rightarrow l'\phi') = (-\Delta\sigma - \Delta\sigma')/2 \,,$$
$$\sigma(l\phi \rightarrow l'\phi') - \sigma(\bar{l}\bar{\phi} \rightarrow \bar{l}'\bar{\phi}') = (-\Delta\sigma + \Delta\sigma')/2 \,,$$
$$\Delta\sigma = \frac{3J\,S}{32\pi^2 M^4} \,, \qquad \Delta\sigma' = \frac{3J'\,S}{32\pi^2 M^4} \,, \tag{5.55}$$

where S is the c.m. energy square,

$$J = \text{Im}\,\text{Tr}[(y^\dagger y)^* g^{-1} (y'^\dagger y') g^{-2} (y^\dagger y) g^{-1}] \tag{5.56}$$

is the CP-violation parameter and J' is obtained from J by exchanging y with y'.

Of course, this is in agreement with CPT theorem that requires that the total cross sections for particle and anti-particle scatterings are equal to each other: $\sigma(l\phi \rightarrow X) = \sigma(\bar{l}\bar{\phi} \rightarrow X)$.
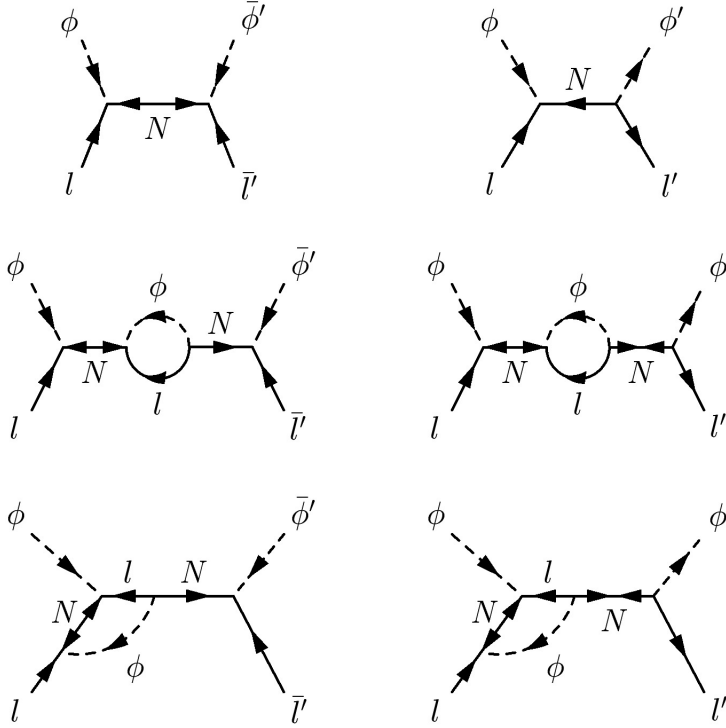
Figure 5.1: Tree-level and one-loop diagrams contributing to the CP-asymmetries in $l\phi \to \bar{l}'\bar{\phi}'$ (left column) and $l\phi \to l'\phi'$ (right column). Figure adopted from [137].

Indeed, taking into account that $\sigma(l\phi \to l\phi) = \sigma(\bar{l}\bar{\phi} \to \bar{l}\bar{\phi})$ by CPT, we see that CP asymmetries in the $\Delta L = 1$ and $\Delta L = 2$ processes should be related as

$$\sigma(l\phi \to \bar{l}\bar{\phi}) - \sigma(\bar{l}\bar{\phi} \to l\phi) = \Delta\sigma \ ,$$
$$\sigma(l\phi \to X') - \sigma(\bar{l}\bar{\phi} \to X') = -\Delta\sigma \ , \qquad (5.57)$$

where X' are the mirror sector final states, either $\bar{l}'\bar{\phi}'$ or $l'\phi'$. That is, the $\Delta L = 1$ and $\Delta L = 2$ reactions have CP asymmetries with equal intensities but opposite signs. But, as L varies in each case by a different amount, a net lepton number decrease is produced, or better, a net increase of $B - L \propto \Delta\sigma$.

As far as we assume that the mirror sector is cooler and thus depleted of particles, the only relevant reactions are the ones with ordinary particles in the initial state. Hence, the evolution of the $B - L$ number density is determined by the CP asymmetries shown in eqs. (5.55) and obeys the equation

$$\frac{dn_{B-L}}{dt} + 3Hn_{B-L} + \Gamma n_{B-L} = \frac{3}{4}\Delta\sigma \, n_{\text{eq}}^2 = 1.8 \times 10^{-3} \frac{T^8}{M^4} \ , \qquad (5.58)$$

where $\Gamma = \Gamma_1 + \Gamma_2$ is the total rate of the $\Delta L = 1$ and $\Delta L = 2$ reactions, and for the CP asymmetric cross section $\Delta\sigma$ we take the thermal average c.m. energy square $S \simeq 17\,T^2$.

It is instructive to first solve this equation in the limit $k_{1,2} \ll 1$, when the out-of-equilibrium conditions are strongly satisfied and thus the term Γn_{B-L} can be neglected. Integrating this equation we obtain for the final $B - L$ asymmetry of the Universe, $Y_{BL} = n_{B-L}/s$, where $s = (2\pi^2/45)g_*T^3$ is the entropy density, the following expression:

$$Y_{BL}^{(0)} \approx 2 \times 10^{-3} \frac{J \, M_{Pl} T_R^3}{g_*^{3/2} M^4}. \qquad (5.59)$$
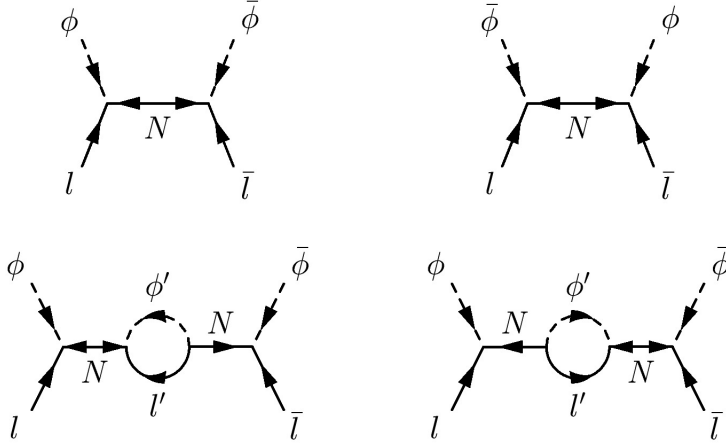
Figure 5.2: Tree-level and one-loop diagrams contributing to the CP-asymmetry of $l\phi \to \bar{l}\bar{\phi}$. The external leg labels identify the initial and final state particles. Figure adopted from [137].

This result (5.59) can be recast as follows

$$Y_{BL}^{(0)} \approx \frac{20 J k^2 T_R}{g_*^{1/2} Q^2 M_{Pl}} \approx 10^{-10} \frac{J k^2}{Q^2} \left(\frac{T_R}{10^9 \text{ GeV}} \right) \tag{5.60}$$

where $Q^2 = Q_1^2 + Q_2^2$, $k = k_1 + k_2$ and we have taken $g_* \approx 100$. This shows that for Yukawa constants spread e.g. in the range $0.1 - 1$, one can achieve $B - L = \mathcal{O}(10^{-10})$ for a reheating temperature as low as $T_R \sim 10^9$ GeV.

Now, solving eq. (5.58) exactly, without assuming $\Gamma \ll H$ gives [138]:

$$Y_{BL} = D(k) \cdot Y_{BL}^{(0)} , \tag{5.61}$$

where the depletion factor $D(k)$ is given by

$$D(k) = \frac{3}{5} e^{-k} F(k) + \frac{2}{5} G(k), \tag{5.62}$$

where

$$F(k) = \frac{1}{4k^4} \left[(2k - 1)^3 + 6k - 5 + 6e^{-2k} \right],$$
$$G(k) = \frac{3}{k^3} \left[2 - (k^2 + 2k + 2)e^{-k} \right]. \tag{5.63}$$

These two terms in $D(k)$ correspond to the integration of (5.58) respectively in the epochs before and after reheating ($T > T_R$ and $T < T_R$). Obviously, for $k \ll 1$ we have $D(k) = 1$ and thus we recover the result as in (5.59) or (5.60). However, for large k the depletion can be reasonable, e.g. for $k = 1, 2$ we have respectively $D(k) = 0.35, 0.15$.

Now, let us discuss how the mechanism considered above produces also the baryon prime asymmetry in the mirror sector. The amount of this asymmetry will depend on the CP-violation parameter $J' = \text{Im} \text{Tr}[(y^\dagger y)g^{-2}(y'^\dagger y')g^{-1}(y'^\dagger y')^* g^{-1}]$ that replaces J in $\Delta\sigma'$ of eqs. (5.55). The mirror P parity under the exchange $\phi \to \phi'^\dagger$, $l \to \bar{l}'$, etc., implies that the Yukawa couplings are essentially the same in both sectors, $y' = y^*$. Therefore, in this case also the CP-violation

parameters are the same, $J' = -J$. Therefore, one naively expects that $n'_{B-L} = n_{B-L}$ and the mirror baryon density should be equal to the ordinary one, $\Omega'_b = \Omega_b$.

However, now we show that if the $\Delta L = 1$ and $\Delta L = 2$ processes are not very far from equilibrium, i.e. $k \sim 1$, the mirror baryon density should be bigger than the ordinary one. Indeed, the evolution of the mirror $B - L$ number density, n'_{B-L}, obeys the equation

$$\frac{dn'_{B-L}}{dt} + 3Hn'_{B-L} + \Gamma'n'_{B-L} = \frac{3}{4}\Delta\sigma' \, n_{\rm eq}^2 \,, \tag{5.64}$$

where now $\Gamma' = (Q_1 + 6Q_2)n'_{\rm eq}/8\pi M^2$ is the total reaction rate of the $\Delta L' = 1$ and $\Delta L' = 2$ processes in the mirror sector, and $n'_{\rm eq} = (1.2/\pi^2)T'^3 = x^3 n_{\rm eq}$ is the equilibrium number density per degree of freedom in the mirror sector. Therefore $k' = \Gamma'/H = x^3 k$, and for the mirror sector we have $Y'_{BL} = D(kx^3) \cdot Y_{BL}^{(0)}$. Hence, if $kx^3 \ll 1$, the depletion can be irrelevant: $D(kx^3) \approx 1$.

Now taking into the account that in both sectors the $B - L$ densities are reprocessed into the baryon number densities by the same sphaleron processes, we have $B = a(B - L)$ and $B' = a(B-L)'$, with coefficients a equal for both sectors. Therefore, we see that the cosmological densities of the ordinary and mirror baryons should be related as

$$\beta = \frac{\Omega'_b}{\Omega_b} \approx \frac{1}{D(k)}. \tag{5.65}$$

If $k \ll 1$, depletion factors in both sectors are $D \approx D' \approx 1$ and thus we have that the mirror and ordinary baryons have the same densities, $\Omega'_b \approx \Omega_b$. In this case mirror baryons are not enough to explain all dark matter and one has to invoke also some other kind of dark matter, presumably cold dark matter.

However, if $k \sim 1$, then we would have $\Omega'_b > \Omega_b$, and thus all dark matter of the Universe could be in the form of mirror baryons. Namely, for $k \simeq 1.5$ we would have from eq. (5.65) that $\Omega'_b/\Omega_b \approx 5$, which is about the best fit relation between the ordinary and dark matter densities.

5.3.3 Mirror Baryons as Dark Matter

We have shown that mirror baryons could provide a significant contribution to the energy density of the Universe and thus they could constitute a relevant component of dark matter. An immediate question arises: how the mirror baryon dark matter (MBDM) behaves and what are the differences from the more familiar dark matter candidates as the cold dark matter (CDM), the hot dark matter (HDM) etc. In this section, following [138] and [139], we briefly address the possible observational consequences of such a cosmological scenario.

In the most general context, the present energy density contains a relativistic (radiation) component Ω_r, a non-relativistic (matter) component Ω_m and the vacuum energy density Ω_Λ (cosmological term). According to the inflationary paradigm the Universe should be almost flat, $\Omega_0 = \Omega_m + \Omega_r + \Omega_\Lambda \approx 1$, which agrees well with the recent results on the cosmic microwave background (CMB) anisotropy and large scale structure (LSS) power spectrum.

The Hubble parameter is known to be $H_0 = 100h$ km s^{-1} Mpc^{-1} with $h \approx 0.7$, and for redshifts of cosmological relevance, $1 + z = T/T_0 \gg 1$, it becomes

$$H(z) = H_0 \left[\Omega_r(1 + z)^4 + \Omega_m(1 + z)^3 + \Omega_\Lambda\right]^{1/2}. \tag{5.66}$$

In the context of mirror world model, the relativistic fraction is represented by the ordinary and mirror photons and neutrinos, $\Omega_r h^2 = 4.2 \times 10^{-5}(1 + x^4)$, and the contribution of the

mirror species is negligible in view of the BBN constraint $x < 0.6$. As for the non-relativistic component, it contains the O-baryon fraction Ω_b and the M-baryon fraction $\Omega'_b = \beta\Omega_b$, while the other types of dark matter, e.g. the CDM, could also be present. Therefore, in general, $\Omega_m = \Omega_b + \Omega'_b + \Omega_{cdm}$.

The important moments for the structure formation are related to the matter-radiation equality (MRE) epoch, to the plasma recombination and matter-radiation decoupling (MRD) epochs. The MRE occurs at the redshift

$$1 + z_{eq} = \frac{\Omega_m}{\Omega_r} \approx 2.4 \cdot 10^4 \frac{\omega_m}{1 + x^4} \tag{5.67}$$

where we denote $\omega_m = \Omega_m h^2$. Therefore, for $x \ll 1$ it is not altered by the additional relativistic component of the M-sector.

The radiation decouples from matter after almost all of electrons and protons recombine into neutral hydrogen and the free electron number density sharply diminishes, so that the photon-electron scattering rate drops below the Hubble expansion rate. In the ordinary Universe the MRD takes place in the matter domination period, at the temperature $T_{dec} \simeq 0.26$ eV, which corresponds to the redshift $1 + z_{dec} = T_{dec}/T_0 \simeq 1100$.

The MRD temperature in the M-sector T'_{dec} can be calculated following the same lines as in the ordinary one [136]. Due to the fact that in either case the photon decoupling occurs when the exponential factor in Saha equations becomes very small, we have $T'_{dec} \simeq T_{dec}$, up to small logarithmic corrections related to B' different from B. Hence

$$1 + z'_{dec} \simeq x^{-1}(1 + z_{dec}) \simeq 1100\, x^{-1} \tag{5.68}$$

so that the MRD in the M-sector occurs earlier than in the ordinary one. Moreover, for x less than $x_{eq} = 0.045\omega_m^{-1} \simeq 0.3$, the mirror photons would decouple yet during the radiation dominated period (see figure (5.3)).

Now we discuss the cosmological evolution of the MBDM. The relevant length scale for the gravitational instabilities is characterized by the mirror Jeans scale $\lambda'_J \simeq v'_s(\pi/G\rho)^{1/2}$, where $\rho(z)$ is the matter density at a given redshift z and $v'_s(z)$ is the sound speed in the M-plasma. The latter contains more baryons and less photons than the ordinary one, $\rho'_b = \beta\rho_b$ and $\rho'_\gamma = x^4\rho_\gamma$. For simplicity we consider the case when dark matter of the Universe is entirely due to M-baryons, $\Omega_m \simeq \Omega'_b$. Then we have:

$$v'_s(z) \simeq \frac{c}{\sqrt{3}}\left(1 + \frac{3\rho'_b}{4\rho'_\gamma}\right)^{-1/2} \approx \frac{c}{\sqrt{3}}\left[1 + \frac{3}{4}\left(1 + x^{-4}\right)\frac{1 + z_{eq}}{1 + z}\right]^{-1/2}. \tag{5.69}$$

Hence, for redshifts of cosmological relevance, $z \sim z_{eq}$, we have $v'_s \sim 2x^2c/3 \ll c/\sqrt{3}$, quite in contrast with the ordinary world, where $v_s \approx c/\sqrt{3}$ practically until the photon decoupling, $z = 1100$.

The M-baryon Jeans mass $M'_J = \frac{\pi}{6}\rho_m\lambda'^3_J$ reaches the maximal value at $z = z'_{dec} \simeq 1100/x$, $M'_J(z'_{dec}) \simeq 2.4 \cdot 10^{16} \times x^6[1 + (x_{eq}/x)]^{-3/2}\omega_m^{-2}\, M_\odot$. Notice, however, that M'_J becomes smaller than the Hubble horizon mass $M_H = \frac{\pi}{6}\rho H^{-3}$ starting from a redshift $z_c = 3750x^{-4}\omega_m$, which is about z_{eq} for $x = 0.64$, but it sharply increases for smaller values of x. So, the density perturbation scales which enter the horizon at $z \sim z_{eq}$ have mass larger than M'_J and thus undergo uninterrupted linear growth immediately after $t = t_{eq}$. The smaller scales for which $M'_J > M_H$ instead would first oscillate. Therefore, the large scale structure formation is not
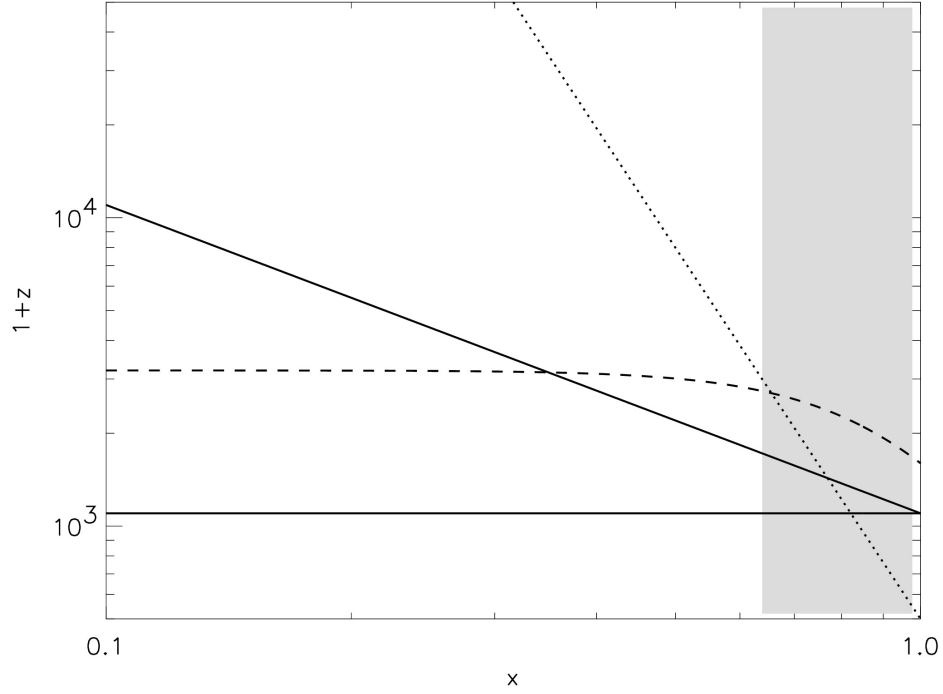
58

Figure 5.3: The M-photon decoupling redshift $1 + z'_{\text{dec}}$ as a function of x (thick solid). The horizontal thin solid line marks the ordinary photon decoupling redshift $1 + z_{\text{dec}} = 1100$. We also show the matter-radiation equality redshift $1 + z_{\text{eq}}$ (dash) and the mirror Jeans-horizon mass equality redshift $1 + z'_c$ (dash-dot) for the case $\omega_m = 0.135$. The shaded area $x > 0.64$ is excluded by the BBN limits. Figure adopted from [138].

delayed even if the mirror MRD epoch did not occur yet, i.e. even if $x > x_{\text{eq}}$. The density fluctuations start to grow in the M-matter and the visible baryons are involved later, when after being recombined they fall into the potential wells of developed mirror structures.

Another important feature of the MBDM scenario is that the M-baryon density fluctuations should undergo strong collisional damping around the time of M-recombination. The photon diffusion from the overdense to underdense regions induce a dragging of charged particles and wash out the perturbations at scales smaller than the mirror Silk scale $\lambda'_S \simeq 3 \times f(x)\omega_m^{-3/4}$ Mpc, where $f(x) = x^{5/4}$ for $x > x_{\text{eq}}$, and $f(x) = (x/x_{\text{eq}})^{3/2}x_{\text{eq}}^{5/4}$ for $x < x_{\text{eq}}$.

Thus, the density perturbation scales which can undergo the linear growth after the MRE epoch are limited by the length λ'_S. This could help in avoiding the excess of small scales (of few Mpc) in the power spectrum without tilting the spectral index. The smallest perturbations that survive the Silk damping will have the mass $M'_S \sim f^3(x)\omega_m^{-5/4} \times 10^{12}\ M_\odot$. Interestingly, for $x \sim x_{\text{eq}}$ we have $M'_S \sim 10^{11}\ M_\odot$, a typical galaxy mass. To some extend, the cutoff effect is analogous to the free streaming damping in the case of warm dark matter (WDM), but there are important differences. The point is that like usual baryons, the MBDM should show acoustic oscillations with an impact on the large scale power spectrum.

In addition, the MBDM oscillations transmitted via gravity to the ordinary baryons, could cause observable anomalies in the CMB angular power spectrum for l's larger than 200. This effect can be observed only if the M-baryon Jeans scale λ'_J is larger than the Silk scale of ordinary baryons, which sets a principal cutoff for CMB oscillations around $l \sim 1200$. As we have seen above, this would require enough large values of x, near the BBN upper bound $x \simeq 0.6$ or so.
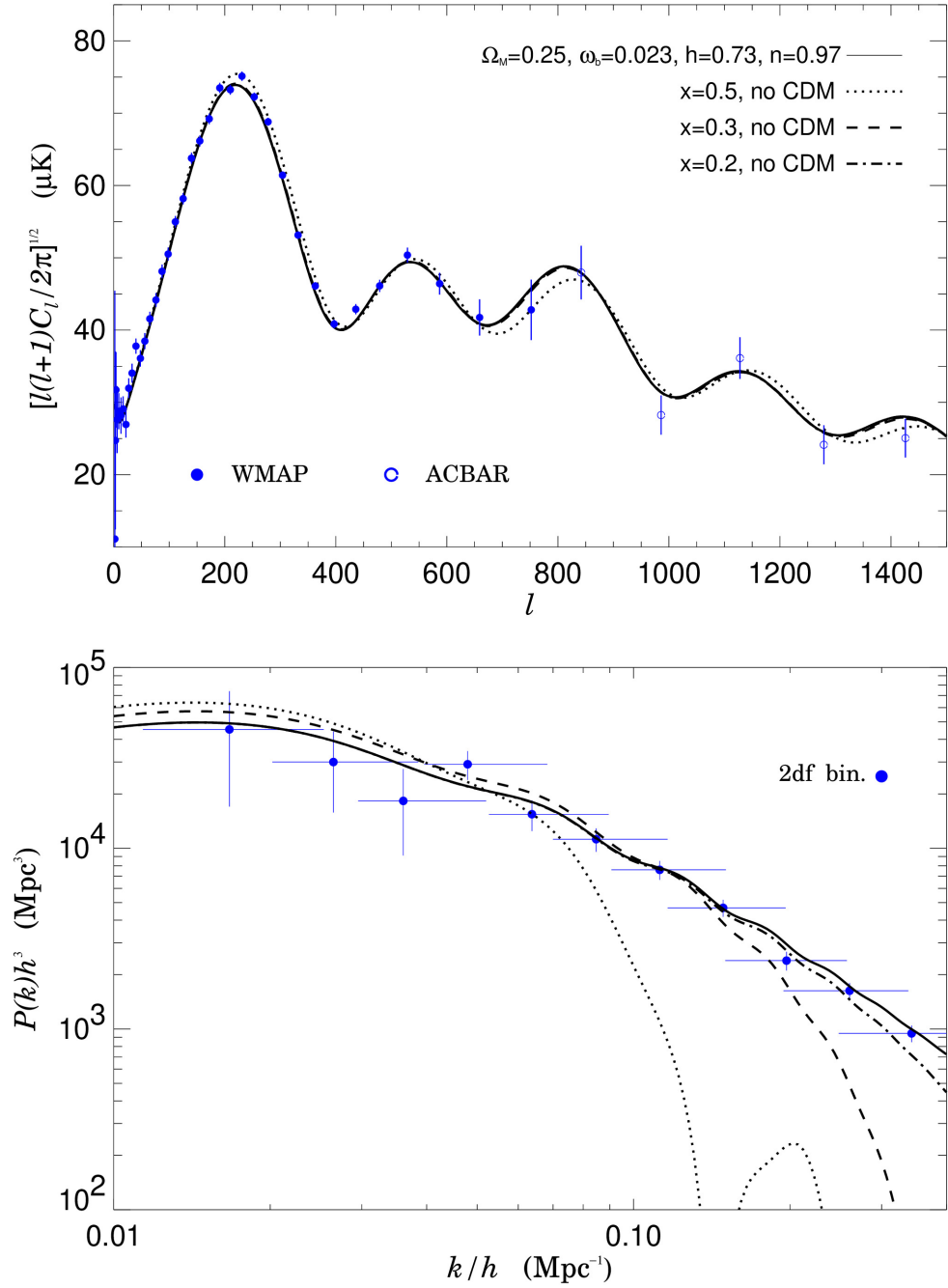
Figure 5.4: The CMB power spectrum (upper panel) and the large scale power spectrum (lower panel) for a "concordance" set of cosmological parameters. The solid curves correspond to the flat ΛCDM model, while dot, dash and dash-dot curves correspond to the situation when the CDM component is completely substituted by the MBDM for different values of x. Figure adopted from [138].

If the dark matter is entirely built up by mirror baryons, large values of x are excluded by the observational data. For the sake of demostration, on the figure (5.4) the CMB and LSS power spectra for different values of x are shown. We see that for $x > 0.3$ the matter power spectrum shows a strong deviation from the experimental data. This is due to Silk damping effects which suppress the small scale power too early, already for $k/h \sim 0.2$. However, the values $x < 0.3$ are compatible with the observational data.

This has a simple explanation. Clearly, for small x the M-matter recombines before the MRE moment, and thus it should rather manifest as the CDM as far as the large scale structure is concerned. However, there still can be a crucial difference at smaller scales which already went non-linear, like galaxies. Then one can question whether the MBDM distribution in halos can be different from that of the CDM? Namely, simulations show that the CDM forms triaxial halos with a density profile too clumped towards the center, and overproduce the small substructures within the halo. As for the MBDM, it constitutes a sort of collisional dark matter and thus potentially could avoid these problems, at least clearly the one related with the excess of small substructures.

Another possibility can also be considered when dark matter in galaxies and clusters contain mixed CDM and MBDM components, $\Omega_d = \Omega_b' + \Omega_{cdm}$. e.g. one can exploit the case when mirror baryons constitute the same fraction of matter as the ordinary ones, $\Omega_b' = \Omega_b$, a situation which emerges naturally in the leptogenesis mechanism.

In the next section we discuss how mirror matter can form stars and galaxies and what potential impact can it has on our observable Universe.

5.3.4 Mirror Stars and Galaxies

If mirror matter exists, then the existence of mirror stars, in a certain sense, is guaranteed by the existence of ordinary stars: given that two sectors have the same microphysics, stars necessarily form in both of them and the only changes are due to the boundary conditions [140]. This is a very favourable condition for the study of M stars, because the necessary knowledge is the same than for the O ones, that we know very well. This means that M stars follow the same evolutionary stages than visible ones. The same physics for both sectors means that the equations governing the mirror stellar evolution and the physical ingredients to put inside them are the same as for visible stars. The only change regards the composition of the M star.

If we consider a single isolated star, its evolutionary and structural properties depend only on the mass and the chemical composition. In particular, the latter is expressed by the abundances by mass of hydrogen (X), helium (Y), and the so-called heavy elements or metals (Z), i.e. all the elements heavier than H and He, so that the condition $X + Y + Z = 1$ is fulfilled. Due to different initial conditions, $x = T'/T < 1$, two sectors have different cosmological evolution, and in particular, different chemical content. Thus, the details of the star and galaxy formation scenarios depend on the exact composition of matter and they can be different in two sectors.

As far as the chemical contents are concerned, for a given value of x, the primordial helium abundances in ordinary and mirror sectors roughly can be given by the following formulas [136]:

$$Y = \frac{2\exp[-t_N/\tau(1+x^4)^{1/2}]}{1 + \exp[\Delta m/T_W(1+x^4)^{1/6}]} , \tag{5.70}$$

and

$$Y' = \frac{2\exp[-t_N/\tau(1+x^{-4})^{1/2}]}{1 + \exp[\Delta m/T_W(1+x^{-4})^{1/6}]} , \tag{5.71}$$

where $\tau = 887$ s is the neutron lifetime, $\Delta m = 1.29$ MeV is the neutron-proton mass difference, $T_W \simeq 0.8$ MeV is a weak interaction freezing temperature in the standard cosmology, and $t_N \sim 200$ s is the cosmological timescale corresponding to the "deuterium bottleneck" temperature $T_N \sim 0.07$ MeV. Therefore, for $x \ll 1$ the standard BBN predictions essentially are not affected. Namely, the smaller is x, the prediction for ordinary helium decreases and gets closer to the standard BBN result $Y \simeq 0.24$, while the prediction for the mirror helium increases and at $x \to 0$ approaches $Y' \to 1$. In particular, for $x = 0.6$ one has $Y' \simeq 0.4$, while for $x = 0.1$, $Y' \simeq 0.8$. Therefore, in two sectors the first stars are formed with different initial abundances of helium.

The evolutionary and structural properties of stars strongly depend on the initial chemical composition, which is fixed by the helium abundance and by the global amount of heavy elements. The primordial abundances of ordinary nuclei heavier than helium are estimated to be very small ($Z \sim 10^{-10}$). This metallicity would be characteristic of the 'first' stellar population, the so-called Population III stars. Concerning the primordial metallicity of mirror matter, it can be some orders of magnitude higher, however there are no reasons to expect that it will be relevant.

Formation of stars and galaxies are strongly coupled. Given the complexity of the physics of galaxy formation (this process in still to be well understood), we can make some general considerations. At a stage during the process of gravitational collapse of the protogalaxy, it fragments into hydrogen clouds with typical Jeans mass (for mirror matter, these gas clouds are rather the hydrogen-helium clouds). Clouds continue to cool and collapse until the opacity of the system becomes so high that the gas prefers to fragment into protostars. This complex phenomenon lead a part of the protogalactic gas to form the first stars. The lack of metals in the Universe for that time should make less efficient the cooling processes within the primordial clouds so their fragmentation could produce only high-mass stars (probably $M \sim 10^2$–$10^3 M_\odot$ and their evolutionary lifetimes are so short that they are no more observable). The cooling rates are mainly determined by hydrogen atoms and molecules, while helium is much less effective. However, even in mirror sector, unless x is extremely small, the number density of hydrogen remains significant and the cooling processes inside the primordial clouds should have also a lower efficiency, so only very massive M stars should form.

Summarizing, one can say that mirror stars are equivalent to ordinary stars, when the latter have converted most of hydrogen into helium and formed a helium core. M stars are born more massive and their evolutionary timescales are shorter as they burn out fuel faster. Increasing the initial helium abundance of a star corresponds to the increase of the mean molecular weight, and correspondingly in both luminosity and effective temperature, which leads to the shorter lifetime. In [140], evolutionary tracks have been simulated for stars with initial helium content in the range $0.24 - 0.8$ and with different initial masses and low metallicity. Analyzing the results, it has been concluded that the mean life of a mirror star can be until 30 times shorter than that of an ordinary one, if we consider the most helium rich stars. It was found that, generally, under large mass ranges and different boundary conditions (in terms of temperatures of the mirror sector, and thus stellar helium contents), the lifetimes of mirror stars are roughly an order of magnitude smaller than the ones of visible stars. As an example, a $10 M_\odot$ star with 70% initial He content has the evolution timescale ~ 10 times faster than the star with ordinary He abundance.

The pattern of galaxy evolution should drastically depend on the mirror star formation and evolution features. Stars play an important role: the fraction of baryonic gas involved in their formation becomes collisionless on galactic scales, and supernova explosions enrich the galaxy of

processed collisional gas (stellar feedback). As far as the MBDM constitutes a dissipative dark matter like the usual baryons, one would question how it can provide extended halos instead of being clumped into the galaxy as usual baryons do. However, one has to take into account the possibility that during the galaxy evolution the bulk of the M-baryons could fastly fragment into the stars. Too fast star formation in mirror component would extinct the mirror gas and thus could avoid that mirror baryons to form disk galaxies as ordinary baryons do. If the mirror protogalaxy, at certain stage of collapse, transforms into the collisionless system of the mirror stars, then it could maintain a typical elliptical structure. Certainly, in this consideration also the galaxy merging process should be taken into account. Efficient merging of mirror disks mostly built up of stars, also would lead to ellipticals. As for ordinary matter, within the dark mirror halo it should typically show up, depending on conditions of the galaxy formation, as an observable elliptic or spiral galaxy, but some anomalous cases can also be possible, like certain types of irregular galaxies or even dark galaxies dominantly made out of mirror baryons. The central part of halo can nevertheless contain a large amount of ionized mirror gas and it is not excluded that it can have a quasi-spherical form, thus possibly avoiding the problem of cusp typical for the CDM halos. Even if mirror star formation is very efficient, the massive mirror stars in the dense central region could fast evolve and explode as supernovae, leaving behind compact objects like neutron stars or black holes, and reproducing the mirror gas and dust.

It is interesting to understand whether these features could help in understanding the process of the formation of the central black holes, with masses $10^6 - 10^9 \, M_\odot$, which are considered as main engines of the quasars and active galactic nuclei. It is also possible that in the galactic halo some fraction of mirror stars exists in the form of compact substructures like globular or open clusters.

5.3.5 Mirror World Observables

In this section we review some main possibilities that can be responsible for detecting mirror matter.

MACHO: If mirror stars do exist, they can be observed as massive compact halo objects (MACHO) in galactic halos in gravitational microlensing experiments. The MACHO Collaboration [143] studied the nature of halo dark matter using microlensing. This experiment has collected 5.7 years of data and provided statistically strong evidence for dark matter in the form of invisible star sized objects, which is what you would expect if there was a significant amount of mirror matter in our galaxy. Their maximum likelihood analysis implies a MACHO halo fraction of 20% for a typical halo model with a 95% confidence interval of 8% to 50%. Their most likely MACHO mass is between $0.15 M_\odot$ and $0.9 M_\odot$ (depending on the halo model), with an average around $M \simeq 0.5 \, M_\odot$, which is difficult to explain in terms of the brown dwarfs with masses below the hydrogen ignition limit $M < 0.1 M_\odot$ or other baryonic objects. In another survey, MACHO Collaboration put a constraint on BH dark matter in the mass range $1 - 30 M_\odot$, concluding that the objects with masses under $30 M_\odot$ cannot make up the entire dark matter halo if the halo is of typical size and that objects with masses under $10 M_\odot$ contribute less than 40% of the dark matter [59]. These observations are consistent with a mirror matter halo because the entire halo would not be expected to be in the form of mirror stars. Mirror gas and dust would also be expected because they are a necessary consequence of stellar evolution and should therefore significantly populate the halo. However, later observations by Eros-2 Collaboration found only one candidate event [60], while ~ 39 were expected depending on the

earlier results by MACHO Collaboration. The disagreement between these two experimental results is not solved yet. Clearly the outcome of the controversy can be crucial for the mirror matter model.

SN: The explosions of mirror supernovae (SN) in our galaxy cannot be directly seen by an ordinary observer [138]. However, it should be observed in terms of gravitational waves. In addition, if the M- and O-neutrinos are mixed, it can lead to an observable neutrino signal, and could be also accompanied by a weak gamma ray burst.

DAMA: Annual-modulation effect, as expected from the relative motion of the Earth with respect to the relic particles responsible for the dark matter in the galactic halo [144, 145], has been measured by DAMA Collaboration using the highly radiopure NaI(Tl) detectors of the former DAMA/NaI and of the second generation DAMA/LIBRA [146]. This annual modulation effect, which fulfills all the requirements of the DM annual modulation signature, has been examined in the context of asymmetric mirror matter model interacting with the ordinary nuclei via the photon-mirror photon kinetic mixing portal, $\frac{\epsilon}{2}F^{\mu\nu}F'_{\mu\nu}$ [147, 148]. It was assumed that mirror atoms constitute a fraction f of the DM in the Galaxy, and allowed physical intervals for some combination of parameters were derived. The obtained values are well compatible with cosmological bounds. However, later the DAMA results have become speculative, as two other studies, attempting to replicate the experiment using the same method have shown no evidence of annual modulation [149, 150].

5.3.6   Neutron Lifetime and $n - n'$ oscillations

In [151] a possibility of oscillations between neutrons (n) and mirror neutrons (n') was discussed. It was argued that, the existing experimental data do not exclude a rather fast $n - n'$ oscillation, with a timescale ~ 1 s, and it can have strong astrophysical implications, in particular for ultra high energy cosmic rays. Moreover, $n - n'$ oscillation can be a solution for a neutron lifetime problem [152]. The neutron lifetime is measured in two types of experiments, which are usually referred as beam and trap methods, that is discussed in our paper [6]. In beam experiments, number of produced protons are counted, as monitored beam of cold neutrons passes through a magnetic field. So this method directly measures the neutron β-decay width $\Gamma_\beta = \tau_\beta^{-1}$. In trap experiments, ultracold neutrons are stored in material or magnetic traps and their disappearance rate determines the neutron total width $\Gamma_n = \tau_n^{-1}$. As far as neutron has only one, β-decay channel and so $\Gamma_n = \Gamma_\beta$, the results of this two types of experiments should agree. But it turns out that trap experiments give neutron lifetime in average

$$\tau_{\text{trap}} = 879.4 \pm 0.6 \ , \tag{5.72}$$

while beam experiments in average yield

$$\tau_{\text{beam}} = 888.0 \pm 2.0 \ , \tag{5.73}$$

showing a discrepancy of about 4σ:

$$\Delta\tau = \tau_{\text{beam}} - \tau_{\text{trap}} = (8.6 \pm 2.1)\text{s} \ . \tag{5.74}$$

The free neutron decay is given by the master formula:

$$\tau_n = \frac{5024.46(30)\text{s}}{|V_{ud}|^2(1 + 3g_A^2)(1 + \Delta_R^V)} \tag{5.75}$$

where V_{ud} is the ud element of CKM matrix (5.25), g_A is the strength of axial coupling and Δ_R^V is radiative correction. Measuring neutron lifetime, axial coupling and knowing the radiative corrections, one can extract V_{ud} from (5.75). However, V_{ud} for today is most precisely determined from superallowed $0^+ \rightarrow 0^+$ β-decays. For making it competitive with the this determination, the neutron lifetime should be measured with precision of 0.1 s and g_A with precision 3 times better than it is now, which can be realistic in future experiments. Once increasing the precisions in neutron experiments, we will be able to estimate $n - n'$ oscillation probabilities more accurately.

Moreover, it was also suggested that $n - n'$ oscillations can take place inside a neutron star (NS), so an ordinary NS could gradually transform into a mixed star consisting in part of mirror dark matter [153]. Mixed stars can be detectable as twin partners of ordinary neutron stars: there can exist compact stars with the same masses but having different radii. If $50\% - 50\%$ proportion between two fractions can be reached asymptotically in time, then the maximum mass of such maximally mixed stars should be $\sqrt{2}$ times smaller than that of ordinary neutron star while the stars exceeding a critical mass value $M_{\text{NS}}^{\text{max}}/\sqrt{2}$ should collapse in black holes. Implications of $n - n'$ transition for the pulsar observations and for the gravitational waves have also been discussed [153].

GW: And finally one good candidate for mirror world observable is gravitational wave. GWs coming from binary mergers detected by LIGO-Virgo-Kagra (LVK), can be produced by mirror binary systems. Lack of electromagnetic counterpart radiation of LVK events, may be indicating to their mirror origin, as mirror photons would be unnoticed for us. The rest part of the thesis is devoted to discussion of LVK events in context of M world scenario.

Chapter 6

Gravitational Waves from Mirror World

In the chapter (4) we discussed gravitational wave data recorded by LIGO-Virgo-KAGRA (LVK) detectors and we have seen what major problems do existing models encounter (4.5). In the previous chapter (5) we reviewed mirror world model and we noted that if M-sector exists, it should form stars and galaxies as well. Therefore, mirror stars can also merge and produce gravitational waves. As gravity freely passes between mirror and ordinary worlds, mirror GW signal can be observed with our detectors, and it will be indistinguishable from the signal coming from ordinary star mergers. However, if coalescence of massive compact objects also produces other type of radiation like gamma-ray bursts, kilonova, neutrinos, etc., then it makes a clear division between O- and M-mergers, as mirror particles will be unnoticed to our detectors. So, in principle, any GW event without counterpart radiation can be associated with M-world. In fact, 98.9% of the event are suchlike; only 1 out of 90 mergers was multimessenger event.

As discussed before, M-world is colder and its cosmological evolution goes in different way compared to our world. If M-sector constitutes dominant part of DM, then an abundance of M-stars is higher than ordinary ones. As the evolution timescales of helium-dominated stars are shorter, this leads to formation of compact objects – neutron stars and black holes in greater amounts. Therefore, merger rates in M-sector could be higher. In our papers [1, 2], we suggested that compact objects' merger rates estimated by LIGO, can be interpreted better in M-world scenario. In [3], we investigated the binary neutron star merger without electromagnetic radiation as a manifestation of mirror world. Furthermore, in papers [4,5], we proposed that the odd mass-gap events in LVK catalog can be explained assuming mergers take place in M-sector. In upcoming sections we describe these schemes in details.

6.1   Lack of Multi-messenger Events

As described precisely in the section (4.4.1), merger of binary neutron stars or neutron star – black hole systems must be followed by emission of jets of electromagnetic radiation. If the Earth falls within the jet opening angle - that should be the case in most occasions, then we should be able to observe short γ-ray bursts and kilonova afterglow accompanying the gravitational wave. LVK data, after completing three observing runs, recorded two NS-NS merger signals, two events from BH-NS coalescence and two mergers of BH with the lower mass gap object, that can potentially be NSs. However, from these six events, only one had counterpart EM

radiation.

In general, merger of BBH system in vacuum is not expected to have follow-up EM signal. However, if BHs still accrete some gas during coalescence, then the merger may emit some kind of highly energetic EM radiation. In fact, Fermi satellite reported the detection of a transient signal at photon energies > 50 keV that lasted $1s$ and appeared $0.4s$ after the BBH event GW150914, overlapping sky localization with 70% [154]. Several mechanisms have been explored that can potentially emit GRB during BBH merger [155–157]. However, due to the lack of confidence that this GRB is actually associated with GW150914, it is admitted that none of GW produced by BBHs detected so far, are multi-messenger events.

So, out of 90 events in LVK catalog, only one has confirmed accompanying electromagnetic radiation. This led us to suggest, that the sources of these gravitational waves reside in mirror world [1, 2]. Mergers of the compact objects produces GW as well as EM radiation - mirror photons. While GWs are observed by our interferometers, mirror photons pass through our detectors and stay unnoticed.

The idea that gravitational waves can originate from the mirror copies of the Standard Model that also constitute dark matter and with the prediction that the amount is expected to be much higher than what would be expected from our world, was also put forward in the paper [158] that predates LIGO experiment.

Possibility of detecting GWs coming from merger of mirror neutron stars was suggested independently in [159]. Authors of the paper modeled equation of state of mirror neutron stars and checked that signal emitted by mirror BNS merger should be exactly the same as for ordinary stars. They concluded that, any GW from BNS without correlation with electromagnetic signal could be an indirect hint on the existence of mirror neutron stars.

6.2 Merger Rates

Lack of EM radiation is not the only indication for the mirror origin of GWs. Abundance of mirror stars must impact merger rates of compact objects, that is discussed in this section.

6.2.1 Binary Black Holes

As we have seen in the section (4.3.1), existence of primordial BHs in the mass intervals relevant for LVK, are tightly constrained. Therefore, we should focus on astrophysical BH (4.3.2). Similar to the formula of merger rates for ordinary BHs, the merger rates for the BHs that formed as a result of the collapse of mirror stars can be written as:

$$\mathcal{R}'_{\text{BBH}} = \frac{1}{2} \; \epsilon P(\tau) N'_{\text{BH}} \; . \tag{6.1}$$

We consider that, dimensionless coefficient $\epsilon < 1$ (4.10) that defines the efficiency of BBH coalescence and the delay time $P(\tau)$ (time elapsed between formation and merger of binary system) are same for ordinary and mirror systems. The difference comes from the number density of BHs, that, following (4.12), for M-sector will have a form:

$$N'_{\text{BH}} = \text{SFR(z')} \int \phi(m) \; N'(m) \int f(Z,m) \int \xi(M) \; dM \; dZ \; dm \; . \tag{6.2}$$

We assume that, stellar initial mass function $\xi(M)$, metallicity distribution function $f(Z,m)$ and galaxy stellar mass function $\phi(m)$ are same for O- and M-sectors and they are integrated in
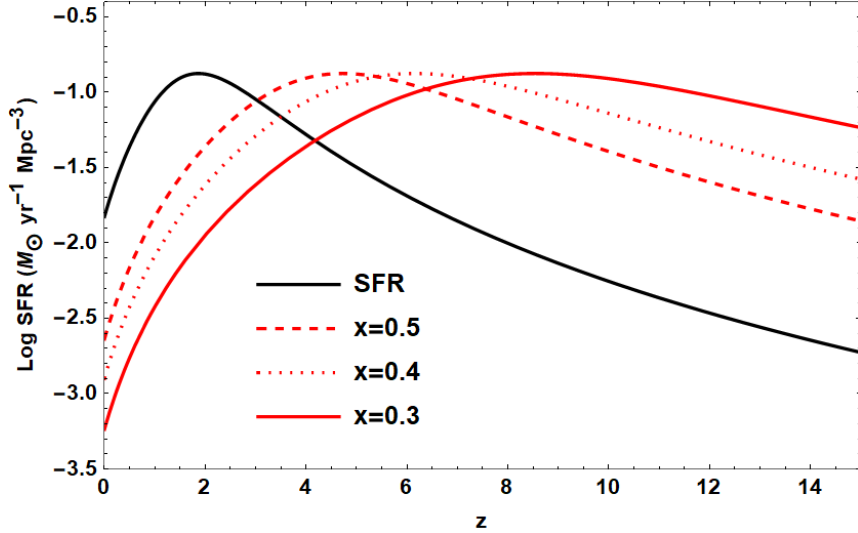
Figure 6.1: Black curve shows the star formation rate formula (4.14) as a function of refshift as given in [66]. Red curves show SFR in mirror world (6.3) for different values of x.

the same interval. But, the star formation rate SFR(z') and the number of stars in the galaxy of mass m, $N(m)$, must be different in mirror world.

SFR is usually adopted from the best-fit-function of experimental data (4.14) and it is a function of redshift. As shown in the section (5.3.3), the consequence of the lower temperature of mirror world, is that important cosmological processes like matter-radiation equality, matter-radiation decoupling, recombination, occur earlier. As a result, neutral atoms and molecules are formed in earlier times and stars start to assemble in M-world prior to ordinary one. So, star formation rate formula (4.14), is modified similar to (5.68) and now has the form:

$$\text{SFR(z')} = 0.015 \frac{(1+z')^{2.7}}{1+[(1+z')/2.9]^{5.6}} \ \text{M}_\odot \ \text{Mpc}^{-3} \ \text{yr}^{-1} \tag{6.3}$$

$$= 0.015 \frac{[x(1+z)]^{2.7}}{1+[x(1+z)/2.9]^{5.6}} \ \text{M}_\odot \ \text{Mpc}^{-3} \ \text{yr}^{-1} \ .$$

This can have a significant impact on the total number of stars and therefore the number of BHs in M-world. In the figure (6.1), we show how SFR curve is modified for different values of $x = T'/T$. As said before, SFR in ordinary world peaks at $z \sim 2$, corresponding to lookback time ~ 10 Gyr. In M-world, lower is its temperature, for higher z the SFR peaks. For $0.3 < x < 0.5$ SFR has peak around $4 < z < 8$, corresponding to lookback time $12 \ \text{Gyr} \lesssim t_{\text{lookback}} \lesssim 13$ Gyr. Furthermore, as wee see from the figure (6.1), lower is the value of x, more is the shape of the curve modified and area under the curve increases substantially. For example, for $x = 0.3$, taking the ratio

$$\frac{\int_0^{14} \text{SFR}' \ dz}{\int_0^{14} \text{SFR} \ dz} = 2.3 \ , \tag{6.4}$$

can be interpreted as ~ 2.3 times more stars were formed in mirror world compared to ordinary one in $0 < z < 14$ period. It will lead to the increase of the number of BHs in (6.2) by the same factor (6.4).

Besides that, as discussed in the section (5.3.3), mirror matter is a candidate of dark matter and certain baryogenesis mechanism (discussed in the section (5.3.2)) can naturally give $\beta =$

$\Omega'/\Omega \sim 5$. It means, mirror matter, therefore mirror stars are ~ 5 times more abundant than ordinary ones, so

$$N' \sim 5 \times N \tag{6.5}$$

in the equation (6.2). Combining (6.3) and (6.5), we get that the number of BHs in mirror sector (6.2) is about one order greater compared to ordinary world,

$$N'_{\mathrm{BH}} \sim 10 \times N_{\mathrm{BH}} . \tag{6.6}$$

As a result, the merger rate in M-world (6.1) is amplified by the same factor

$$\mathcal{R}'_{\mathrm{BBH}} \sim 10 \times \mathcal{R}^{\mathrm{theor}}_{\mathrm{BBH}} . \tag{6.7}$$

Of course, total merger rate that will be observed through gravitational waves, is

$$\mathcal{R}^{\mathrm{total}}_{\mathrm{BBH}} = \mathcal{R}^{\mathrm{theor}}_{\mathrm{BBH}} + \mathcal{R}'_{\mathrm{BBH}} , \tag{6.8}$$

but, in the configuration when $x = 0.3$ and $\beta = 5$, $\mathcal{R}^{\mathrm{total}}_{\mathrm{BBH}} \approx \mathcal{R}'_{\mathrm{BBH}}$. However, this is an extreme case, in reality, mirror matter density can be smaller $\beta < 5$. So we conclude that, BBH merger rate in mirror sector can be up to 10 times higher. Now, we remember that the merger rate in majority of models was given by the equation (4.15) and is equal to $\mathcal{R}^{\mathrm{theor}}_{\mathrm{BBH}} \sim 5 - 10$ Gpc^{-3} yr^{-1}. Inserting it into the equation (6.7), we get:

$$\mathcal{R}'_{\mathrm{BBH}} \sim 50 - 100 \ \mathrm{Gpc}^{-3} \ \mathrm{yr}^{-1} , \tag{6.9}$$

in the case all DM is made of mirror matter. Comparing it with the LVK estimations given by the equation (4.1), $\mathcal{R}_{\mathrm{BBH}} = 17.9 - 44$ Gpc^{-3}yr^{-1}, we see that (6.9) resides near the LVK upper bound. In the configuration when DM is not entirely composed of M-matter, or the SFR' is not as effective as considered, then we can reduce amplification factor by 2, getting:

$$\mathcal{R}'_{\mathrm{BBH}} \sim 25 - 50 \ \mathrm{Gpc}^{-3} \ \mathrm{yr}^{-1} , \tag{6.10}$$

that fits perfectly with LVK estimations (4.1).

6.2.2 Binary Neutron Stars

For the merger rate of binary neutron stars, similar to (6.1), one can use the formula:

$$\mathcal{R} = \frac{1}{2} \epsilon \int P(\tau) N_{\mathrm{NS}} \ d\tau , \tag{6.11}$$

where now N_{NS} is a number density of neutron stars and it is obtained by integrating IMF in the mass range $5 \ M_\odot < M < 25 \ M_\odot$ in the equation (4.12). Following the arguments from the previous section and using the results (6.4) and (6.5), merger rate for mirror BNSs will get amplified by up to the same factor 10,

$$\mathcal{R}'_{\mathrm{BNS}} \sim 10 \times \mathcal{R}^{\mathrm{theor}}_{\mathrm{BNS}} . \tag{6.12}$$

However, the uncertainty of calculated merging rate (4.4) is large, namely $\mathcal{R}_{\mathrm{BNS}} = 10 - 1700$ Gpc^{-3}yr^{-1} and it spans over more than one order of magnitude. So almost any sane theoretical estimate can be well reconciled with the results of LVK on BNS coalescence rates.

Future runs with increased sensitivity will shrink the allowed intervals making models which rely on predictions of rates more falsifiable. However, in our scenario, we can predict with a confidence that most of the detected GW events classified as BNS or BH-NS mergers will not have any electromagnetic counterparts. More precisely, we foresee that roughly only one out of ten BNS mergers will be detected as a multi-messenger event to be seen in both GWs and at least one of the canonical electromagnetic counterparts discussed above. The forecast becomes more rigorous if we restrict ourselves with those BNS (BH-NS) mergers detected not too much off from its face on position with respect to GWs observations. Although, in this case, the amount of the statistics needed for confirmation of the hypothesis should be substantially increased. In case if the mirror world contributes less than total amount of the dark matter, the rate of joint GW electromagnetic observations will increase inversely proportion to the ratio $\Omega_{B'}/\Omega_B$. Hence the measurements of the joint detection rate potentially can be used as an independent constraint on the cosmology of the mirror world dark matter.

Our forecast can be stated in another way, namely, the NS mergers rate derived from the measurements of GWs signals will be ~ 10 times higher than that one obtained from SGRB data. The same arguments are valued for BH-NS mergers, although the mass ratio of the components of such binary systems as well as configuration of angular parameters can play more critical role for such kind of estimations.

6.3   Mass Gap Objects

In the sections (4.3.3) and (4.4.2), we have discussed that there may exist so-called upper and lower mass gaps for compact objects. Pulsational pair instability forbids formation of BHs in the mass interval $\sim 65 - 150 M_\odot$. Many models of star evolution predict, that transition between NS and BH masses cannot be smooth and there should be a gap in $2.5 - 5 M_\odot$ mass range, that is supported by the observations of X-ray binaries. Nevertheless, LVK data contains reasonable amount of events with the masses within these disallowed intervals (4.3.3,4.4.2). In [4,5], we suggested that such unexpected events may be explained better, if one assumes that they originated from mirror world.

6.3.1   Upper Mass Gap

Firstly, we consider the possible M-World origin of the upper-mass-gap BHs of the LVK catalog. In principle, BH-BH mergers, which account for the most amount of LVK events, should not have optical counterparts, so they can be originated from both normal stars and mirror ones. However, as discussed above, BH binaries of mirror origin amplifies the chance of BH-BH mergers. As the microphysics of mirror stars is similar to that of ordinary stars, they probably also are subject to pair instability and produce the mass gap for intermediate mass BHs. However, as already seen, stars in M-World are born with higher initial mass, compared to ordinary stars and they evolve faster. As a result, considering SFR in M-sector shown in the figure (6.1), higher quantities of massive BHs are formed in a short period of time. Also, adding the fact that the mirror matter density can be ~ 5 times the ordinary matter density, BHs formed in the mirror matter environment, can increase in mass by accretion of mirror matter. Altogether, collisions of BHs formed by mirror stars are more frequent, increasing merger rate naturally as discussed previously.

As a consequence, hierarchical mergers can form intermediate mass BHs in M-World more

easily. As merger rates are amplified in M-sector, the extreme assumptions made by [71] in equation (4.17) can be relaxed and one can still obtain merger rates of GW190521-like systems within the LVK interval (4.16). To be more specific, as the formation of BHs is ~ 10 times more efficient (6.2) in M-world, one can decrease the product $f \equiv f_{\text{triple}} \times f_{\text{survival}} \times f_{\text{merger}}$ in the equation (4.17) by one order of magnitude and the obtained value (4.19) will remain unchanged. Such reduced value of f is not so extreme anymore and it looks more plausible. In this way, the obtained merger rate for the first generation BHs, that formed the heavy components of GW190426_190642 and GW190521, look more natural. So, discussing hierarchical BBH mergers in the framework of the M-World scenario can stand as a good interpretation for LVK's upper-mass-gap events.

6.3.2   Lower Mass Gap

Another outcome of the M-World scenario can be explanation of issues relating the compact objects residing in or next to the lower-mass-gap in LVK catalog. As stated before, NS-NS or BH-NS mergers, in case they contain normal NSs, should be typically accompanied by GRB and optical afterglows. However, neither NS-NS event GW190425, or BH-NS mergers GW200105 and GW200115, nor BH-mass gap events GW190814 and GW200210_092254 had such associations, that can potentially stand as a manifestation of their mirror origin.

So, the fact that "heavy" NSs are not detected through electromagnetic spectrum but are observed through gravitational radiation, may be an indication that they exist in the mirror world. As discussed above, in order to form a binary NS system like GW190425, an ultra-tight binary with NS and massive He-star is required. As M-World is dominated by helium and so it is inhabited mostly by He-stars, such configuration can be achieved easily. The formation of GW190814-like systems is also challenging for current theories and their abundance is expected to be extremely low. However, as in M-World the abundance of matter exceeds ~ 5 times the abundance of ordinary matter and stars in M-World evolve a way faster, the probability of hierarchical mergers is increased by an order of magnitude, and the formation of GW190814-like systems should be more common.

6.4   Future Prospects

Gravitational-wave physics is just at its dawn. The first generation detectors LIGO and Virgo were unable to observe GWs. However, after upgrades to Advanced LIGO and Advanced Virgo, these second generation observatories reached enough sensitivity to detect signals. From 2015 to 2020, three observing runs were conducted with total runtime of approximately 2 years. During this time, LIGO and Virgo, with KAGRA joining for last few months, detected 90 confirmed signals. In average, it was one verified event in every ≈ 8 days.

Fourth observing run of LVK is planned to start in march 2023. LIGO India (IndIGO) is intended to join in 2024. The sensitivities of the detectors will remain same, however, upgrading their performance and adding more new observatories will increase number of detected events significantly. Building of Third generation ground-based GW observatories Einstein Telescope and Cosmic explorer are proposed and planned to be fulfilled in 2030s. Also, the first space-based detector LISA (Laser Interferometer Space Antenna) was approved as one of the main research missions of European Space Agency.

Drastic increase in GW data, that is expected in the near future, will allow to confirm or

reject many of the proposals. Our suggestion, that mirror objects can emit GWs is among the theories that can be tested through this path. Raise in number of detected GWs will ease the search of associated electromagnetic radiation and increase the number of multi-messenger events. This will help to shed light on many existing problems. However, the main prediction of M-world scenario is, that quantity of multi-messenger event will be low, as most of mergers are accompanied by mirror photons that are invisible for us.

One interesting prospect for future studies in this field are GWs from the objects that compound both ordinary and mirror matter. As mentioned earlier, it has been suggested that $n \to n'$ oscillations can take place inside a neutrons star, so an ordinary NS could gradually transform into a mixed star consisting $50\% - 50\%$ of ordinary and mirror matter [153]. In this case, mass-size ration for the star changes and modify a GW signal.

Another intriguing case can be a merger of ordinary and mirror NSs. In principle, it is possible to form the binary of ordinary and mirror stars. Even though they do not 'see' each other, gravitational attraction will force them to merge. While merging, although they both are neutron stars and should be impact companions tidal field, they actually 'touch' each other at later times compared to normal case. This should leave an imprint of produced gravitational waveform.

Once studying these cases and knowing what kind of corrections should be expected in gravitational waveform, one can search for indications on such exotic events in gravitational-wave data.

Chapter 7

Conclusion

Gravitational waves, predicted long time ago by Albert Einstein in his theory of general relativity, were directly detected for the first time in 2015 by LIGO. This served as a beginning of completely new era in multi-messenger astronomy. 90 confirmed events in GWTC-3 opened up a novel window for models of binary stars evolution. Being in agreement with GR predictions, some properties of observed GWs are still hard to be explained using existing models. Among the peculiar features are: absence of accompanying electromagnetic radiation in all events except one; high merger rates compared to predictions; events containing objects that have mass in the forbidden intervals, where majority of models expect gaps.

In order to deal with this confusions, we suggested the mirror world scenario. About 27% of the total energy budget of the Universe is thought to be occupied by dark matter, composition of which is still unknown. Mirror matter is a long-standing candidates of DM and may constitute it entirely or just some part of it. According to M-world theory, there exist an exact mirror copy of standard model of particle physics, that have a right-handed weak interactions. These twin mirror particles have properties similar to ordinary ones: exactly same masses, charges, interaction laws, etc. With such extension, global theory has left-right symmetry, that was broken in SM.

If M-sector do exists, it was created by Big Bang, along with ordinary matter. However cosmological evolution of M-world cannot be identical to ordinary one, as it would be in immediate conflict with the bounds from BBN. To avoid this, M-sector must have had a lower initial reheating temperature. Then, if two sectors interact weakly, only through gravity, they do not come into thermal equilibrium with each other and maintain a constant temperature ratio $x = T'/T (< 0.65$ from BBN). Certain mechanism of lepto-baryogenesis can produce baryon asymmetry in both sectors simultaneously. In fact, under certain circumstances it is possible to have $\beta = \Omega'_b/\Omega_b \approx 5$ and mirror matter can explain dark matter completely.

One of the consequence of the lower temperature is a fact that M-world should be dominated by helium. This will affect the formation and evolution properties of stars and galaxies. It has been shown that early fragmentation of mirror gas into stars, can guarantee mirror matter to maintain a spherical form and do not collapse into disk, as does ordinary matter. In this way, M-matter can form spherical DM halos observed in galaxies.

Having the microphysics similar to ordinary matter, mirror sector is destined to form stars, compact objects like NS and BH, as well binary systems that can merge and produce GWs. In our papers [1–5], we built up a model, that implements GWs detected by LVK in the framework of mirror matter. In this thesis, we summarized our model and demonstrated that some of the inconsistencies arisen in LVK data can be solved in M-world scenario.

In particular, lack of multi-messenger events is natural in our model. If GWs detected by LVK were produced by mergers of mirror binaries, then electromagnetic radiation emitted as mirror photons would be unnoticed by our detectors as they are made of ordinary matter. Furthermore, He-rich stars formed at early times in mirror sector, evolve faster and their path to remnant compact objects - mirror NSs and BHs are shorter. Besides that, star formation rate formula that has a peak at $z \approx 2$ in ordinary world, peaks earlier in M-sector, at about $4 < z < 8$. Altogether amplifies the merger rate in M-sector by factor ~ 10. Existing models of binary compact objects formation and coalescence predicted merger rates lower than observed by LVK. We suggested, that accounting for the GWs coming from mirror matter, total merger rates will get amplified by the factor ~ 10, that comes in accordance with detections.

Besides that, the events that fall in the mass gaps and are hard to be described using typical models, can be better interpreted in M-world scenario. As helium-rich stars evolve faster and their abundance is higher, they form NSs and BHs at early stages at greater amounts. As a result, possibility of hierarchical mergers in M-world is increased and objects with the masses in the gaps are formed more easily.

Abbreviations:

BA	Baryon Asymmetry
BBH	Binary Black Hole
BBN	Big Bang Nucleosynthesis
BH	Black Hole
BNS	Binary Neutron Star
CDM	Cold Dark Matter
CMB	Cosmic Microwave Background
CP	Charge-Parity
CPT	Charge-Parity-Time
DE	Dark Energy
DM	Dark Matter
EM	ElectroMagnetic
EW	ElectroWeak
GR	General Relativity
HDM	Hot Dark Matter
GRB	Gamma Ray Burst
GW	Gravitational Wave
GWTC	Gravitational-Wave Transient Catalog
KAGRA	Kamioka Gravitational Wave Detector
LSS	Large Scale Structure
LIGO	The Laser Interferometer Gravitational-Wave Observatory
LVK	LIGO-Virgo-KAGRA
MACHO	Massive Compact Halo Object
MBDM	Mirror Baryon Dark Matter
MRD	Matter-Radiation Decoupling
MRE	Matter-Radiation Equality
M-World	Mirror World
NS	Neutron Star
O1(2,3)	Observing run 1(2,3)
O-World	Ordinary World
PBH	Primordial Black Hole
QCD	Quantum ChromoDynamics
QED	Quantum ElectroDynamics
QFT	Quantum Field Theory
SFR	Star Formation Rate
SGRB	Short Gamma Ray Burst
SM	Standard Model
SN	Supernova
SR	Special Relativity
SSB	Spontaneous Symmetry Breaking
VEV	Vacuum Expectation Value
WDM	Warm Dark Matter
WIMP	Weakly Interacting Massive Particle
ΛCDM	Lambda Cold Dark Matter

Bibliography

[1] R. Beradze and M. Gogberashvili, "LIGO Signals from the Mirror World," Mon. Not. Roy. Astron. Soc. **487** (2019) no.1, 650-652 doi:10.1093/mnras/stz1295 [arXiv:1902.05425 [gr-qc]].

[2] R. Beradze and M. Gogberashvili, "Gravitational Waves from Mirror World," MDPI Physics **1** (2019) no.1, 67-75 doi:10.3390/physics1010007 [arXiv:1905.02787 [gr-qc]].

[3] R. Beradze, M. Gogberashvili and A. S. Sakharov, "Binary Neutron Star Mergers with Missing Electromagnetic Counterparts as Manifestations of Mirror World," Phys. Lett. B **804** (2020), 135402 doi:10.1016/j.physletb.2020.135402 [arXiv:1910.04567 [astro-ph.HE]].

[4] R. Beradze and M. Gogberashvili, "Unexpected LIGO events and the Mirror World," Mon. Not. Roy. Astron. Soc. **503** (2021) no.2, 2882-2886 doi:10.1093/mnras/stab685 [arXiv:2101.12532 [astro-ph.CO]].

[5] R. Beradze and M. Gogberashvili, "LIGO signals from mirror world," PoS **Regio2021** (2022), 029 doi:10.22323/1.412.0029

[6] B. Belfatto, R. Beradze and Z. Berezhiani, "The CKM unitarity problem: A trace of new physics at the TeV scale?," Eur. Phys. J. C **80** (2020) no.2, 149 doi:10.1140/epjc/s10052-020-7691-6 [arXiv:1906.02714 [hep-ph]].

[7] R. Beradze and M. Gogberashvili, "Can the quasi-molecular mechanism of recombination decrease the Hubble tension?," Phys. Dark Univ. **32** (2021), 100841 doi:10.1016/j.dark.2021.100841 [arXiv:2001.05874 [astro-ph.CO]].

[8] S. Carroll, "Spacetime and Geometry: An Introduction to General Relativity," Cambridge: Cambridge University Press. doi:10.1017/9781108770385

[9] P. A. Zyla *et al.* [Particle Data Group], "Review of Particle Physics," PTEP **2020** (2020) no.8, 083C01 doi:10.1093/ptep/ptaa104

[10] N. Aghanim *et al.* [Planck], "Planck 2018 results. VI. Cosmological parameters," Astron. Astrophys. **641** (2020), A6 [erratum: Astron. Astrophys. **652** (2021), C4] doi:10.1051/0004-6361/201833910 [arXiv:1807.06209 [astro-ph.CO]].

[11] T. Kereselidze, I. Noselidze and J. F. Ogilvie, "Influence of a quasi-molecular mechanism of recombination on the formation of hydrogen in the early universe," Mon. Not. Roy. Astron. Soc. **501** (2021) no.1, 1160-1167 doi:10.1093/mnras/staa3622 [arXiv:2008.01660 [physics.atom-ph]], T. Kereselidze and I. Noselidze, "A quasi-molecular mechanism of formation of hydrogen in the early Universe – a scheme of calculation," [arXiv:2104.11584 [astro-ph.CO]].

[12] G. Bertone, D. Hooper and J. Silk, "Particle dark matter: Evidence, candidates and constraints," Phys. Rept. **405** (2005), 279-390 doi:10.1016/j.physrep.2004.08.031 [arXiv:hep-ph/0404175 [hep-ph]].

[13] J. L. Feng, "Dark Matter Candidates from Particle Physics and Methods of Detection," Ann. Rev. Astron. Astrophys. **48** (2010), 495-545 doi:10.1146/annurev-astro-082708-101659 [arXiv:1003.0904 [astro-ph.CO]].

[14] G. Arcadi, M. Dutra, P. Ghosh, M. Lindner, Y. Mambrini, M. Pierre, S. Profumo and F. S. Queiroz, "The waning of the WIMP? A review of models, searches, and constraints," Eur. Phys. J. C **78** (2018) no.3, 203 doi:10.1140/epjc/s10052-018-5662-y [arXiv:1703.07364 [hep-ph]].

[15] L. Roszkowski, E. M. Sessolo and S. Trojanowski, "WIMP dark matter candidates and searches—current status and future prospects," Rept. Prog. Phys. **81** (2018) no.6, 066201 doi:10.1088/1361-6633/aab913 [arXiv:1707.06277 [hep-ph]].

[16] J. Preskill, M. B. Wise and F. Wilczek, "Cosmology of the Invisible Axion," Phys. Lett. B **120** (1983), 127-132 doi:10.1016/0370-2693(83)90637-8

[17] D. J. E. Marsh, "Axion Cosmology," Phys. Rept. **643** (2016), 1-79 doi:10.1016/j.physrep.2016.06.005 [arXiv:1510.07633 [astro-ph.CO]].

[18] S. Dodelson and L. M. Widrow, "Sterile-neutrinos as dark matter," Phys. Rev. Lett. **72** (1994), 17-20 doi:10.1103/PhysRevLett.72.17 [arXiv:hep-ph/9303287 [hep-ph]].

[19] G. Jungman, M. Kamionkowski and K. Griest, "Supersymmetric dark matter," Phys. Rept. **267** (1996), 195-373 doi:10.1016/0370-1573(95)00058-5 [arXiv:hep-ph/9506380 [hep-ph]].

[20] S. L. Dubovsky, P. G. Tinyakov and I. I. Tkachev, "Massive graviton as a testable cold dark matter candidate," Phys. Rev. Lett. **94** (2005), 181102 doi:10.1103/PhysRevLett.94.181102 [arXiv:hep-th/0411158 [hep-th]].

[21] B. P. Abbott *et al.* [LIGO Scientific and Virgo], "The basic physics of the binary black hole merger GW150914," Annalen Phys. **529** (2017) no.1-2, 1600209 doi:10.1002/andp.201600209 [arXiv:1608.01940 [gr-qc]].

[22] B. P. Abbott *et al.* [LIGO Scientific and Virgo], "Observation of Gravitational Waves from a Binary Black Hole Merger," Phys. Rev. Lett. **116** (2016) no.6, 061102 doi:10.1103/PhysRevLett.116.061102 [arXiv:1602.03837 [gr-qc]].

[23] B. P. Abbott *et al.* [LIGO Scientific and Virgo], "GW151226: Observation of Gravitational Waves from a 22-Solar-Mass Binary Black Hole Coalescence," Phys. Rev. Lett. **116** (2016) no.24, 241103 doi:10.1103/PhysRevLett.116.241103 [arXiv:1606.04855 [gr-qc]].

[24] B. P. Abbott *et al.* [LIGO Scientific and VIRGO], "GW170104: Observation of a 50-Solar-Mass Binary Black Hole Coalescence at Redshift 0.2," Phys. Rev. Lett. **118** (2017) no.22, 221101 [erratum: Phys. Rev. Lett. **121** (2018) no.12, 129901] doi: 10.1103/PhysRevLett.118.221101 [arXiv:1706.01812 [gr-qc]].

[25] B. P. Abbott *et al.* [LIGO Scientific and Virgo], "GW170814: A Three-Detector Observation of Gravitational Waves from a Binary Black Hole Coalescence," Phys. Rev. Lett. **119** (2017) no.14, 141101 doi:10.1103/PhysRevLett.119.141101 [arXiv:1709.09660 [gr-qc]].

[26] B. P. Abbott *et al.* [LIGO Scientific and Virgo], "GW170608: Observation of a 19-solar-mass Binary Black Hole Coalescence," Astrophys. J. Lett. **851** (2017), L35 doi:10.3847/2041-8213/aa9f0c [arXiv:1711.05578 [astro-ph.HE]].

[27] B. P. Abbott *et al.* [LIGO Scientific and Virgo], "GW170817: Observation of Gravitational Waves from a Binary Neutron Star Inspiral," Phys. Rev. Lett. **119** (2017) no.16, 161101 doi:10.1103/PhysRevLett.119.161101 [arXiv:1710.05832 [gr-qc]].

[28] B. P. Abbott *et al.* [LIGO Scientific and Virgo], "GWTC-1: A Gravitational-Wave Transient Catalog of Compact Binary Mergers Observed by LIGO and Virgo during the First and Second Observing Runs," Phys. Rev. X **9** (2019) no.3, 031040 doi:10.1103/PhysRevX.9.031040 [arXiv:1811.12907 [astro-ph.HE]].

[29] B. P. Abbott *et al.* [LIGO Scientific and Virgo], "GW190425: Observation of a Compact Binary Coalescence with Total Mass $\sim 3.4 M_{\odot}$," Astrophys. J. Lett. **892** (2020) no.1, L3 doi:10.3847/2041-8213/ab75f5 [arXiv:2001.01761 [astro-ph.HE]].

[30] R. Abbott *et al.* [LIGO Scientific and Virgo], "GW190521: A Binary Black Hole Merger with a Total Mass of $150 M_{\odot}$," Phys. Rev. Lett. **125** (2020) no.10, 101102 doi:10.1103/PhysRevLett.125.101102 [arXiv:2009.01075 [gr-qc]].

[31] R. Abbott *et al.* [LIGO Scientific and Virgo], "GW190412: Observation of a Binary-Black-Hole Coalescence with Asymmetric Masses," Phys. Rev. D **102** (2020) no.4, 043015 doi:10.1103/PhysRevD.102.043015 [arXiv:2004.08342 [astro-ph.HE]].

[32] R. Abbott *et al.* [LIGO Scientific and Virgo], "GW190814: Gravitational Waves from the Coalescence of a 23 Solar Mass Black Hole with a 2.6 Solar Mass Compact Object," Astrophys. J. Lett. **896** (2020) no.2, L44 doi:10.3847/2041-8213/ab960f [arXiv:2006.12611 [astro-ph.HE]].

[33] R. Abbott *et al.* [LIGO Scientific and Virgo], "GWTC-2: Compact Binary Coalescences Observed by LIGO and Virgo During the First Half of the Third Observing Run," Phys. Rev. X **11** (2021), 021053 doi:10.1103/PhysRevX.11.021053 [arXiv:2010.14527 [gr-qc]].

[34] R. Abbott *et al.* [LIGO Scientific and VIRGO], "GWTC-2.1: Deep Extended Catalog of Compact Binary Coalescences Observed by LIGO and Virgo During the First Half of the Third Observing Run," [arXiv:2108.01045 [gr-qc]].

[35] R. Abbott *et al.* [LIGO Scientific, KAGRA and VIRGO], "Observation of Gravitational Waves from Two Neutron Star–Black Hole Coalescences," Astrophys. J. Lett. **915** (2021) no.1, L5 doi:10.3847/2041-8213/ac082e [arXiv:2106.15163 [astro-ph.HE]].

[36] R. Abbott *et al.* [LIGO Scientific, VIRGO and KAGRA], "GWTC-3: Compact Binary Coalescences Observed by LIGO and Virgo During the Second Part of the Third Observing Run," [arXiv:2111.03606 [gr-qc]].

[37] A. Goldstein *et al.*, "An ordinary short gamma-ray burst with extraordinary implications: Fermi-GBM detection of GRB 170817A," Astrophys. J. Lett. **848** (2017) L14 doi: 10.3847/2041-8213/aa8f41 [arXiv: 1710.05446 [astro-ph.HE]].

[38] V. Savchenko *et al.*, "INTEGRAL detection of the first prompt gamma-ray signal coincident with the gravitational-wave event GW170817," Astrophys. J. Lett. **848** (2017) L15 doi: 10.3847/2041-8213/aa8f94 [arXiv: 1710.05449 [astro-ph.HE]].

[39] R. Abbott *et al.* [LIGO Scientific and Virgo], "Search for Gravitational Waves Associated with Gamma-Ray Bursts Detected by Fermi and Swift During the LIGO-Virgo Run O3a," Astrophys. J. **915** (2021) 86, doi: 10.3847/1538-4357/abee15 [arXiv: 2010.14550 [astro-ph.HE]].

[40] R. Abbott *et al.* [LIGO Scientific, KAGRA and VIRGO], "Search for Gravitational Waves Associated with Gamma-Ray Bursts Detected by Fermi and Swift during the LIGO–Virgo Run O3b," Astrophys. J. **928** (2022) no.2, 186 doi:10.3847/1538-4357/ac532b [arXiv:2111.03608 [astro-ph.HE]].

[41] B. P. Abbott *et al.* [LIGO Scientific and Virgo], "Binary Black Hole Population Properties Inferred from the First and Second Observing Runs of Advanced LIGO and Advanced Virgo," Astrophys. J. Lett. **882** (2019) no.2, L24 doi:10.3847/2041-8213/ab3800 [arXiv:1811.12940 [astro-ph.HE]].

[42] R. Abbott *et al.* [LIGO Scientific and Virgo], "Population Properties of Compact Objects from the Second LIGO-Virgo Gravitational-Wave Transient Catalog," Astrophys. J. Lett. **913** (2021) no.1, L7 doi:10.3847/2041-8213/abe949 [arXiv:2010.14533 [astro-ph.HE]].

[43] R. Abbott *et al.* [LIGO Scientific, VIRGO and KAGRA], "The population of merging compact binaries inferred using gravitational waves through GWTC-3," [arXiv:2111.03634 [astro-ph.HE]].

[44] A. Heger, C. L. Fryer, S. E. Woosley, N. Langer and D. H. Hartmann, "How massive single stars end their life," Astrophys. J. **591** (2003), 288-300 doi:10.1086/375341 [arXiv:astro-ph/0212469 [astro-ph]].

[45] K. Belczynski, D. E. Holz, T. Bulik and R. O'Shaughnessy, "The first gravitational-wave source from the isolated evolution of two 40-100 Msun stars," Nature **534** (2016), 512 doi:10.1038/nature18322 [arXiv:1602.04531 [astro-ph.HE]].

[46] N. Giacobbo and M. Mapelli, "The progenitors of compact-object binaries: impact of metallicity, common envelope and natal kicks," Mon. Not. Roy. Astron. Soc. **480** (2018) no.2, 2011-2030 doi:10.1093/mnras/sty1999 [arXiv:1806.00001 [astro-ph.HE]].

[47] E. P. J. van den Heuvel, S. F. Portegies Zwart and S. E. de Mink, "Forming short-period Wolf–Rayet X-ray binaries and double black holes through stable mass transfer," Mon. Not. Roy. Astron. Soc. **471** (2017) no.4, 4256-4264 doi:10.1093/mnras/stx1430 [arXiv:1701.02355 [astro-ph.SR]].

[48] A. Olejak, K. Belczynski and N. Ivanova, "Impact of common envelope development criteria on the formation of LIGO/Virgo sources," Astron. Astrophys. **651** (2021), A100 doi:10.1051/0004-6361/202140520 [arXiv:2102.05649 [astro-ph.HE]].

[49] I. Mandel and S. E. de Mink, "Merging binary black holes formed through chemically homogeneous evolution in short-period stellar binaries," Mon. Not. Roy. Astron. Soc. **458** (2016) no.3, 2634-2647 doi:10.1093/mnras/stw379 [arXiv:1601.00007 [astro-ph.HE]].

[50] P. Marchant, N. Langer, P. Podsiadlowski, T. M. Tauris and T. J. Moriya, "A new route towards merging massive black holes," Astron. Astrophys. **588** (2016), A50 doi:10.1051/0004-6361/201628133 [arXiv:1601.03718 [astro-ph.SR]].

[51] A. Askar, M. Szkudlarek, D. Gondek-Rosińska, M. Giersz and T. Bulik, "MOCCA-SURVEY Database – I. Coalescing binary black holes originating from globular clusters," Mon. Not. Roy. Astron. Soc. **464** (2017) no.1, L36-L40 doi:10.1093/mnrasl/slw177 [arXiv:1608.02520 [astro-ph.HE]].

[52] F. Antonini, S. Toonen and A. S. Hamers, "Binary black hole mergers from field triples: properties, rates and the impact of stellar evolution," Astrophys. J. **841** (2017) no.2, 77 doi:10.3847/1538-4357/aa6f5e [arXiv:1703.06614 [astro-ph.GA]].

[53] G. Fragione and B. Kocsis, "Black hole mergers from quadruples," Mon. Not. Roy. Astron. Soc. **486** (2019) no.4, 4781-4789 doi:10.1093/mnras/stz1175 [arXiv:1903.03112 [astro-ph.GA]].

[54] T. Nakamura, M. Sasaki, T. Tanaka and K. S. Thorne, "Gravitational waves from coalescing black hole MACHO binaries," Astrophys. J. Lett. **487** (1997), L139-L142 doi:10.1086/310886 [arXiv:astro-ph/9708060 [astro-ph]].

[55] M. Sasaki, T. Suyama, T. Tanaka and S. Yokoyama, "Primordial Black Hole Scenario for the Gravitational-Wave Event GW150914," Phys. Rev. Lett. **117** (2016) no.6, 061101 [erratum: Phys. Rev. Lett. **121** (2018) no.5, 059901] doi:10.1103/PhysRevLett.117.061101 [arXiv:1603.08338 [astro-ph.CO]].

[56] M. Sasaki, T. Suyama, T. Tanaka and S. Yokoyama, "Primordial black holes—perspectives in gravitational wave astronomy," Class. Quant. Grav. **35** (2018) no.6, 063001 doi:10.1088/1361-6382/aaa7b4 [arXiv:1801.05235 [astro-ph.CO]].

[57] A. Dolgov and K. Postnov, "Why the mean mass of primordial black hole distribution is close to $10M_\odot$," JCAP **07** (2020), 063 doi:10.1088/1475-7516/2020/07/063 [arXiv:2004.11669 [astro-ph.CO]].

[58] A. D. Dolgov, A. G. Kuranov, N. A. Mitichkin, S. Porey, K. A. Postnov, O. S. Sazhina and I. V. Simkin, "On mass distribution of coalescing black holes," JCAP **12** (2020), 017 doi:10.1088/1475-7516/2020/12/017 [arXiv:2005.00892 [astro-ph.CO]].

[59] R. A. Allsman *et al.* [Macho], "MACHO project limits on black hole dark matter in the 1-30 solar mass range," Astrophys. J. Lett. **550** (2001), L169 doi:10.1086/319636 [arXiv:astro-ph/0011506 [astro-ph]].

[60] P. Tisserand *et al.* [EROS-2], "Limits on the Macho Content of the Galactic Halo from the EROS-2 Survey of the Magellanic Clouds," Astron. Astrophys. **469** (2007), 387-404 doi:10.1051/0004-6361:20066017 [arXiv:astro-ph/0607207 [astro-ph]].

[61] J. Yoo, J. Chaname and A. Gould, "The end of the MACHO era: limits on halo dark matter from stellar halo wide binaries," Astrophys. J. **601** (2004), 311-318 doi:10.1086/380562 [arXiv:astro-ph/0307437 [astro-ph]].

[62] M. Ricotti, J. P. Ostriker and K. J. Mack, "Effect of Primordial Black Holes on the Cosmic Microwave Background and Cosmological Parameter Estimates," Astrophys. J. **680** (2008), 829 doi:10.1086/587831 [arXiv:0709.0524 [astro-ph]].

[63] S. Bird, I. Cholis, J. B. Muñoz, Y. Ali-Haïmoud, M. Kamionkowski, E. D. Kovetz, A. Raccanelli and A. G. Riess, "Did LIGO detect dark matter?," Phys. Rev. Lett. **116** (2016) no.20, 201301 doi:10.1103/PhysRevLett.116.201301 [arXiv:1603.00464 [astro-ph.CO]].

[64] O. D. Elbert, J. S. Bullock and M. Kaplinghat, "Counting Black Holes: The Cosmic Stellar Remnant Population and Implications for LIGO," Mon. Not. Roy. Astron. Soc. **473** (2018) no.1, 1186-1194 doi:10.1093/mnras/stx1959 [arXiv:1703.02551 [astro-ph.GA]].

[65] H. Sana, S. E. de Mink, A. de Koter, N. Langer, C. J. Evans, M. Gieles, E. Gosset, R. G. Izzard, J. B. L. Bouquin and F. R. N. Schneider, "Binary interaction dominates the evolution of massive stars," Science **337** (2012), 444 doi:10.1126/science.1223344 [arXiv:1207.6397 [astro-ph.SR]].

[66] P. Madau and M. Dickinson, "Cosmic Star Formation History," Ann. Rev. Astron. Astrophys. **52** (2014), 415-486 doi:10.1146/annurev-astro-081811-125615 [arXiv:1403.0007 [astro-ph.CO]].

[67] S. E. Woosley, S. Blinnikov and A. Heger, "Pulsational pair instability as an explanation for the most luminous supernovae," Nature **450** (2007) 390 doi: 10.1038/nature06333 [arXiv: 0710.3314 [astro-ph]].

[68] S. E. Woosley, "Pulsational pair-instability supernovae," Astrophys. J. **836** (2017) 244 doi: 10.3847/1538-4357/836/2/244 [arXiv: 1608.08939 [astro-ph.HE]].

[69] C. Kimball *et al.*, "Black hole genealogy: Identifying hierarchical mergers with gravitational waves," Astrophys. J. **900** (2020) 177 doi: 10.3847/1538-4357/aba518 [arXiv: 2005.00023 [astro-ph.HE]].

[70] M. Mapelli *et al.*, "Hierarchical mergers in young, globular and nuclear star clusters: black hole masses and merger rates," Symmetry **13** (2021) 1678 [arXiv: 2007.15022 [astro-ph.HE]].

[71] B. Liu and D. Lai, "Hierarchical black-hole mergers in multiple systems: Constrain the formation of GW190412, GW190814 and GW190521-like events," Mon. Not. Roy. Astron. Soc. **502** (2021) 2049 doi: 10.1093/mnras/stab178 [arXiv: 2009.10068 [astro-ph.HE]].

[72] C. O. Lousto and Y. Zlochower, "Hangup kicks: Still larger recoils by partial spin/orbit alignment of black-hole binaries," Phys. Rev. Lett. **107** (2011) 231102 doi: 10.1103/PhysRevLett.107.231102 [arXiv: 1108.2009 [gr-qc]].

[73] B. Bruegmann, J. A. Gonzalez, M. Hannam, S. Husa and U. Sperhake, "Exploring black hole superkicks," Phys. Rev. D **77** (2008) 124047 doi: 10.1103/PhysRevD.77.124047 [arXiv: 0707.0135 [gr-qc]].

[74] V. Varma, M. Isi and S. Biscoveanu, "Extracting the gravitational recoil from black hole merger signals," Phys. Rev. Lett. **124** (2020) 101104 doi: 10.1103/PhysRevLett.124.101104 [arXiv: 2002.00296 [gr-qc]].

[75] M. A. Sedda, M. Mapelli, M. Spera, M. Benacquista and N. Giacobbo, "Fingerprints of binary black hole formation channels encoded in the mass and spin of merger remnants," Astrophys. J. **894** (2020) 133 doi: 10.3847/1538-4357/ab88b2 [arXiv: 2003.07409 [astro-ph.GA]].

[76] V. Baibhav *et al.*, "The mass gap, the spin gap, and the origin of merging binary black holes," Phys. Rev. D **102** (2020) 043002 doi: 10.1103/PhysRevD.102.043002 [arXiv: 2004.00650 [astro-ph.HE]].

[77] R. Abbott *et al.* [LIGO Scientific and Virgo], "Properties and Astrophysical Implications of the 150 M$_\odot$ Binary Black Hole Merger GW190521," Astrophys. J. Lett. **900** (2020) no.1, L13 doi:10.3847/2041-8213/aba493 [arXiv:2009.01190 [astro-ph.HE]].

[78] T. Chiba and S. Yokoyama, "Spin Distribution of Primordial Black Holes," PTEP **2017** (2017) no.8, 083E01 doi:10.1093/ptep/ptx087 [arXiv:1704.06573 [gr-qc]].

[79] V. De Luca, G. Franciolini, P. Pani and A. Riotto, "The evolution of primordial black holes and their final observable spins," JCAP **04** (2020), 052 doi:10.1088/1475-7516/2020/04/052 [arXiv:2003.02778 [astro-ph.CO]].

[80] V. De Luca, V. Desjacques, G. Franciolini, P. Pani and A. Riotto, "GW190521 Mass Gap Event and the Primordial Black Hole Scenario," Phys. Rev. Lett. **126** (2021) no.5, 051101 doi:10.1103/PhysRevLett.126.051101 [arXiv:2009.01728 [astro-ph.CO]].

[81] A. Sadowski, K. Belczynski, T. Bulik, N. Ivanova, F. A. Rasio and R. W. O'Shaughnessy, "The Total Merger Rate of Compact Object Binaries In The Local Universe," Astrophys. J. **676** (2008) 1162 doi: 10.1086/528932 [arXiv: 0710.0878 [astro-ph]].

[82] J. A. Faber and F. A. Rasio, "Binary Neutron Star Mergers," Living Rev. Rel. **15** (2012) 8 doi: 10.12942/lrr-2012-8 [arXiv:1204.3858 [gr-qc]].

[83] E. Burns, "Neutron Star Mergers and How to Study Them," Living Rev. Rel. **23** (2020) no.1, 4 doi:10.1007/s41114-020-00028-7 [arXiv:1909.06085 [astro-ph.HE]].

[84] K. Belczynski, V. Kalogera and T. Bulik, "A Comprehensive study of binary compact objects as gravitational wave sources: Evolutionary channels, rates, and physical properties," Astrophys. J. **572** (2001) 407 doi: 10.1086/340304 [astro-ph/0111452].

[85] F. Zappa, S. Bernuzzi, D. Radice, A. Perego and T. Dietrich, "Gravitational-wave luminosity of binary neutron stars mergers," Phys. Rev. Lett. **120** (2018) 111101 doi: 10.1103/PhysRevLett.120.111101 [arXiv:1712.04267 [gr-qc]].

[86] B. F. Schutz, "Networks of gravitational wave detectors and three figures of merit," Class. Quant. Grav. **28** (2011) 125023 doi: 10.1088/0264-9381/28/12/125023 [arXiv: 1102.5421 [astro-ph.IM]].

[87] R. Fernández and B. D. Metzger, "Electromagnetic Signatures of Neutron Star Mergers in the Advanced LIGO Era," Ann. Rev. Nucl. Part. Sci. **66** (2016) 23 doi: 10.1146/annurev-nucl-102115-044819 [arXiv: 1512.05435 [astro-ph.HE]].

[88] B. D. Metzger and R. Fernández, "Red or blue? A potential kilonova imprint of the delay until black hole formation following a neutron star merger," Mon. Not. Roy. Astron. Soc. **441** (2014) 3444 doi: 10.1093/mnras/stu802 [arXiv: 1402.4803 [astro-ph.HE]].

[89] B. D. Metzger, "Kilonovae," Living Rev. Rel. **23** (2020) 1 doi:10.1007/s41114-019-0024-0 [arXiv: 1910.01617 [astro-ph.HE]].

[90] M. Tanaka, "Kilonova/Macronova Emission from Compact Binary Mergers," Adv. Astron. **2016** (2016) 6341974 doi: 10.1155/2016/6341974 [arXiv: 1605.07235 [astro-ph.HE]].

[91] W. f. Fong, E. Berger, R. Margutti and B. A. Zauderer, "A Decade of Short-duration Gamma-ray Burst Broadband Afterglows: Energetics, Circumburst Densities, and jet Opening Angles," Astrophys. J. **815** (2015) 102 doi: 10.1088/0004-637X/815/2/102 [arXiv: 1509.02922 [astro-ph.HE]].

[92] E. Nakar and T. Piran, "Radio Remnants of Compact Binary Mergers - the Electromagnetic Signal that will follow the Gravitational Waves," Nature **478** (2011) 82 doi: 10.1038/nature10365 [arXiv:1102.1020 [astro-ph.HE]].

[93] T. Piran, E. Nakar and S. Rosswog, "The Electromagnetic Signals of Compact Binary Mergers," Mon. Not. Roy. Astron. Soc. **430** (2013) 2121 doi: 10.1093/mnras/stt037 [arXiv: 1204.6242 [astro-ph.HE]].

[94] K. Hotokezaka and T. Piran, "Mass ejection from neutron star mergers: different components and expected radio signals," Mon. Not. Roy. Astron. Soc. **450** (2015) 1430 doi: 10.1093/mnras/stv620 [arXiv: 1501.01986 [astro-ph.HE]].

[95] R. Sari, T. Piran and J. Halpern, "Jets in GRBs," Astrophys. J. **519** (1999) L17 doi: 10.1086/312109 [astro-ph/9903339].

[96] Z. P. Jin *et al.*, "Short GRBs: opening angles, local neutron star merger rate and off-axis events for GRB/GW association," Astrophys. J. **857** (2018) 128 doi: 10.3847/1538-4357/aab76d [arXiv: 1708.07008 [astro-ph.HE]].

[97] I. Mandel, "The Orbit of GW170817 Was Inclined by Less Than 28° to the Line of Sight," Astrophys. J. **853** (2018) L12 doi: 10.3847/2041-8213/aaa6c1 [arXiv: 1712.03958 [astro-ph.HE]].

[98] O. D. Elbert, J. S. Bullock and M. Kaplinghat, "Counting Black Holes: The Cosmic Stellar Remnant Population and Implications for LIGO," Mon. Not. Roy. Astron. Soc. **473** (2018) 1186 doi: 10.1093/mnras/stx1959 [arXiv: 1703.02551 [astro-ph.GA]].

[99] D. Guetta and T. Piran, "The batse-swift luminosity and redshift distributions of short-duration grbs," Astron. Astrophys. **453** (2006) 823 doi: 10.1051/0004-6361:20054498 [astro-ph/0511239].

[100] P. D'Avanzo, "Short gamma-ray bursts: A review," JHEAp **7** (2015) 73 doi:10.1016/j.jheap.2015.07.002

[101] M. Mapelli and N. Giacobbo, "The cosmic merger rate of neutron stars and black holes," Mon. Not. Roy. Astron. Soc. **479** (2018) 4391 doi: 10.1093/mnras/sty1613 [arXiv: 1806.04866 [astro-ph.HE]].

[102] F. Ozel, D. Psaltis, R. Narayan and A. S. Villarreal, "On the mass distribution and birth masses of neutron stars," Astrophys. J. **757** (2012) 55 doi: 10.1088/0004-637X/757/1/55 [arXiv: 1201.1006 [astro-ph.HE]].

[103] W. M. Farr *et al.*, "The mass distribution of stellar-mass black holes," Astrophys. J. **741** (2011) 103 doi: 10.1088/0004-637X/741/2/103 [arXiv: 1011.1459 [astro-ph.GA]].

[104] C. S. Kochanek, "Failed supernovae explain the compact remnant mass function," Astrophys. J. **785** (2014) 28 doi: 10.1088/0004-637X/785/1/28 [arXiv: 1308.0013 [astro-ph.HE]].

[105] O. Pejcha and T. A. Thompson, "The landscape of the neutrino mechanism of core-collapse supernovae: Neutron star and black hole mass functions, explosion energies and nickel yields," Astrophys. J. **801** (2015) 90 doi: 10.1088/0004-637X/801/2/90 [arXiv: 1409.0540 [astro-ph.HE]].

[106] S. E. Woosley, A. Heger and T. A. Weaver, "The evolution and explosion of massive stars," Rev. Mod. Phys. **74** (2002) 1015. doi: 10.1103/RevModPhys.74.1015.

[107] T. Ertl, S. E. Woosley, T. Sukhbold and H. T. Janka, "The explosion of helium stars evolved with mass loss," Astrophys. J. **890** (2020) 51 doi: 10.3847/1538-4357/ab6458 [arXiv: 1910.01641 [astro-ph.HE]].

[108] P. Demorest, T. Pennucci, S. Ransom, M. Roberts and J. Hessels, "Shapiro Delay Measurement of A Two Solar Mass Neutron Star," Nature **467** (2010) 1081 doi: 10.1038/nature09466 [arXiv: 1010.5788 [astro-ph.HE]].

[109] J. Antoniadis *et al.*, "A Massive Pulsar in a Compact Relativistic Binary," Science **340** (2013) 6131 doi: 10.1126/science.1233232 [arXiv: 1304.6875 [astro-ph.HE]].

[110] V. Kalogera, K. Belczynski, C. Kim, R. W. O'Shaughnessy and B. Willems, "Formation of double compact objects," Phys. Rept. **442** (2007) 75 doi: 10.1016/ j.physrep.2007.02.008 [arXiv: astro-ph/0612144 [astro-ph]].

[111] T. M. Tauris *et al.*, "Formation of double neutron star systems," Astrophys. J. **846** (2017) 170 doi:10.3847/1538-4357/aa7e89 [arXiv: 1706.09438 [astro-ph.HE]].

[112] T. M. Tauris, N. Langer and P. Podsiadlowski, "Ultra-stripped supernovae: progenitors and fate," Mon. Not. Roy. Astron. Soc. **451** (2015) 2123 doi:10.1093/mnras/stv990 [arXiv: 1505.00270 [astro-ph.SR]].

[113] Y. Yang *et al.*, "Black hole formation in the lower mass gap through mergers and accretion in AGN disks," Astrophys. J. **901** (2020) L34 doi: 10.3847/2041-8213/abb940 [arXiv: 2007.04781 [astro-ph.HE]].

[114] Y. Lim and J. W. Holt, "Bayesian modeling of the nuclear equation of state for neutron star tidal deformabilities and GW170817," Eur. Phys. J. A **55** (2019) 209 doi:10.1140/epja/i2019-12917-9 [arXiv: 1902.05502 [nucl-th]].

[115] R. Essick, P. Landry and D. E. Holz, "Nonparametric inference of neutron star composition, equation of state, and maximum mass with GW170817," Phys. Rev. D **101** (2020) 063007 doi: 10.1103/PhysRevD.101.063007 [arXiv: 1910.09740 [astro-ph.HE]].

[116] H. Mueller and B. D. Serot, "Relativistic mean field theory and the high density nuclear equation of state," Nucl. Phys. A **606** (1996) 508 doi:10.1016/0375-9474(96)00187-X [arXiv: nucl-th/9603037].

[117] Z. Berezhiani, I. Bombaci, A. Drago, F. Frontera and A. Lavagno, "Gamma-ray bursts from delayed collapse of neutron stars to quark matter stars," Astrophys. J. **586** (2003) 1250 doi: 10.1086/367756 [arXiv: astro-ph/0209257].

[118] D. J. Kaup, "Klein-Gordon geon," Phys. Rev. **172** (1968) 1331. doi: 10.1103/ PhysRev.172.1331

[119] P. O. Mazur and E. Mottola, "Gravitational vacuum condensate stars," Proc. Nat. Acad. Sci. **101** (2004) 9545 doi:10.1073/pnas.0402717101 [arXiv: gr-qc/0407075 [gr-qc]].

[120] I. Bombaci, A. Drago, D. Logoteta, G. Pagliara and I. Vidaña, "Was GW190814 a Black Hole–Strange Quark Star System?," Phys. Rev. Lett. **126** (2021) 162702, doi: 10.1103/PhysRevLett.126.162702 [arXiv: 2010.01509 [nucl-th]].

[121] Z. Cao, L. W. Chen, P. C. Chu and Y. Zhou, "GW190814: Circumstantial evidence for up-down quark star," arXiv: 2009.00942 [astro-ph.HE].

[122] G. Fragione and A. Loeb, "Black hole-neutron star mergers from triples," Mon. Not. Roy. Astron. Soc. **486** (2019) 4443 doi:10.1093/mnras/stz1131 [arXiv: 1903.10511 [astro-ph.GA]].

[123] F. Antonini and H. B. Perets, "Secular evolution of compact binaries near massive black holes: Gravitational wave sources and other exotica," Astrophys. J. **757** (2012) 27 doi:10.1088/0004-637X/757/1/27 [arXiv: 1203.2938 [astro-ph.GA]].

[124] G. Fragione, E. Grishin, N. W. C. Leigh, H. B. Perets and R. Perna, "Black hole and neutron star mergers in galactic nuclei," Mon. Not. Roy. Astron. Soc. **488** (2019) 47 doi:10.1093/mnras/stz1651 [arXiv: 1811.10627 [astro-ph.GA]].

[125] M. E. Peskin and D. V. Schroeder, "An Introduction to quantum field theory,"

[126] T. D. Lee and C. N. Yang, "Question of Parity Conservation in Weak Interactions," Phys. Rev. **104** (1956), 254-258 doi:10.1103/PhysRev.104.254

[127] C. S. Wu, E. Ambler, R. W. Hayward, D. D. Hoppes and R. P. Hudson, "Experimental Test of Parity Conservation in β Decay," Phys. Rev. **105** (1957), 1413-1414 doi:10.1103/PhysRev.105.1413

[128] A. D. Sakharov, "Violation of CP Invariance, C asymmetry, and baryon asymmetry of the universe," Pisma Zh. Eksp. Teor. Fiz. **5** (1967), 32-35 doi:10.1070/PU1991v034n05ABEH002497

[129] I. Y. Kobzarev, L. B. Okun and I. Y. Pomeranchuk, "On the possibility of experimental observation of mirror particles," Sov. J. Nucl. Phys. **3** (1966) no.6, 837-841

[130] E. W. Kolb, D. Seckel and M. S. Turner, "The Shadow World," Nature **314** (1985), 415-419 doi:10.1038/314415a0

[131] Z. Berezhiani, "Through the looking-glass: Alice's adventures in mirror world," doi:10.1142/9789812775344_0055 [arXiv:hep-ph/0508233 [hep-ph]].

[132] L. B. Okun, "Mirror particles and mirror matter: 50 years of speculations and search," Phys. Usp. **50** (2007), 380-389 doi:10.1070/PU2007v050n04ABEH006227 [arXiv:hep-ph/0606202 [hep-ph]].

[133] M. Khlopov, "Fundamentals of Cosmic Particle Physics," doi:10.1007/978-1-907343-72-8

[134] R. Foot, "Mirror dark matter: Cosmology, galaxy structure and direct detection," Int. J. Mod. Phys. A **29** (2014), 1430013 doi:10.1142/S0217751X14300130 [arXiv:1401.3965 [astro-ph.CO]].

[135] Z. G. Berezhiani, A. D. Dolgov and R. N. Mohapatra, "Asymmetric inflationary reheating and the nature of mirror universe," Phys. Lett. B **375** (1996), 26-36 doi:10.1016/0370-2693(96)00219-5 [arXiv:hep-ph/9511221 [hep-ph]].

[136] Z. Berezhiani, D. Comelli and F. L. Villante, "The Early mirror universe: Inflation, baryogenesis, nucleosynthesis and dark matter," Phys. Lett. B **503** (2001), 362-375 doi:10.1016/S0370-2693(01)00217-9 [arXiv:hep-ph/0008105 [hep-ph]].

[137] L. Bento and Z. Berezhiani, "Leptogenesis via collisions: The Lepton number leaking to the hidden sector," Phys. Rev. Lett. **87** (2001), 231304 doi:10.1103/PhysRevLett.87.231304 [arXiv:hep-ph/0107281 [hep-ph]].

[138] Z. Berezhiani, "Mirror world and its cosmological consequences," Int. J. Mod. Phys. A **19** (2004), 3775-3806 doi:10.1142/S0217751X04020075 [arXiv:hep-ph/0312335 [hep-ph]].

[139] Z. Berezhiani, P. Ciarcelluti, D. Comelli and F. L. Villante, "Structure formation with mirror dark matter: CMB and LSS," Int. J. Mod. Phys. D **14** (2005), 107-120 doi:10.1142/S0218271805005165 [arXiv:astro-ph/0312605 [astro-ph]].

[140] Z. Berezhiani, S. Cassisi, P. Ciarcelluti and A. Pietrinferni, "Evolutionary and structural properties of mirror star MACHOs," Astropart. Phys. **24** (2006), 495-510 doi:10.1016/j.astropartphys.2005.10.002 [arXiv:astro-ph/0507153 [astro-ph]].

[141] E. Lisi, S. Sarkar and F. L. Villante, "The big bang nucleosynthesis limit on N(neutrino)," Phys. Rev. D **59** (1999), 123520 doi:10.1103/PhysRevD.59.123520 [arXiv:hep-ph/9901404 [hep-ph]].

[142] A. Y. Ignatiev and R. R. Volkas, "Mirror dark matter and large scale structure," Phys. Rev. D **68** (2003), 023518 doi:10.1103/PhysRevD.68.023518 [arXiv:hep-ph/0304260 [hep-ph]].

[143] C. Alcock *et al.* [MACHO], "The MACHO project: Microlensing results from 5.7 years of LMC observations," Astrophys. J. **542** (2000), 281-307 doi:10.1086/309512 [arXiv:astro-ph/0001272 [astro-ph]].

[144] A. K. Drukier, K. Freese and D. N. Spergel, "Detecting Cold Dark Matter Candidates," Phys. Rev. D **33** (1986), 3495-3508 doi:10.1103/PhysRevD.33.3495

[145] K. Freese, J. A. Frieman and A. Gould, "Signal Modulation in Cold Dark Matter Detection," Phys. Rev. D **37** (1988), 3388-3405 doi:10.1103/PhysRevD.37.3388

[146] R. Bernabei, P. Belli, F. Cappella, V. Caracciolo, S. Castellano, R. Cerulli, C. J. Dai, A. d'Angelo, S. d'Angelo and A. Di Marco, *et al.* "Final model independent result of DAMA/LIBRA-phase1," Eur. Phys. J. C **73** (2013), 2648 doi:10.1140/epjc/s10052-013-2648-7 [arXiv:1308.5109 [astro-ph.GA]].

[147] A. Addazi, Z. Berezhiani, R. Bernabei, P. Belli, F. Cappella, R. Cerulli and A. Incicchitti, "DAMA annual modulation effect and asymmetric mirror matter," Eur. Phys. J. C **75** (2015) no.8, 400 doi:10.1140/epjc/s10052-015-3634-z [arXiv:1507.04317 [hep-ex]].

[148] R. Cerulli, P. Villar, F. Cappella, R. Bernabei, P. Belli, A. Incicchitti, A. Addazi and Z. Berezhiani, "DAMA annual modulation and mirror Dark Matter," Eur. Phys. J. C **77** (2017) no.2, 83 doi:10.1140/epjc/s10052-017-4658-3 [arXiv:1701.08590 [hep-ex]].

[149] G. Adhikari, P. Adhikari, E. Barbosa de Souza, N. Carlin, S. Choi, M. Djamal, A. C. Ezeribe, C. H. Ha, I. Hahn and A. J. F. Hubbard, *et al.* "An experiment to search for dark-matter interactions using sodium iodide detectors," Nature **564** (2018) no.7734, 83-86 [erratum: Nature **566** (2019) no.7742, E2] doi:10.1038/s41586-018-0739-1 [arXiv:1906.01791 [astro-ph.IM]].

[150] J. Amare, S. Cebrian, D. Cintas, I. Coarasa, E. Garcia, M. Martinez, M. A. Olivan, Y. Ortigoza, A. O. de Solorzano and J. Puimedon, *et al.* "Annual Modulation Results from Three Years Exposure of ANAIS-112," Phys. Rev. D **103** (2021) no.10, 102005 doi:10.1103/PhysRevD.103.102005 [arXiv:2103.01175 [astro-ph.IM]].

[151] Z. Berezhiani and L. Bento, "Neutron - mirror neutron oscillations: How fast might they be?," Phys. Rev. Lett. **96** (2006), 081801 doi:10.1103/PhysRevLett.96.081801 [arXiv:hep-ph/0507031 [hep-ph]].

[152] Z. Berezhiani, "Neutron lifetime puzzle and neutron–mirror neutron oscillation," Eur. Phys. J. C **79** (2019) no.6, 484 doi:10.1140/epjc/s10052-019-6995-x [arXiv:1807.07906 [hep-ph]].

[153] Z. Berezhiani, R. Biondi, M. Mannarelli and F. Tonelli, "Neutron-mirror neutron mixing and neutron stars," Eur. Phys. J. C **81** (2021) no.11, 1036 doi:10.1140/epjc/s10052-021-09806-1 [arXiv:2012.15233 [astro-ph.HE]].

[154] V. Connaughton, E. Burns, A. Goldstein, M. S. Briggs, B. B. Zhang, C. M. Hui, P. Jenke, J. Racusin, C. A. Wilson-Hodge and P. N. Bhat, *et al.* "Fermi GBM Observations of LIGO Gravitational Wave event GW150914," Astrophys. J. Lett. **826** (2016) no.1, L6 doi:10.3847/2041-8205/826/1/L6 [arXiv:1602.03920 [astro-ph.HE]].

[155] A. Loeb, "Electromagnetic Counterparts to Black Hole Mergers Detected by LIGO," Astrophys. J. Lett. **819** (2016) no.2, L21 doi:10.3847/2041-8205/819/2/L21 [arXiv:1602.04735 [astro-ph.HE]].

[156] R. Perna, D. Lazzati and B. Giacomazzo, "Short Gamma-Ray Bursts from the Merger of Two Black Holes," Astrophys. J. Lett. **821** (2016) no.1, L18 doi:10.3847/2041-8205/821/1/L18 [arXiv:1602.05140 [astro-ph.HE]].

[157] K. Murase, K. Kashiyama, P. Mészáros, I. Shoemaker and N. Senno, "Ultrafast Outflows from Black Hole Mergers with a Minidisk," Astrophys. J. Lett. **822** (2016) no.1, L9 doi:10.3847/2041-8205/822/1/L9 [arXiv:1602.06938 [astro-ph.HE]].

[158] N. Arkani-Hamed, S. Dimopoulos, G. R. Dvali and N. Kaloper, "Many fold universe," JHEP **12** (2000), 010 doi:10.1088/1126-6708/2000/12/010 [arXiv:hep-ph/9911386 [hep-ph]].

[159] A. Addazi and A. Marciano, "Testing merging of Dark Exotic Stars from Gravitational Waves in the Multi-messenger approach," Int. J. Mod. Phys. A **33** (2018) no.29, 1850167 doi:10.1142/S0217751X18501671 [arXiv:1710.08822 [hep-ph]].